Age-Dependent Variability in Immune Host Responses to SARS-CoV-2: Implications for Inclusive Clinical Trial Design

Taylor Johnson

A dissertation

submitted in partial fulfillment of the

requirements for the degree of

Doctor of Philosophy

University of Washington

2025

Reading Committee:

Alison Fohner, Chair

Michael Gale Jr.

Helen Chu

Program Authorized to Offer Degree:

Public Health Genetics

University of Washington

Abstract

Age-Dependent Variability in Immune Host Responses to SARS-CoV-2: Implications for Inclusive Clinical Trial Design

Taylor Johnson

Chair of the Supervisory Committee:

Alison Fohner

Epidemiology

The COVID-19 pandemic, caused by SARS-CoV-2 has disproportionately affected older adults, who account for the majority of COVID-19-related hospitalizations and deaths. Although disease severity has declined, periodic surges continue to pose significant risks to aging populations, exacerbated by age-associated immune dysfunction, or immunosenescence. This dissertation investigates the immune responses that contribute to protection against SARS-CoV-2 and how these responses become dysregulated with increasing age. Given the evidence of impaired antiviral immunity in aged models, we also evaluated the representation of older adults in COVID-19 vaccine clinical trials to assess whether key age-associated immune differences are being adequately captured in clinical research.

In Chapter 1, we examined the effects of IFNβ pre-treatment on SARS-CoV-2 infection dynamics in lung epithelial cell models. We identified interferon-stimulated gene signatures

associated with antiviral protection, and found that pre-activation of the IFN pathway significantly reduced viral replication and dampened inflammatory responses associated with severe disease.

In Chapter 2, leveraging a cohort of young, mature, and aged mice infected with mouse-adapted SARS-CoV-2, we performed temporally resolved transcriptomic analyses of lung tissues. Aged mice exhibited impaired early cytokine and IFN signaling, dysregulated T cell activation during recovery, and elevated baseline inflammatory signatures, all of which contributed to delayed viral clearance and worsened disease outcomes. Moreover, these immune response are crucial for effective vaccine-induced protection against COVID-19.

In Chapter 3, we conducted a cross-sectional analysis of COVID-19 vaccine clinical trials, quantifying the underrepresentation of older adults and identifying exclusion criteria disproportionately impacting this group. Our analysis reveals significant underrepresentation of older adults in these trials, key barriers to their enrollment, and provides recommendations for improving inclusivity of this group in clinical trials. Together, these studies provide new insights into the molecular mechanisms underlying age-associated susceptibility to SARS-CoV-2 and offer a framework for improving immune protection and clinical trial participation for older adults.

TABLE OF CONTENTS

ACKNOWLEDGEMENTS

First and foremost, I want to thank my family for their unwavering support throughout this journey. My dad taught me the value of hard work and dedication, and I've tried to carry that with me. My mom instilled in me a belief in the power of education and importance of following your dreams. Their steady encouragement and pride have guided and lifted me every step of the way. To my sister, Riley–your constant support and belief in me have meant the world.

To my wife, Amber—I am endlessly grateful for your presence in my life. Your encouragement during the application process and our move across the country was invaluable. When we arrived in Seattle, we only had each other, and your grace and support during that transition meant everything. Together, we built a new life that not only sustained me through graduate school but made it the most meaningful chapter of my life so far. I could not have done this without you, nor would I want to.

I would also like to thank my undergraduate mentors, whose early guidance helped shape my path in science. Their mentorship sparked my curiosity and gave me the foundation to pursue graduate study. To my graduate mentors–especially Dr. Michael Gale—thank you for welcoming me into your lab and providing a supportive environment in which I could grow as a scientist. I am especially grateful for your mentorship, thoughtful feedback, and the trust you placed in me throughout this project. To the members of the Gale Lab—thank you for your generosity, insight, and friendship. Your guidance and collaboration were instrumental in completing this dissertation. To the Public Health Genetics program–thank you for being an incredible home. I am especially grateful to Dr. Alison Fohner for her mentorship and support. To my cohort, thank you for becoming family.

Chapter 1. EARLY INTERFERON RESPONSES SHAPE ANTIVIRAL IMMUNITY AND LIMIT INFLAMMATION DURING ANCESTRAL SARS-COV-2 INFECTION: A FUNCTIONAL GENOMIC ANALYSIS

Chapter 1. SUMMARY

Dysregulation of the interferon (IFN) signaling pathway has been implicated in severe cases of COVID-19. Type I IFNs have shown promise in reducing viral load in some patients, but their efficacy depends on multiple factors, including timing, duration, IFN subtype, and host transcriptional responses. Here, we analyzed the transcriptional response to IFN-β and SARS-CoV-2 infection in Calu-3 and HSAEC1-KT lung epithelial cells, revealing distinct IFN-stimulated gene (ISG) and virus-stimulated gene (VSG) signatures, including waves of ISGs that define antiviral immunity, immune modulation, and cellular recovery. IFN-β treatment prior to SARS-CoV-2 infection induced a robust ISG response, accelerating viral RNA clearance and dampening inflammatory pathways linked to severe disease, including NF-κB activation and cytokine-mediated signaling. In contrast, post-infection treatment with IFN-β had minimal impact on gene expression, with no significant reduction in viral RNA levels. Furthermore, we identified a viral-load associated transcriptional signature that was enriched in severe COVID-19 patients, but was mitigated by IFN-β pre-treatment. These findings underscore the importance of early ISG activation in shaping antiviral defenses and highlight the role of IFN timing in reducing inflammation and limiting viral replication. Our results provide a comprehensive atlas of ISG sets with potential therapeutic potential, offering a framework for optimizing IFN-based therapies against SARS-CoV-2.

1.1 INTRODUCTION

1.1.1 *Novel coronavirus outbreak*

The coronavirus disease 2019 (COVID-19) pandemic marks the third pathogenic coronavirus outbreak in the past two decades. Severe acute respiratory syndrome coronavirus 2 (SARS-CoV-2), the virus responsible for COVID-19, was first identified in Wuhan, Hubei Province, China in December 2019, and quickly spread worldwide[1]. The first confirmed case of SARS-CoV-2 infection in the United States was identified in Snohomish County, Washington State on January 19, 2020[2]. Phylogenetic analysis revealed that this strain, designated USA/WA1/2020 (WA1), was closely related to early virus samples from China[3]. The WA1 isolate has since become the primary reference strain for research in the United States, serving as a critical tool for investigating the mechanisms of SARS-CoV-2 infection and immune activation.

1.1.2 *SARS-CoV-2 evolution*

Like other RNA viruses, SARS-CoV-2 undergoes continuous genomic mutations, resulting in the emergence of variants that pose significant global public health challenges. Variants of concern (VOCs), including Alpha (B.1.1.7), Beta (B.1.351), Gamma (P.1), Delta (B.1.617.2), and Omicron (B.1.1.529), have raised concerns regarding vaccine efficacy, transmissibility, and disease severity. Despite the emergence of these variants, the WA1 remains a critical reference strain for investigating fundamental mechanisms of SARS-CoV-2 infection. Given that innate immune pathways, including IFN signaling and ISG responses are broadly conserved across SARS-CoV-2 variants, studying WA1 provides essential insights into antiviral defense mechanisms that remain relevant to understanding both ancestral and emerging variant strains.

1.1.3 *Clinical features of COVID-19*

SARS-CoV-2/WA1 primarily causes lower respiratory tract infections, presenting with symptoms such as cough, fever, shortness of breath, and muscle aches[4]. It has been widely

reported that over 80% of COVID-19 patients experience mild disease, requiring neither hospitalization nor intensive medical care[5,6]. Risk factors for severe disease include advanced age, male sex, racial and social inequities, and pre-existing comorbidities such as diabetes and coronary heart disease[5,7]. Despite these known risk factors, the reasons some individuals recover quickly while others experience severe illness or fail to recover remain unclear.

Early studies suggest that worsening COVID-19 severity is associated with a delayed and dysregulated interferon (IFN) response, leading to excessive inflammatory cytokine production characteristic of cytokine storm syndrome[8-11]. For example, Hadjadj et al. reported reduced expression of IFN-stimulated genes (ISGs) in severe and critical COVID-19 cases, coupled with the absence of IFN-beta (IFN-β) mRNA or protein in infected patients[10]. Other studies have confirmed insufficient type I and III IFN responses alongside elevated levels of inflammatory cytokines[11]. While cytokine signaling is crucial for regulating the innate immune response to viral infections, dysregulation or hyperactivation of this response can result in significant host damage[12-14]. Elevated levels of pro-inflammatory cytokines, including interleukin (IL)-1, IL-2, IL-6, tumor necrosis factor (TNF), and IFN-gamma (IFN-γ) have been linked to severe COVID-19 complications, including acute respiratory distress syndrome (ARDS), hemophagocytic lymphohistiocytosis (HLH), and multi-organ failure[15]. These findings suggest that effective IFN signaling and coordinated ISG production may drive mild COVID-19 outcomes, highlighting their role in mitigating hyperinflammation and dysregulated responses characteristic of severe cases.

1.1.4 *Canonical antiviral host defenses*

Canonical host defense signaling against viruses begins with the detection of pathogen-associated molecular patterns (PAMPs) by pattern-recognition receptors (PRRs)[16]. In the context

of SARS-CoV-2 infection, PRR-mediated immune signaling is initiated primarily through retinoic acid-inducible gene-I (RIG-I)-like receptors (RLRs), including RIG-I and melanoma differentiation-associated gene 5 (MDA5)[17]. This recognition triggers the production of type I and III IFNs and other antiviral cytokines. Binding of type I/III IFNs to their respective receptor induces the expression of hundreds of ISGs, collectively combating viral infections through a variety of mechanisms including inhibition of viral entry, replication, translation, and egress[18]. However, ISG composition and expression kinetics can fluctuate in response to pathogen-specific factors, cell type specificity, receptor expression levels, and host genetic variation[19]. While numerous ISGs with established antiviral properties, such as *MX1*, *RSAD2*, and *IFIT2*, are induced upon SARS-CoV-2 infection, a substantial knowledge gap persists in defining the specific ISGs induced by SARS-CoV-2.

1.1.5 *Uncovering SARS-CoV-2 specific gene signatures*

Understanding the ISG signature unique to SARS-CoV-2 is crucial for elucidating how the disrupted IFN response contributes to inflammatory cytokine production and severe disease outcomes. Moreover, rather than focusing solely on individual effector ISGs, it is essential to consider how ISGs function collectively to restrict viral infection. Given that IFNs exert their potency through the concerted action of multiple ISGs, a better understanding of these group dynamics may provide more clinically relevant insights into therapeutic strategies that mimic IFN's broad antiviral properties while mitigating its adverse side effects.

Despite significant progress in understanding host-virus interactions, further research is essential to understand the mechanisms underlying COVID-19 pathogenesis and inform effective public health interventions. In this study, we analyzed the response to type I IFN and SARS-CoV-2 infection to reveal the ISG and VSG signature of human lung epithelial cells. Calu-3 cells,

derived from the human airway epithelium, represent the upper respiratory tract, while HSAEC1-KT/ACE2 cells, primary human small airway epithelial cells engineered to express ACE2, model the distal lung. These complementary models capture distinct regional and functional responses to IFN and viral infection across the respiratory tract. We hypothesized that early induction of ISGs in lung epithelial cells would restrict SARS-CoV-2 replication *in vitro*, leading to rapid viral clearance and inhibition of infection. Our findings identify SARS-CoV-2 (WA1)-specific ISG subsets that, when activated early, can directly control viral replication and mitigate virus-induced inflammatory programming.

1.2 RESULTS

1.2.1 *IFN-β induces canonical type I IFN signaling in human lung epithelial cells*

To evaluate the type I IFN response, we used two human lung epithelial cell lines, Calu-3 and HSAEC1-KT, highly relevant models for SARS-CoV-2 studies. Human ACE2 was stably introduced into parental HSAEC1-KT cells to facilitate infection. Upon IFN-β treatment, both cell lines exhibited canonical IFN signaling, evidenced by STAT1 and STAT2 phosphorylation and a dose-dependent increase in ISG expression, including IFIT1 and IFITM1 (Fig. 1A). Bulk RNA sequencing (RNA-seq) was performed across four time points (6, 12, 24, and 48 h) and three IFN-β doses (10, 100, 1,000 IU/mL) (Fig. 1B). Principal component analysis (PCA) on the mean $\log_2$ counts per million (CPM) revealed distinct separation between treatments and time points, validating that the experimental conditions induced distinct transcriptional signatures (Fig. S1A).

1.2.2 *Characterizing the IFNβ-stimulated gene signature*

Differential expression (DE) analysis revealed 652 and 2,766 interferon-stimulated genes (ISGs) in Calu-3 and HSAEC1-KT/ACE2 cells, respectively, with 383 shared ISGs (Fig. 1C). Here,

ISGs are defined as genes significantly upregulated or downregulated following IFN-β treatment. The number of DEGs increased proportionally with IFN-β dose across time points (Fig. 1D). Unsupervised clustering of $\log_2$ fold changes (LFC) revealed five temporally distinct co-expression clusters: *Immediate Early*, *Early*, *Late*, *Downregulated 1*, and *Downregulated 2* (Fig. 1D). Despite differences in gene composition, clusters exhibited similar dynamic expression patterns across cell lines, with *Immediate Early* genes peaking at 12 h, *Early* genes at 24 h, and *Late* genes steadily increasing over time (Fig. 1E).

Pathway enrichment analysis revealed that *Immediate Early* clusters were enriched for canonical type I IFN responses, complement activation, and viral defense pathways, while *Early* clusters were associated with IFN-γ response and TNF-α signaling (Fig. 1F). *Late* clusters showed enrichment for pathways related to structural organization and cellular regulation pathways, though with divergent gene membership between cell lines (Fig. S2). Downregulated clusters revealed reduced expression of genes involved in RNA catabolism, ribosome function, and translation initiation (Fig. 1F , Fig. S2).

Given the strong cytokine pathway enrichment, we further examined cytokine induction following IFN-β treatment. Both cell lines upregulated *CXCL10, CXCL8, IL-15, IFNL1, IFNL3, CXCL9, CCL5, IL-7,* and *IL-6,* while HSAEC1-KT/ACE2 cells uniquely showed stronger induction of anti-inflammatory cytokines *IL-1RN* and *IL-36RN*, enhanced modulation of inflammation (Fig 1G).

Upstream regulator analysis implicated canonical IFN-driven regulators, including IRF1, IRF7, and STAT1 in *Immediate Early* and *Early* clusters (Fig. 1H). Additional immune and stress-responsive regulators (NONO, SMAD4, SPI1, NFKB1, and RELA) were also associated with gene regulation following IFN-β treatment, potentially reflecting secondary regulatory layers.

Late cluster genes were driven by regulators of chromatin remodeling and cell differentiation (SMARCA4, EP300, and EOMES) which downregulated clusters showed suppression of metabolic and proliferative programs regulated by ID1, HNF1A, and E2F4. Notably, most TFs in HSAEC1-KT/ACE2 cells were predicted to regulate genes across all clusters, suggesting a more globally coordinated response to IFN-β (Fig. 1H).

1.2.3 *SARS-CoV-2 elicits type I IFN signaling*

Following SARS-CoV-2 (MOI:5) infection for up to 48 hpi, we identified 3,584 and 3,691 DE genes, referred to as virus-stimulated genes (VSGs), in Calu-3 and HSAEC1-KT/ACE2 cells, respectively (Fig. 2A-B). In Calu-3 cells, nearly all VSGs were DE by 48 h post-infection (hpi), with peak upregulation at this time, while HSAEC1-KT/ACE2 displayed a faster transcriptional response, with approximately half of the VSGs responding by 24 hpi (Fig. S3A-S3B). Cytokine activation mirrored this trend, with antiviral mediators (*IFN-β, IFN-λs, CXCL10*) and pro-inflammatory cytokines (*TNF-α, IL-6, CCL5*) peaking at 48 hpi in Calu-3 cells and 24 hpi in HSAEC1-KT/ACE2 cells (Fig. S2C). Again, immunomodulatory cytokines *IL1RN* and *IL36RN* were only DE after SARS-CoV-2 infection in HSAEC1-KT/ACE2 cells (Fig. S3C).

1.2.4 *Characterizing the SARS-CoV-2 gene signature*

Pathway enrichment analysis revealed that Calu-3 cells activated TNF-α/NF-κB signaling, IFN-γ response, and RNA Pol II activity at 48 hpi, whereas HSAEC1-KT/ACE2 cells showed earlier activation of these pathways at 24 hpi (Fig. S3D). Enrichment of IL-2/STAT2 signaling pathways at earlier time points in HSAEC1-KT/ACE2 cells suggests a more rapid transition toward immune activation. Both cell lines downregulated metabolic pathways (Fig. S3D). Upstream regulator analysis highlighted activation of immune-related TFs (STATs, IRFs, RELA, NFKB1),

stress-related TFs (ATF4, SMARCA4, TP53, NUPR1), and tissue remodeling TFs (SMAD3, FOXM1, CDKN2B), with earlier activation predicted in HSAEC1-KT/ACE2 cells (Fig. S2E).

1.2.5 *ISG signature during infection*

Following SARS-CoV-2 infection, the transcriptional dynamics of ISGs identified in Fig. 1D mirrored the patterns observed during IFN-β treatment (Fig. 2C). HSAEC1-KT/ACE2 cells quickly induced innate immune signaling, with *Immediate Early* and *Early* ISG expression peaking at 24 hpi compared to 48 hpi in Calu-3 cells, and showing a higher average LFC in these early time points (Fig. 2D). In both cell lines, ISG induction was greater during infection than during IFN-β treatment alone, likely due to viral RNA sensing through PRRs and autocrine amplification of the IFN response (Fig 2D). These timing and strength differences suggest that HSAEC1-KT/ACE2 cells may limit viral replication more effectively than Calu-3.

1.2.6 *IFN-β-independent VSG signature*

To identify genes regulated independently of IFN signaling, ISGs were excluded, yielding 2,654 and 1,417 IFN-independent VSGs in Calu-3 and HSAEC1-KT/ACE2 cells, respectively, with 464 shared genes (Fig. S3A). In both cell lines, early transcriptional responses were largely IFN-mediated, with virus-specific responses emerging predominantly between 24 and 48 hi. HSAEC1-KT/ACE2 cells exhibited accelerated transcriptional dynamics compared to Calu-3, consistent with earlier innate immune activation.

Pathway enrichment of IFN-independent VSGs revealed activation of TNFα/NF-κB and MAPK signaling, along with epithelial morphogenesis pathways, while metabolic and structural organization pathways were downregulated (Fig. S4B). Upstream regulator analysis implicated inflammation-related (NFKB1, RELA, FOS, JUN), stress-responsive (ATF4, KLF6, MYC), and tissue remodeling (SMAD3, FOXA1, EZH2) TFs (Fig. S4C). These findings demonstrate that

although ISG responses dominate early infection, IFN-independent antiviral pathways emerge later, providing additional layers of host defense that may be particularly important in the context of impaired IFN signaling or viral immune evasion strategies.

1.2.7 *Early IFN signaling attenuates SARS-CoV-2 replication*

To investigate the role of early IFN signaling on SARS-CoV-2 infection, viral kinetics were assessed following 24 h of IFN-β pre-treatment (Fig. 3A). Pre-treatment significantly reduced viral production in a dose-dependent manner in Calu-3 cells and conferred complete protection in HSAEC1-KT/ACE2 cells across all IFN-β doses (Fig. 3B). While high IFN-β doses (100, 1000 IU/mL) induced mild cytotoxicity in mock-treated Calu-3 cells, HSAEC1-KT/ACE2 cells maintained 100% cell survival across all doses (Fig. 3C). qPCR analysis demonstrated significant reductions in viral RNA levels (orf1ab and N) following IFN-β pre-treatment (Fig. 3D).

Immunoblot analysis confirmed induction of canonical ISGs, including IFIT1 and IFITM1, within 24 h, indicating successful IFN pathway activation prior to infection (Fig. 3E). Higher IFN-β doses were associated with greater reductions in viral N protein levels and suppression of virus-induced signaling proteins, including phosphorylated (p)-IRF3, p-STAT1, and p-STAT2 levels (Fig. 3E, Fig. 3F). These findings indicate that IFN-β pre-treatment effectively attenuates both viral replication and virus-triggered signaling pathways, mitigating infection-associated cellular stress.

1.2.8 *IFN-β pre-treatment reprograms the host response*

To investigate the impact of IFN-β pre-treatment on host responses to SARS-CoV-2, we compared gene expression in pre-treated versus untreated infected cells (Fig. 5A). IFN-β priming significantly reprogrammed transcriptional responses, with 2,995 DE genes in Calu-3 cells, and

5,830 DE genes in HSAEC1-KT/ACE2 cells (Fig. S5A). Pre-activated antiviral modules were already elevated at 0 hpi in pre-treated cells and dampened by 24-48 hpi, consistent with viral suppression (Fig. S5A, Fig. 3B). Pro-inflammatory cytokines (*TNF-α, IFN-β, IFNL1-3, IFNL2,* and *CXCL9)* strongly upregulated in infection were markedly reduced in IFN-β pre-treated cells (Fig. S5B). Pathway analysis revealed upregulation of ciliary function, motility, and metabolism pathways– which were suppressed during infection–suggesting restoration of epithelial homeostasis (Fig. S5C). Upstream regulators shifted from early ISG drivers (IRFs, STATs) to metabolic and cell cycle factors (TEAD1, SPI1, E2F4, HNF1A, and MGA) over time (Fig. S5D). Pre-treatment enhanced early ISG induction, with *Immediate Early* and *Early* ISGs peaking at 0 hpi, followed by reduction at later time points compared to untreated infection (Fig 4A). Conversely, Downregulated ISG modules exhibited progressive upregulation relative to untreated infection consistent with transcriptional recovery (Fig. 4A).

1.2.9 *IFN-β induces early expression of antiviral ISGs*

Among cell line-specific ISGs, 383 genes were conserved across cell lines (Fig. 1C). These ISGs were clustered into five co-expression modules, and nearly all remained significantly regulated during IFN-β pre-treatment compared to infection alone (Fig. 4B). Cluster 3 contained key antiviral ISGs, including *RIG-I, OAS1, IFITM1, BST2, IFNL1, HERC5,* and *ISG15*, which are known SARS-CoV-2 restriction factors (Fig. 4C). Cluster 3 expression was stronger in HSAEC1-KT/ACE2 cells at early time points but more rapidly attenuated at later timepoints compared to Calu-3, suggesting a more dynamic antiviral response (Fig. 4C). Pro-inflammatory ISGs, such as *CXCL10, CXCL11, IFNL1,* and *IFNL3* were also attenuated by IFN-β pre-treatment beginning at 24 hpi in both cell lines. These findings suggest that early IFN-β priming

enhances antiviral gene expression while mitigating excessive inflammatory-related genes, potentially limiting tissue damage and promoting recovery.

IFN-β pre-treatment suppressed immune-related ISG expression (Clusters 1-4) at later time points in a dose-dependent manner, except at the lowest dose in Calu-3 (Fig. 4D). While 100 and 1,000 IU/mL effectively suppressed late ISG expression, 10 IU/mL failed to do so, resulting in sustained activation similar to untreated infection (Fig 4D). This pattern correlated with viral replication outcomes, where 10 IU/mL IFN-β only modestly reduced viral plaques in Calu-3 cells (Fig. 3B). In contrast, HSAEC1-KT/ACE2 cells exhibited complete viral suppression and tightly regulated ISG expression across all doses (Fig. 4D).

1.2.10 *IFNβ post-treatment has limited protective effects*

To evaluate the protective potential of IFN-β administered after SARS-CoV-2 infection, Calu-3 and HSAEC1-KT/ACE2 cells were treated with IFN-β at 24 hpi (Fig. 5A). Plaque assays revealed a slight dose-dependent reduction in infectious virus in Calu-3 cells, though the effect was not statistically significant (Fig. 5B). IFN-β post-treatment had no significant impact on cytotoxicity (Fig. 5C) or viral RNA levels, with untreated, infected cells showing naturally declining RNA levels by 72 hpi (Fig. 5D).

Immunoblot analysis confirmed activation of antiviral pathways by SARS-CoV-2 infection at 24 hpi, including phosphorylation of IRF3 (S386), STAT1 (Y701), and STAT2 (Y689), and elevated ISG expression at 36 hpi (Fig. 5E). However, IFN-β post-treatment did not significantly alter the levels of p-Stat1, p-Stat2, or p-IRF3 across doses (Fig. 5F). These findings suggest that by 24 hpi, SARS-CoV-2 infection is already well-established, limiting the protective effects of subsequent IFN-β administration.

1.2.11 *Post-treatment IFN-β weakly alters SARS-CoV-2-induced transcription*

To identify ISGs capable of overcoming virus-induced transcriptional dominance, we compared the transcriptomic response to increasing doses of IFN-β administered at 24 hpi relative to untreated. infected cells. DE analysis identified only 65 DE genes in Calu-3 and 15 in HSAEC1-KT/ACE2, suggesting that SARS-CoV-2-driven transcriptional program remains largely unaffected by IFN-β post-treatment (Fig. S6A). Restricting the analysis to ISGs revealed 12 significant DE ISGs per cell line, with *CXCL10* and *GMPR* as the only shared genes (Fig. 6A). These inducible ISGs included antiviral effectors (*ZBP1*, *TRIM22*, *GBP4*, *IFIT2*, *RSAD2*) and immune regulators (*CD38*, *CXCL10*, *UBD*, *BATF2*, *CXCL11*, *IDO1*, *XAF1*). Upstream regulator analyses predicted IRF3, STAT1, and NONO as key TFs orchestrating these responses (Fig. 1H, Fig. S3E). Interaction networks linking IFN-β-induced ISGs with these regulators revealed cell line-specific modules capable of residual induction despite established infection, highlighting potential pathways that remain responsive to IFN signaling at later stages (Fig. 6B).

1.2.12 *IFN-β protects against severe COVID-19 signature*

To identify gene networks associated with viral load, we performed weighted gene co-expression network analysis (WGCNA) across all treatment groups in both cell lines, using a soft-thresholding power of 8 to achieve a scale-free R^2 value of 0.8 (Fig. S7A). This analysis identified 36 co-expression modules, with the blue module showing the strongest correlation with viral reads ($r=0.73$, $p \leq 0.001$), suggesting its key role in host responses to SARS-CoV-2 infection (Fig. S7B-C). A significant correlation between gene significance (GS) and module membership (MM) ($r=0.79$, $p \leq 0.001$) further confirmed that hub genes in this module are strongly associated with viral load (Fig. 57D).

To assess clinical relevance, we compared the blue module gene signature to a publicly available transcriptomic dataset (GSE171110) consisting of whole blood RNA-seq from 10 healthy

controls and 44 severe COVID-19 patients. DE analysis identified 221 of the 2,087 blue module genes as significantly DE in severe disease (Fig. S7E). Expression analysis of these genes across experimental conditions (Mock, IFN-β treatment, SARS-CoV-2 infection, and IFN-β post-treatment) revealed highly consistent expression patterns across, except for a distinct subset of 14 genes in Cluster 6 (Fig. 7A).

These 14 genes exhibited low expression in Mock, IFN-β treatment, and IFN-β pre-treatment conditions, but were strongly upregulated during SARS-CoV-2 infection and IFN-B post-treatment, suggesting they are primarily virus-induced rather than IFN-induced (Fig. 7A). Further analysis of normalized expression counts revealed that early IFN-β pre-treatment mitigated the induction of these genes, likely due to early viral suppression and prevention of persistently activated host stress and immune pathways, whereas IFN-β post-treatment had minimal impact.

Comparison to severe COVID-19 patient samples confirmed significant upregulation of these genes in severe disease, except *IFNL1*, which was reduced (Fig. 7C). Together, these findings reinforce that early IFN-β priming effectively attenuates gene signatures associated with viral-load and severe COVID-19, while late IFN-β intervention fails to reprogram the host transcriptional landscape once infection is established.

1.3 DISCUSSION

1.3.1 *Principle findings*

This study provides critical insights into the transcriptional responses of human lung epithelial cells to IFN-β treatment and SARS-CoV-2 infection, revealing temporally distinct waves of ISG expression that define antiviral immunity, immune modulation, and cellular recovery. By categorizing ISGs into coordinated transcriptional clusters, we identified pathways critical for

early viral suppression, inflammation regulation, and homeostasis, highlighting the dynamic and context-dependent nature of IFN signaling. HSAEC1-KT/ACE2 cells exhibited a more rapid and robust transcriptional response to both IFN-β and SARS-CoV-2 compared to Calu-3 cells, correlating with more effective viral suppression at lower IFN-β doses (Fig. 1D, Fig. S3A, Fig. 5B). This suggests innate differences in epithelial cell responsiveness between these cell lines. Early IFN-β priming not only suppressed viral replication but also mitigated inflammatory pathways linked to severe COVID-19, including NF-κB activation, IL-8 production, complement activation, and PRR signaling (Fig. 3B-F, Fig. 4D). IFN-β pre-treatment also suppressed adaptive immune pathways, such as T cell-mediated immunity and antigen processing (Fig. 4D), and dampened pro-inflammatory ISGs (*CXCL10*, *CXCL11*, *IFNL1*, and *IFNL3)* at later stages (Fig. 3C). Given that CXCL10 and CXCL11 recruit effector cells and IFN-λs modulate epithelial antiviral defenses, their downregulation by IFN-β pre-treatment suggests a coordinated mechanism to limit immune-mediated tissue damage and promote recovery.

1.3.2 *Clinical implications*

Our findings also reinforce the critical importance of timing in IFN responses. Consistent with previous studies, such as Viox et al., which demonstrated IFN-α-mediated viral suppression in Calu-3 cells and rhesus macaques, our work extends these observations by defining distinct ISG waves and coordinated transcriptional drivers of protection [20]. Despite the potency of early IFN-β priming, IFN-β post-treatment at 24 hpi failed to substantially reprogram virus-driven transcription. Nevertheless, select ISGs (*TRIM22*, *RSAD2*, *IFIT2, CXCL10, CXCL11, CD38*) remained inducible. We did not observe evidence of SARS-CoV-2-mediated inhibition of ISG activation as no ISGs remained uninduced during infection. Rather, the limited impact of IFN-β post-treatment likely reflects ISG saturation in infected cells.

The intersection of the viral load-associated transcriptional signatures with severe COVID-19 patient datasets revealed a 14-gene cluster mitigated by early IFN-β treatment (Fig. 7B). Genes involved in chromatin remodeling (*H1-4*, *H2AC8*, *H2BC18*, and *HSPA6*) suggest that SARS-CoV-2 may exploit host epigenetic machinery to sustain infection and inflammation. RNA viruses, including SARS-CoV-2, have been shown to hijack host chromatin remodeling pathways to evade immune detection and promote inflammatory cytokine production[21,22]. Early ISG induction may counteract virus-driven epigenetic modifications, preserving transcriptional integrity and limiting viral exploitation of host chromatin dynamics. Moreover, prior reports have associated increased expression of *DNAH17*, *ITGAM, FAP, HSPA6,* and *IL-11* with COVID-19 infection, further linking this IFN-suppressed signature to dysregulated immune activation[24-27]. Given that early IFN priming suppressed all genes in this signature, future studies should investigate whether these genes contribute mechanistically to severe COVID-19 pathogenesis or are secondary to immune dysregulation.

Although early IFN priming suppressed this severe COVID-19 gene signature, most viral load-associated genes identified in lung epithelial cells were not DE in severe COVID-19 blood samples, likely reflecting differences in tissue-specific responses and timing (epithelial vs. blood, early vs. late infection). These findings underscore the need to integrate *in vitro* and *in vivo* models to fully capture host-pathogen dynamics.

1.3.3 *Strengths and limitations*

While our study provides a detailed temporal framework for ISG dynamics, several limitations exist. This use of WA1 strain does not fully encompass mutations present in later variants (e.g., Delta, Omicron) or current circulating variants that could alter IFN sensitivity. The use of high MOI may noy fully replicate natural infection dynamics. Moreover, our *in vitro* system, while

mechanistically informative, does not capture the complexity of multicellular immune responses in vivo. Longitudinal patient studies with consistent IFN dose, timing, and sample collection would complement these findings and provide insights into ISG regulation during convalescence.

1.3.4 *Conclusions*

In summary, this work defines temporally distinct ISG modules and demonstrates that early IFN signaling is a critical determinant of effective antiviral responses to SARS-CoV-2. Early activation of cytokine and IFN pathways promotes viral clearance while preventing downstream inflammation. These findings provide a foundation for optimizing IFN-based therapies that leverage endogenous antiviral pathways. Future studies should explore the functions of uncharacterized ISGs and the therapeutic potential of targeting upstream regulators to enhance early antiviral responses.

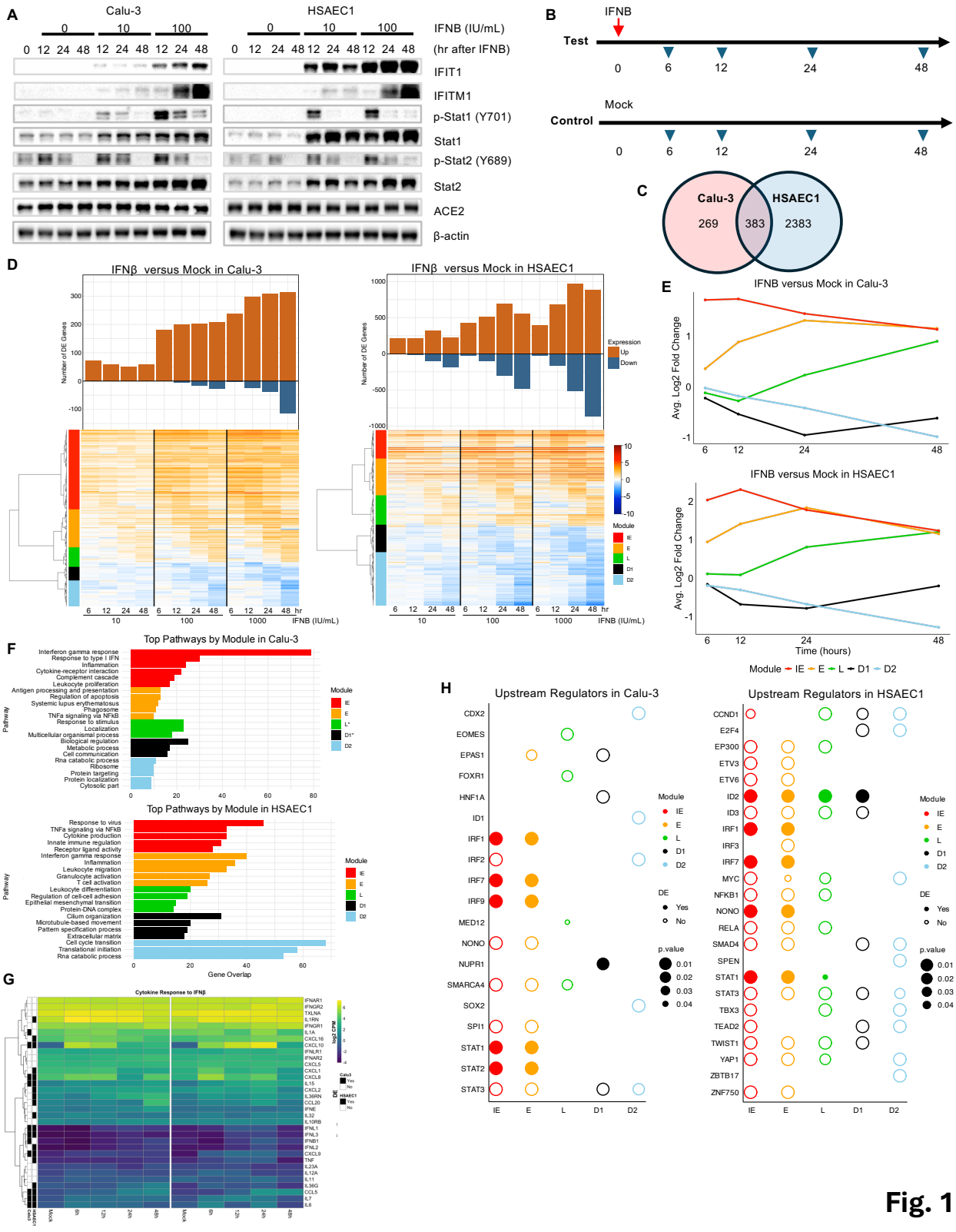
A
Calu-3
HSAEC1
IFNB (IU/mL)
(hr after IFNB)
IFIT1
IFITM1
p-Stat1 (Y701)
Stat1
p-Stat2 (Y689)
Stat2
ACE2
β-actin
B
IFNB
Test
Mock
Control
C
Calu-3
HSAEC1
269
383
2383
D
IFNβ versus Mock in Calu-3
IFNβ versus Mock in HSAEC1
Number of DE Genes
Expression
Up
Down
Module
IFNB (IU/mL)
E
IFNB versus Mock in Calu-3
IFNB versus Mock in HSAEC1
Avg. Log2 Fold Change
Time (hours)
Module IE E L D1 D2
F
Top Pathways by Module in Calu-3
Top Pathways by Module in HSAEC1
Pathway
Gene Overlap
G
Cytokine Response to IFNβ
H
Upstream Regulators in Calu-3
Upstream Regulators in HSAEC1
DE
Yes
No
p.value
0.01
0.02
0.03
0.04

Fig. 1

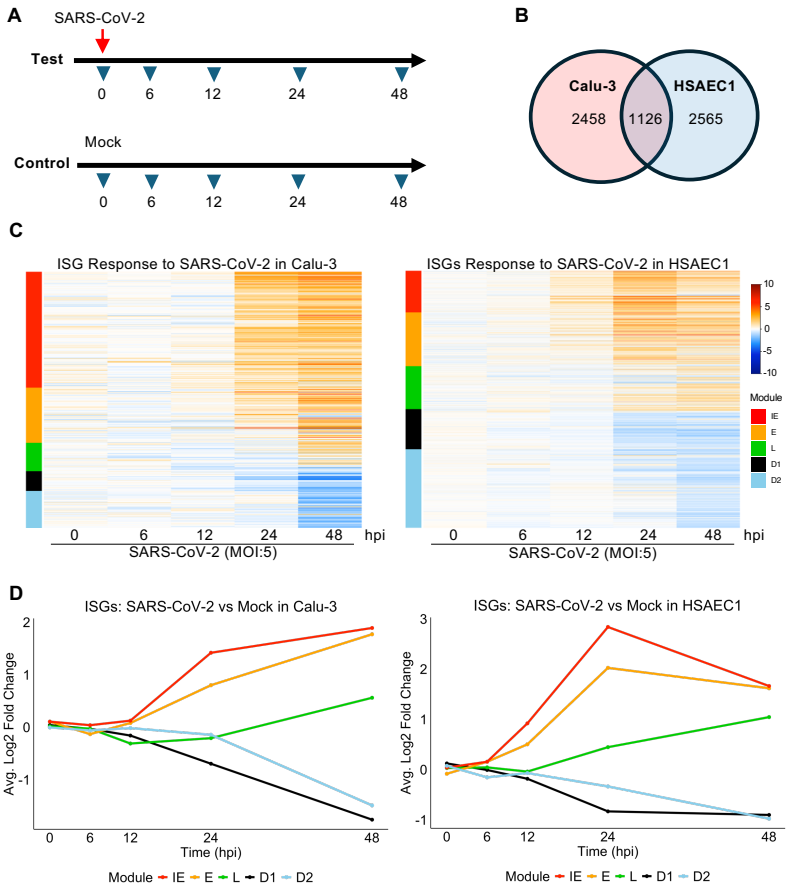
A
SARS-CoV-2
Test
0
6
12
24
48
Mock
Control
0
6
12
24
48
B
Calu-3
HSAEC1
2458
1126
2565
C
ISG Response to SARS-CoV-2 in Calu-3
ISGs Response to SARS-CoV-2 in HSAEC1
10
5
0
-5
-10
Module
IE
E
L
D1
D2
0
6
12
24
48
hpi
SARS-CoV-2 (MOI:5)
D
ISGs: SARS-CoV-2 vs Mock in Calu-3
ISGs: SARS-CoV-2 vs Mock in HSAEC1
Avg. Log2 Fold Change
Time (hpi)
Module IE E L D1 D2

Fig. 2

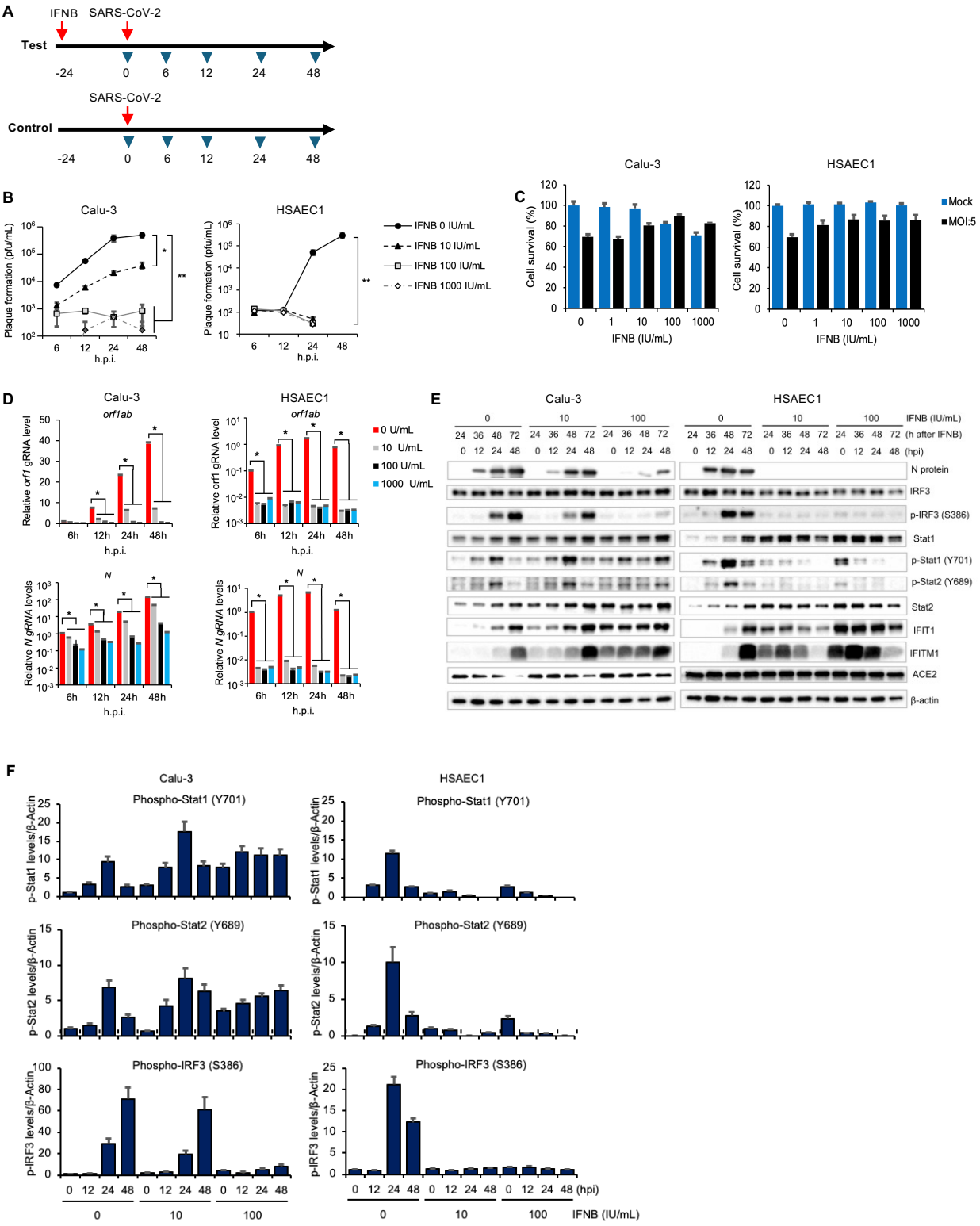
A
IFNB
SARS-CoV-2
Test
-24
0
6
12
24
48
SARS-CoV-2
Control
-24
0
6
12
24
48
B
Calu-3
HSAEC1
Plaque formation (pfu/mL)
h.p.i.
IFNB 0 IU/mL
IFNB 10 IU/mL
IFNB 100 IU/mL
IFNB 1000 IU/mL
C
Calu-3
HSAEC1
Cell survival (%)
IFNB (IU/mL)
Mock
MOI:5
D
Calu-3
HSAEC1
orf1ab
Relative orf1 gRNA level
N
Relative N gRNA levels
h.p.i.
0 U/mL
10 U/mL
100 U/mL
1000 U/mL
E
Calu-3
HSAEC1
IFNB (IU/mL)
(h after IFNB)
(hpi)
N protein
IRF3
p-IRF3 (S386)
Stat1
p-Stat1 (Y701)
p-Stat2 (Y689)
Stat2
IFIT1
IFITM1
ACE2
β-actin
F
Calu-3
HSAEC1
Phospho-Stat1 (Y701)
p-Stat1 levels/β-Actin
Phospho-Stat2 (Y689)
p-Stat2 levels/β-Actin
Phospho-IRF3 (S386)
p-IRF3 levels/β-Actin
(hpi)
IFNB (IU/mL)

Fig. 3

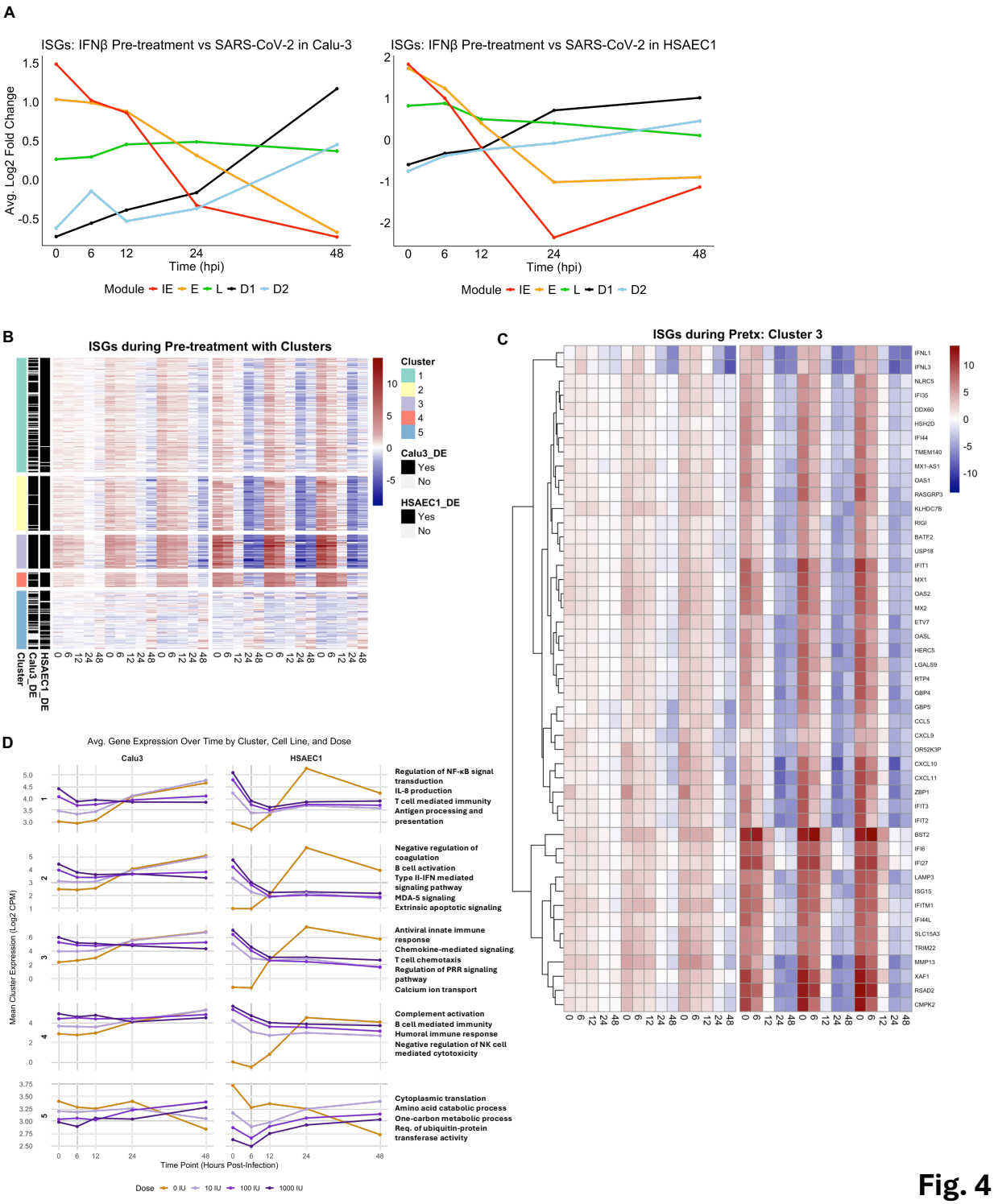
A
ISGs: IFNβ Pre-treatment vs SARS-CoV-2 in Calu-3
ISGs: IFNβ Pre-treatment vs SARS-CoV-2 in HSAEC1
Avg. Log2 Fold Change
Time (hpi)
Module IE E L D1 D2
B
ISGs during Pre-treatment with Clusters
Cluster
Calu3_DE
HSAEC1_DE
C
ISGs during Pretx: Cluster 3
D
Avg. Gene Expression Over Time by Cluster, Cell Line, and Dose
Calu3
HSAEC1
Mean Cluster Expression (Log2 CPM)
Regulation of NF-κB signal transduction
IL-8 production
T cell mediated immunity
Antigen processing and presentation
Negative regulation of coagulation
B cell activation
Type II-IFN mediated signaling pathway
MDA-5 signaling
Extrinsic apoptotic signaling
Antiviral innate immune response
Chemokine-mediated signaling
T cell chemotaxis
Regulation of PRR signaling pathway
Calcium ion transport
Complement activation
B cell mediated immunity
Humoral immune response
Negative regulation of NK cell mediated cytotoxicity
Cytoplasmic translation
Amino acid catabolic process
One-carbon metabolic process
Req. of ubiquitin-protein transferase activity
Time Point (Hours Post-Infection)
Dose 0 IU 10 IU 100 IU 1000 IU

Fig. 4

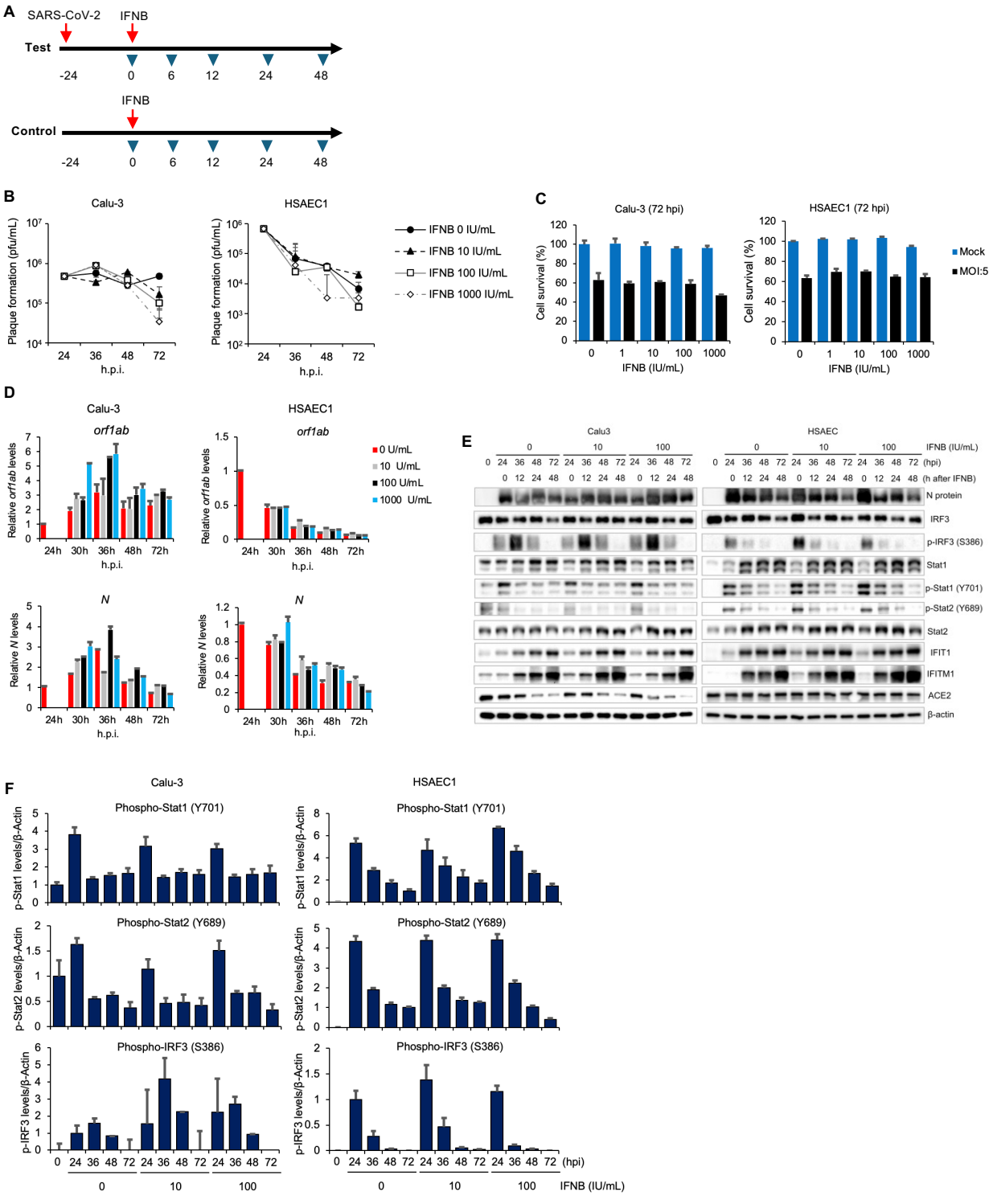
A
SARS-CoV-2
IFNB
Test
-24
0
6
12
24
48
IFNB
Control
-24
0
6
12
24
48
B
Calu-3
HSAEC1
Plaque formation (pfu/mL)
h.p.i.
IFNB 0 IU/mL
IFNB 10 IU/mL
IFNB 100 IU/mL
IFNB 1000 IU/mL
C
Calu-3 (72 hpi)
HSAEC1 (72 hpi)
Cell survival (%)
IFNB (IU/mL)
Mock
MOI:5
D
Calu-3
HSAEC1
orf1ab
Relative orf1ab levels
N
Relative N levels
h.p.i.
0 U/mL
10 U/mL
100 U/mL
1000 U/mL
E
Calu3
HSAEC
IFNB (IU/mL)
(hpi)
(h after IFNB)
N protein
IRF3
p-IRF3 (S386)
Stat1
p-Stat1 (Y701)
p-Stat2 (Y689)
Stat2
IFIT1
IFITM1
ACE2
β-actin
F
Calu-3
HSAEC1
Phospho-Stat1 (Y701)
p-Stat1 levels/β-Actin
Phospho-Stat2 (Y689)
p-Stat2 levels/β-Actin
Phospho-IRF3 (S386)
p-IRF3 levels/β-Actin
(hpi)
IFNB (IU/mL)

Fig. 5

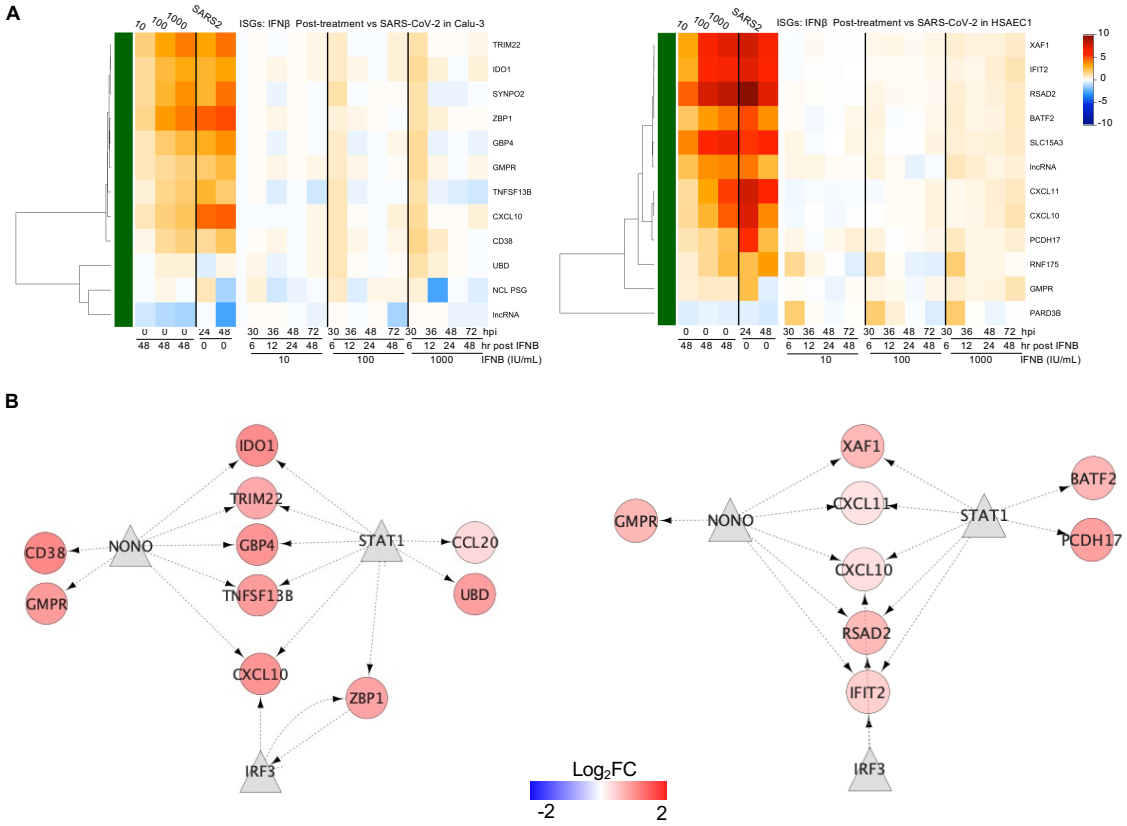
A
ISGs: IFNβ Post-treatment vs SARS-CoV-2 in Calu-3
TRIM22
IDO1
SYNPO2
ZBP1
GBP4
GMPR
TNFSF13B
CXCL10
CD38
UBD
NCL PSG
lncRNA
hpi
hr post IFNB
IFNB (IU/mL)
ISGs: IFNβ Post-treatment vs SARS-CoV-2 in HSAEC1
XAF1
IFIT2
RSAD2
BATF2
SLC15A3
lncRNA
CXCL11
CXCL10
PCDH17
RNF175
GMPR
PARD3B
B
IDO1
TRIM22
CD38
NONO
GBP4
STAT1
CCL20
GMPR
TNFSF13B
UBD
CXCL10
ZBP1
IRF3
XAF1
CXCL11
GMPR
NONO
STAT1
BATF2
PCDH17
CXCL10
RSAD2
IFIT2
IRF3
Log2FC
-2
2

Fig. 6

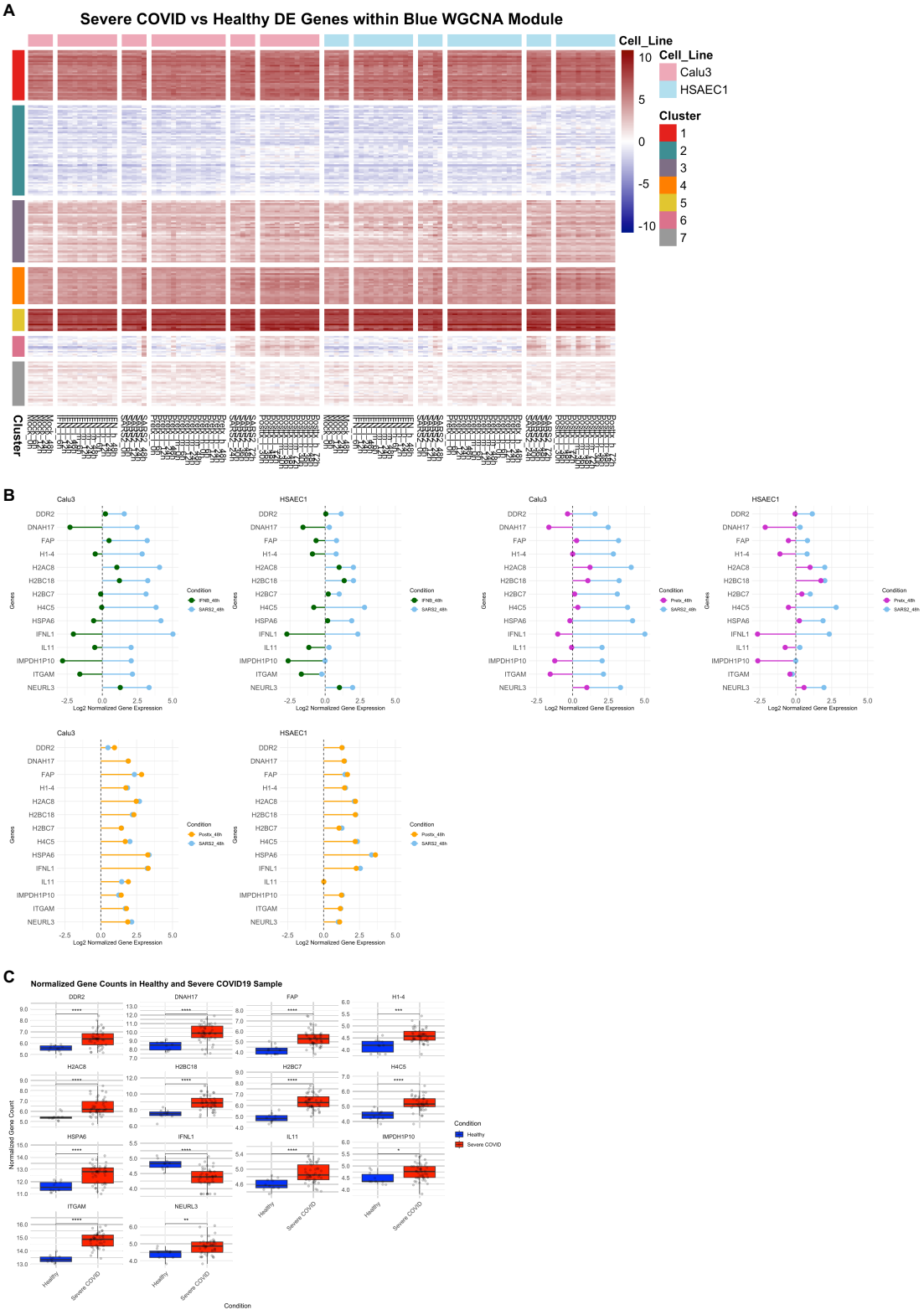
A
Severe COVID vs Healthy DE Genes within Blue WGCNA Module
Cell_Line
Calu3
HSAEC1
Cluster
1
2
3
4
5
6
7
10
5
0
-5
-10
B
Calu3
HSAEC1
DDR2
DNAH17
FAP
H1-4
H2AC8
H2BC18
H2BC7
H4C5
HSPA6
IFNL1
IL11
IMPDH1P10
ITGAM
NEURL3
Genes
Condition
IFNB_48h
SARS2_48h
Prstx_48h
Postx_48h
Log2 Normalized Gene Expression
C
Normalized Gene Counts in Healthy and Severe COVID19 Sample
Normalized Gene Count
Healthy
Severe COVID
Condition

Fig. 7

A

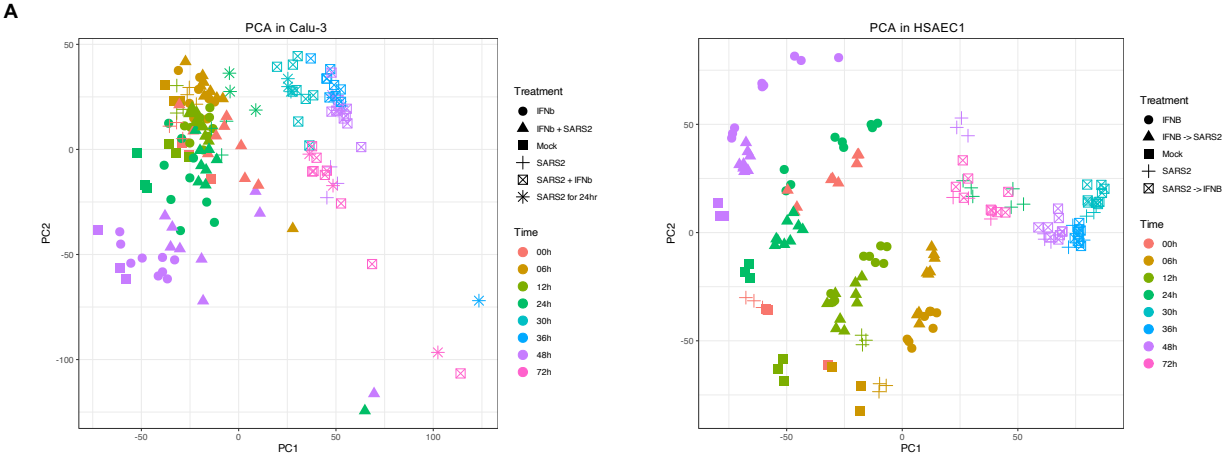
PCA in Calu-3
PC1
PC2
Treatment
IFNb
IFNb + SARS2
Mock
SARS2
SARS2 + IFNb
SARS2 for 24hr
Time
00h
06h
12h
24h
30h
36h
48h
72h
PCA in HSAEC1
PC1
PC2
Treatment
IFNB
IFNB -> SARS2
Mock
SARS2
SARS2 -> IFNB
Time
00h
06h
12h
24h
30h
36h
48h
72h

Fig. S1

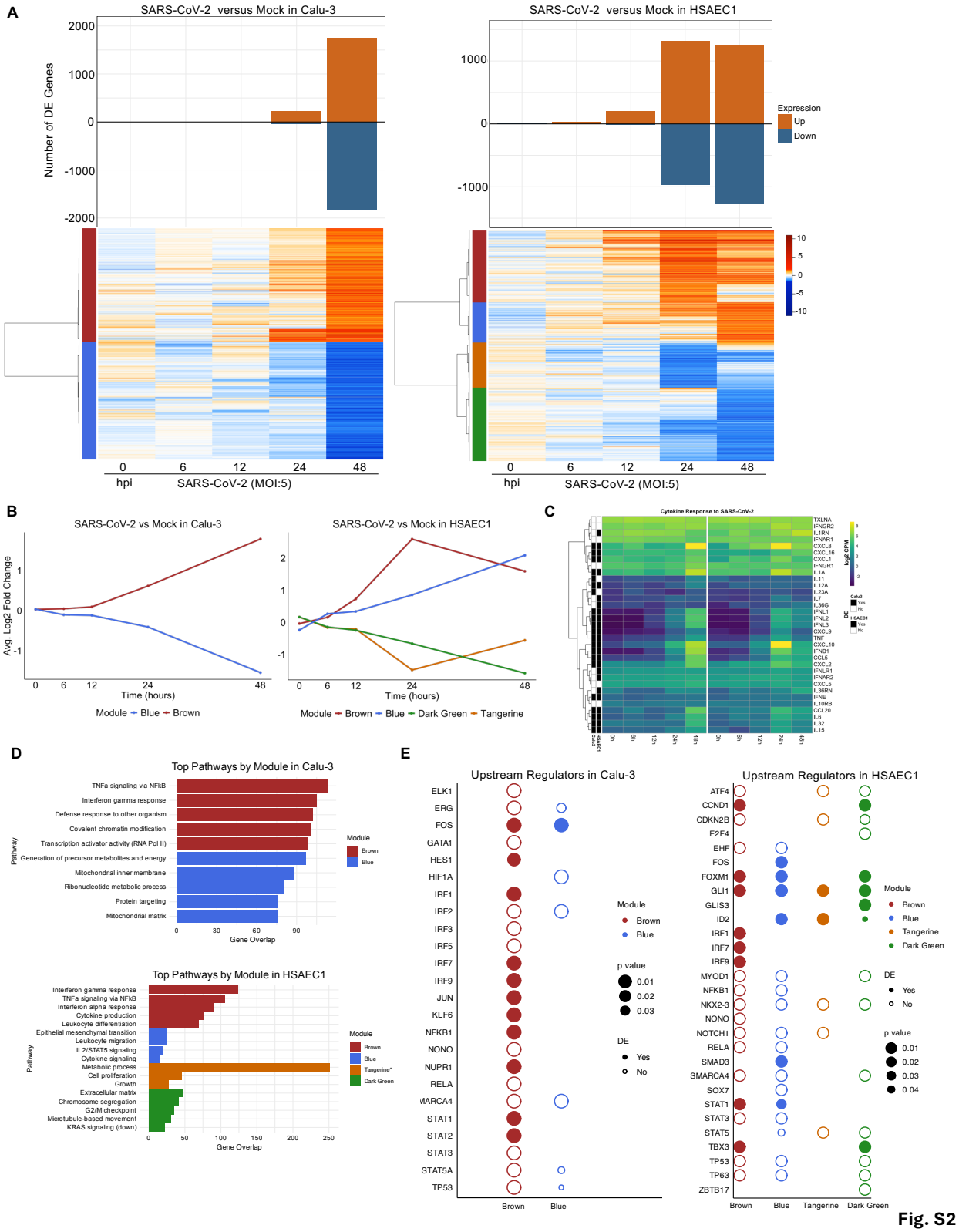
A
SARS-CoV-2 versus Mock in Calu-3
SARS-CoV-2 versus Mock in HSAEC1
Number of DE Genes
Expression
Up
Down
hpi
SARS-CoV-2 (MOI:5)
B
SARS-CoV-2 vs Mock in Calu-3
SARS-CoV-2 vs Mock in HSAEC1
Avg. Log2 Fold Change
Time (hours)
Module Blue Brown
Module Brown Blue Dark Green Tangerine
C
Cytokine Response to SARS-CoV-2
log2 CPM
DE
D
Top Pathways by Module in Calu-3
TNFa signaling via NFkB
Interferon gamma response
Defense response to other organism
Covalent chromatin modification
Transcription activator activity (RNA Pol II)
Generation of precursor metabolites and energy
Mitochondrial inner membrane
Ribonucleotide metabolic process
Protein targeting
Mitochondrial matrix
Pathway
Gene Overlap
Module
Brown
Blue
Top Pathways by Module in HSAEC1
Interferon gamma response
TNFa signaling via NFkB
Interferon alpha response
Cytokine production
Leukocyte differentiation
Epithelial mesenchymal transition
Leukocyte migration
IL2/STAT5 signaling
Cytokine signaling
Metabolic process
Cell proliferation
Growth
Extracellular matrix
Chromosome segregation
G2/M checkpoint
Microtubule-based movement
KRAS signaling (down)
Tangerine*
Dark Green
E
Upstream Regulators in Calu-3
ELK1
ERG
FOS
GATA1
HES1
HIF1A
IRF1
IRF2
IRF3
IRF5
IRF7
IRF9
JUN
KLF6
NFKB1
NONO
NUPR1
RELA
STAT1
STAT2
STAT3
STAT5A
TP53
Brown
Blue
Module
p.value
0.01
0.02
0.03
DE
Yes
No
Upstream Regulators in HSAEC1
ATF4
CCND1
CDKN2B
E2F4
EHF
FOS
FOXM1
GLI1
GLIS3
ID2
IRF1
IRF7
IRF9
MYOD1
NFKB1
NKX2-3
NONO
NOTCH1
RELA
SMAD3
SMARCA4
SOX7
STAT1
STAT3
STAT5
TBX3
TP53
TP63
ZBTB17
Tangerine
Dark Green
0.04

Fig. S2

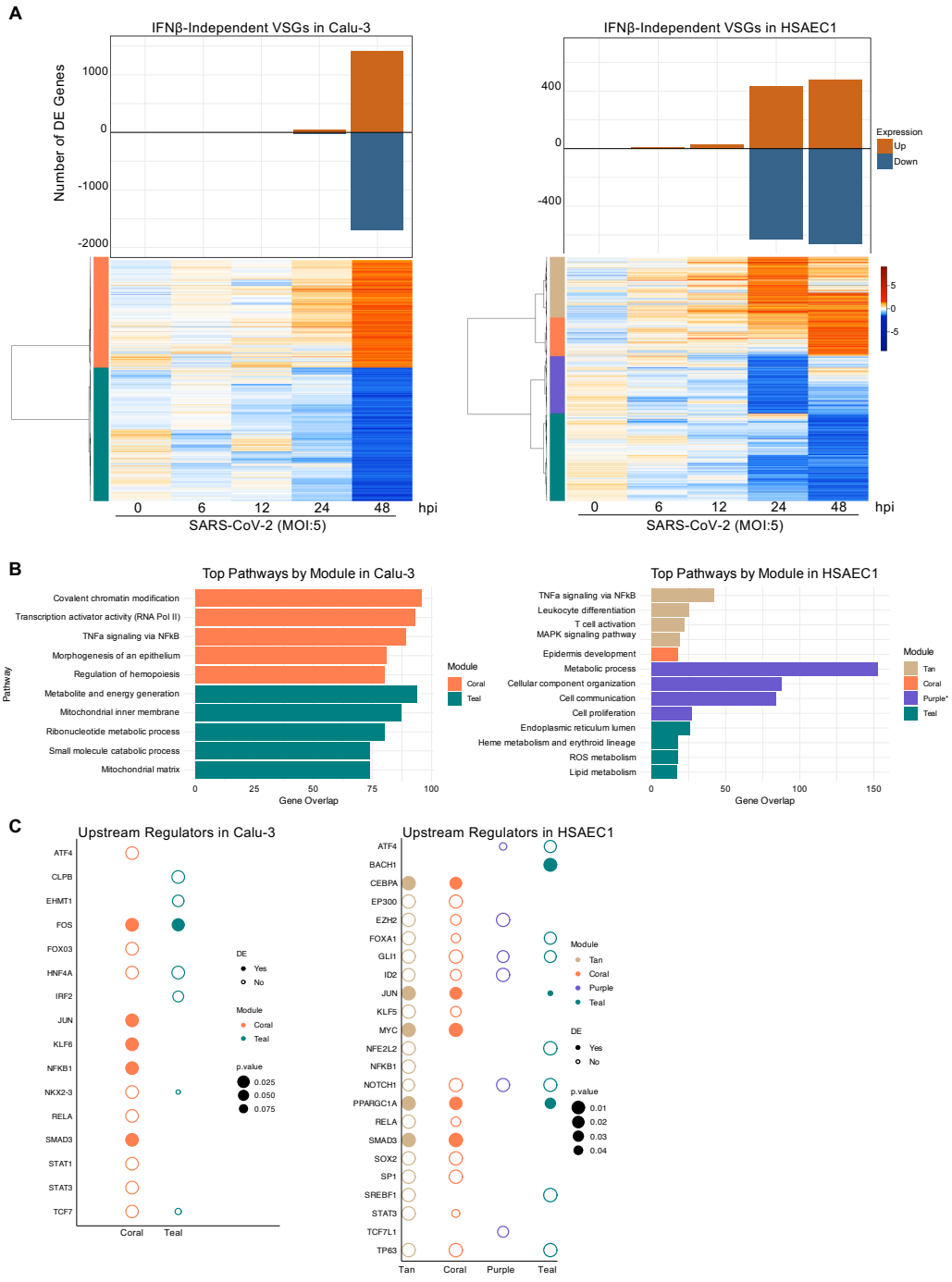
A
IFNβ-Independent VSGs in Calu-3
IFNβ-Independent VSGs in HSAEC1
Number of DE Genes
1000
0
-1000
-2000
400
0
-400
Expression
Up
Down
5
0
-5
0
6
12
24
48
hpi
SARS-CoV-2 (MOI:5)
B
Top Pathways by Module in Calu-3
Top Pathways by Module in HSAEC1
Pathway
Covalent chromatin modification
Transcription activator activity (RNA Pol II)
TNFa signaling via NFkB
Morphogenesis of an epithelium
Regulation of hemopoiesis
Metabolite and energy generation
Mitochondrial inner membrane
Ribonucleotide metabolic process
Small molecule catabolic process
Mitochondrial matrix
Module
Coral
Teal
0
25
50
75
100
Gene Overlap
TNFa signaling via NFkB
Leukocyte differentiation
T cell activation
MAPK signaling pathway
Epidermis development
Metabolic process
Cellular component organization
Cell communication
Cell proliferation
Endoplasmic reticulum lumen
Heme metabolism and erythroid lineage
ROS metabolism
Lipid metabolism
Tan
Coral
Purple*
Teal
0
50
100
150
Gene Overlap
C
Upstream Regulators in Calu-3
Upstream Regulators in HSAEC1
ATF4
CLPB
EHMT1
FOS
FOX03
HNF4A
IRF2
JUN
KLF6
NFKB1
NKX2-3
RELA
SMAD3
STAT1
STAT3
TCF7
Coral
Teal
DE
Yes
No
Module
Coral
Teal
p.value
0.025
0.050
0.075
ATF4
BACH1
CEBPA
EP300
EZH2
FOXA1
GLI1
ID2
JUN
KLF5
MYC
NFE2L2
NFKB1
NOTCH1
PPARGC1A
RELA
SMAD3
SOX2
SP1
SREBF1
STAT3
TCF7L1
TP63
Tan
Coral
Purple
Teal
Module
Tan
Coral
Purple
Teal
DE
Yes
No
p.value
0.01
0.02
0.03
0.04

Fig. S3

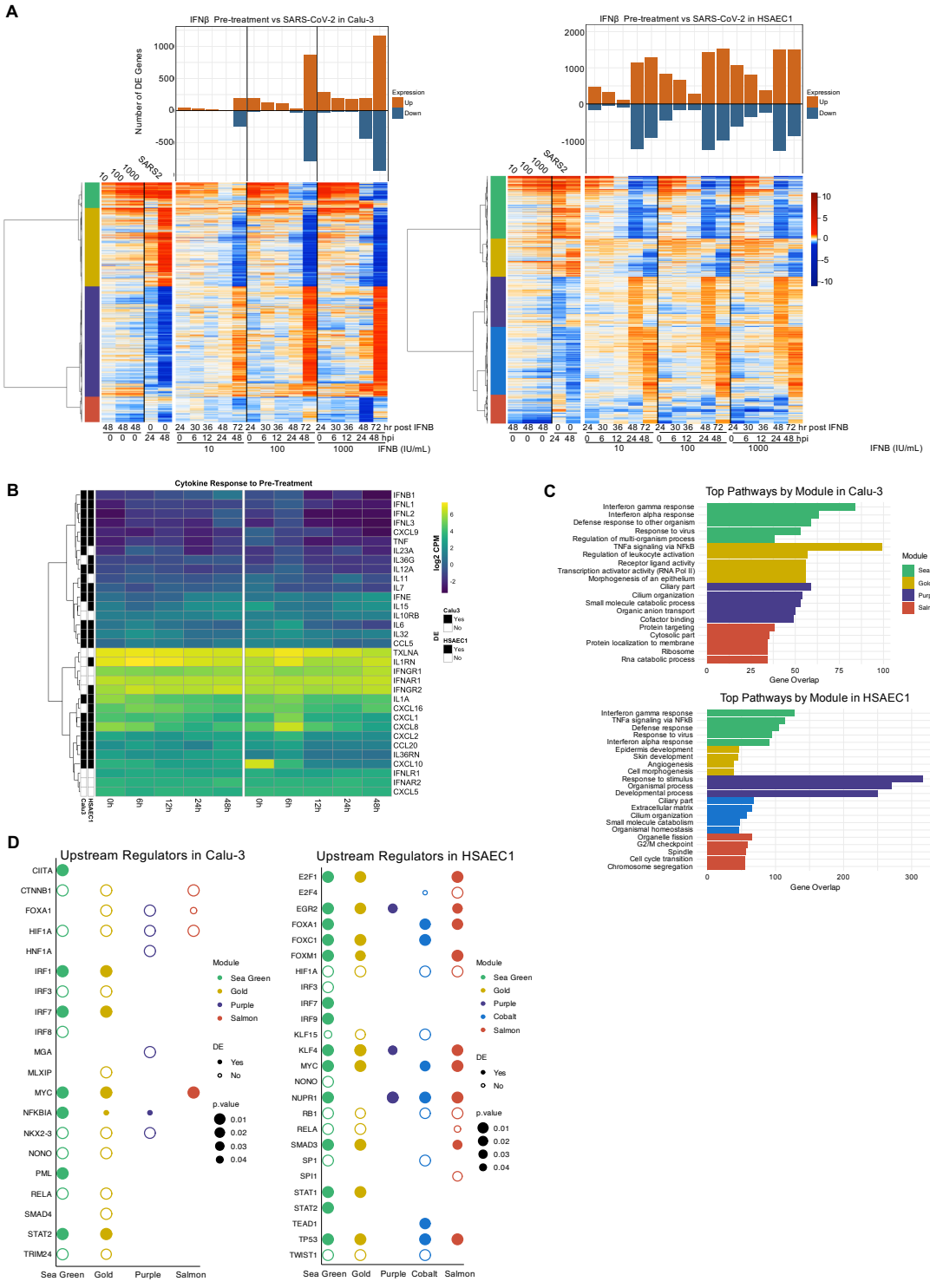
A
IFNβ Pre-treatment vs SARS-CoV-2 in Calu-3
IFNβ Pre-treatment vs SARS-CoV-2 in HSAEC1
Number of DE Genes
Expression
Up
Down
SARS2
hr post IFNB
hpi
IFNB (IU/mL)
B
Cytokine Response to Pre-Treatment
log2 CPM
DE
Calu3
HSAEC1
Yes
No
C
Top Pathways by Module in Calu-3
Top Pathways by Module in HSAEC1
Module
Sea Green
Gold
Purple
Purple*
Salmon
Cobalt
Gene Overlap
D
Upstream Regulators in Calu-3
Upstream Regulators in HSAEC1
p.value
0.01
0.02
0.03
0.04

Fig. S4

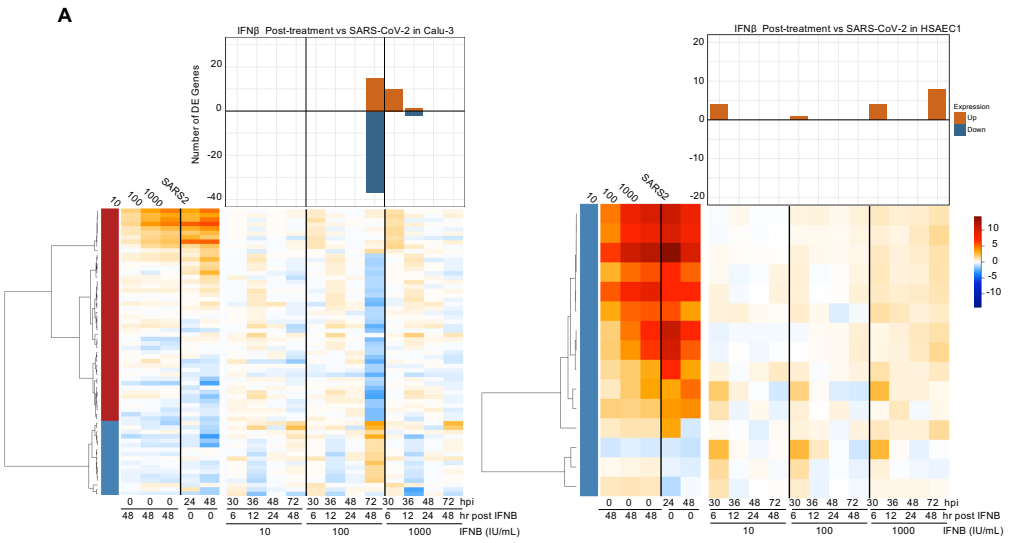
A
IFNβ Post-treatment vs SARS-CoV-2 in Calu-3
IFNβ Post-treatment vs SARS-CoV-2 in HSAEC1
Number of DE Genes
Expression
Up
Down
SARS2
10
100
1000
hpi
hr post IFNB
IFNB (IU/mL)

Fig. S5

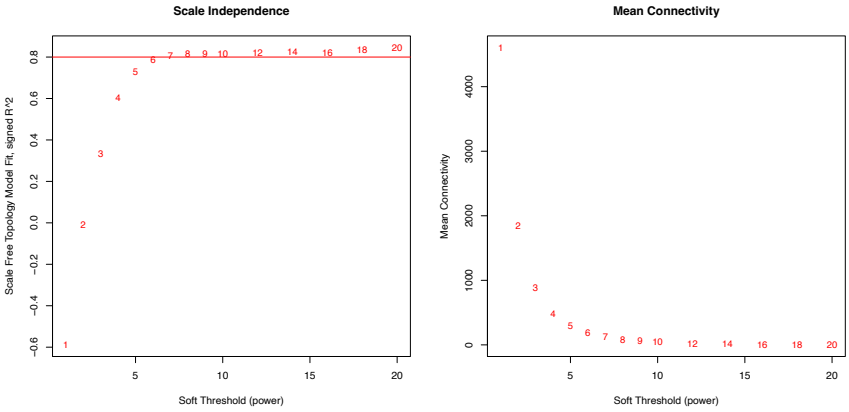
Scale Independence
Scale Free Topology Model Fit, signed R^2
Soft Threshold (power)
Mean Connectivity
Mean Connectivity
Soft Threshold (power)

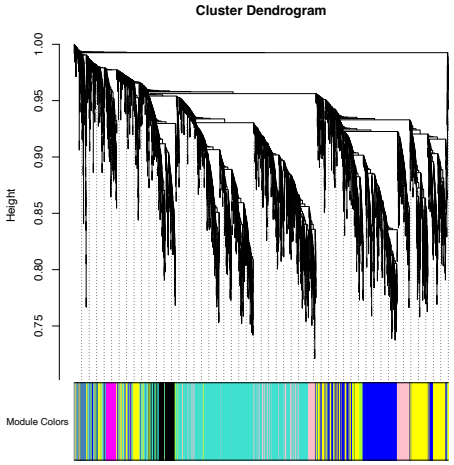
Cluster Dendrogram
Height
Module Colors

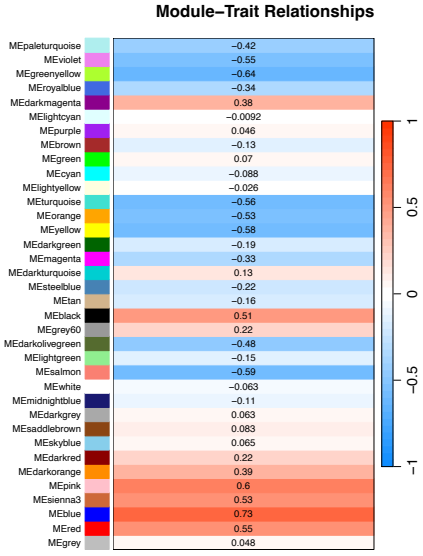
Module–Trait Relationships
MEpaleturquoise −0.42
MEviolet −0.55
MEgreenyellow −0.64
MEroyalblue −0.34
MEdarkmagenta 0.38
MElightcyan −0.0092
MEpurple 0.046
MEbrown −0.13
MEgreen 0.07
MEcyan −0.088
MElightyellow −0.026
MEturquoise −0.56
MEorange −0.53
MEyellow −0.58
MEdarkgreen −0.19
MEmagenta −0.33
MEdarkturquoise 0.13
MEsteelblue −0.22
MEtan −0.16
MEblack 0.51
MEgrey60 0.22
MEdarkolivegreen −0.48
MElightgreen −0.15
MEsalmon −0.59
MEwhite −0.063
MEmidnightblue −0.11
MEdarkgrey 0.063
MEsaddlebrown 0.083
MEskyblue 0.065
MEdarkred 0.22
MEdarkorange 0.39
MEpink 0.6
MEsienna3 0.53
MEblue 0.73
MEred 0.55
MEgrey 0.048

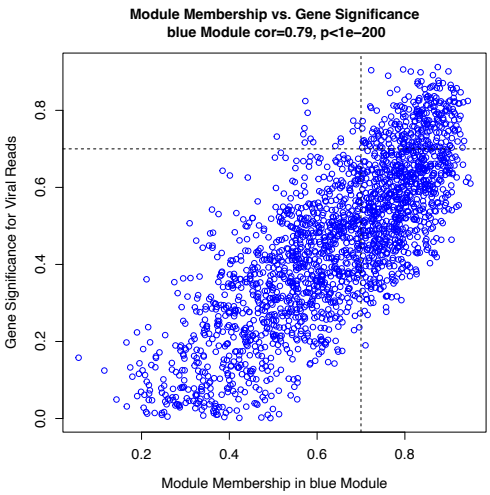
Module Membership vs. Gene Significance
blue Module cor=0.79, p<1e−200
Gene Significance for Viral Reads
Module Membership in blue Module

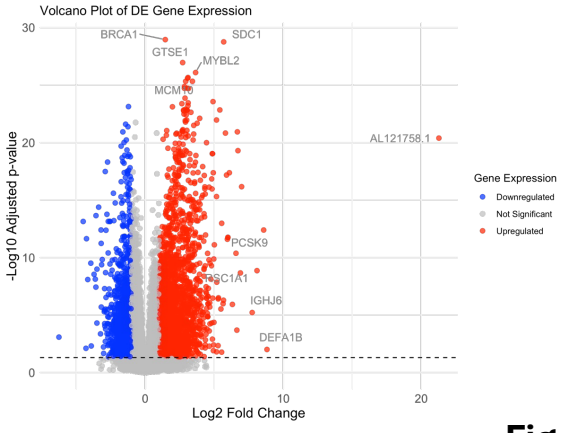
Volcano Plot of DE Gene Expression
BRCA1
GTSE1
SDC1
MYBL2
MCM10
AL121758.1
PCSK9
TSC1A1
IGHJ6
DEFA1B
-Log10 Adjusted p-value
Log2 Fold Change
Gene Expression
Downregulated
Not Significant
Upregulated

Fig. S6

1.6 FIGURE LEGENDS

1.6.1 *Figure 1. The effect of IFN-β on lung epithelial cells.*

Human lung adenocarcinoma Calu-3 (ACE2+) and immortalized small airway epithelial HSAEC1-KT/ACE2 cells were treated with the indicated concentration of IFN-β (0, 10, 100, and 1,000 IU/mL) for 6, 12, 24, and 48 h. (A) Western blot analysis of ISG protein expression (IFIT1, IFITM1) and phosphorylation of STAT1 and STAT2 following IFN-β treatment. (B) Schematic summary of IFN-β treatment. Samples treated with IFN-β (10, 100, and 1,000 IU/mL) were compared to their respective mock-treated controls, matched by time point (6, 12, 24, 48 h). (C) Overlap of differentially expressed genes (DEGs) between Calu-3 (652 DEGs) and HSAEC1-KT/ACE2 (2,766 DEGs) cells following IFN-β treatment. (D) Hierarchical clustering of DEGs (p.adj ≤ 0.01, LFC ≥1) in Calu-3 and HSAEC1-KT/ACE2. Five interferon-stimulated gene (ISG) clusters were identified based on expression kinetics: Immediate Early (IE), Early (E), Late (L), Downregulated 1 (D1), and Downregulated 2 (D2). The accompanying bar plot reflects the number of upregulated and downregulated DEGs at each time point. (E) Line plot of average log2 fold change (LFC) for each ISG subset at 6, 12, 24, and 48 h post IFN-β (100 IU/mL) treatment relative to mock controls in both cell lines. (F) Pathway enrichment analysis using Over Representation Analysis (ORA) with Gene Ontology (GO), KEGG, and Hallmark databases for clusters identified in panel D. Modules marked with an asterisk (*) did not meet the statistical significance threshold (FDR ≤ 0.05) for pathway enrichment, but associated Gene Ontology (GO) terms are shown for biological context. (G) Heatmap of log2 counts per million (CPM) for cytokine expression during IFN-β (100 IU/mL) treatment at 6, 12, 24 and 48 h in both cell lines. A mock treatment time point (0 IU/mL) was included as a reference. DE annotations are shown next to the heatmap. (H) Upstream Regulator analysis of the ISG subsets identified in

panel D, performed using Ingenuity Pathway Analysis (IPA). Transcription factor (TFs) were filtered for significance, and significantly predicted TFs were assessed across ISG subsets. Dot color represents the ISG subset where the TF was significant, dot size corresponds to the p-value within that subset, and TFs DE by IFN-β are filled in.

1.6.2 *Figure 2. Effect of SARS-CoV-2 on ISG expression in lung epithelial cells.*

(A) Schematic summary of SARS-CoV-2 infection (MOI:5). Samples infected with SARS-CoV-2 were compared to their respective mock-treated samples matched by time point (0, 6, 12, 24, and 48 hpi). (B) Overlap of VSGs between Calu-3 (3,584 VSGs) and HSAEC1-KT/ACE2 (3,691 VSGs) cells. (C) Heatmap of the average LFC expression of ISGs identified in Figure 1D, showing their behavior in Calu-3 and HSAEC1-KT/ACE2 cells infected with SARS-CoV-2. Genes are ordered to match the ISG subsets (Immediate Early, Early, Late, Downregulated 1, and Downregulated 2) defined in Figure 1D. (D) Line plot of the average LFC for each ISG subset at 0, 6, 12, 24, and 48 hpi compared to time-matched mock samples in both cell lines.

1.6.3 *Figure 3. IFN-β pre-treatment readily suppresses SARS-CoV-2 virus activity.*

(A) Schematic summary of IFN-β pre-treatment. Calu-3 and HSAEC1-KT/ACE2 cells were pre-treated with increasing concentrations of IFN-β (0, 10, 100, and 1,000 IU/mL) for 24 h prior to infection with SARS-CoV-2 (MOI:5), followed by incubation for 6, 12, 24, or 48 h. (B) Plaque assay results quantifying SARS-CoV-2 viral activity in supernatants collected at the indicated time points. Viral titers are expressed as plaque-forming units per milliliter (PFU/mL). Statistically significant differences are indicated by *$p \leq 0.05$ and **$p \leq 0.001$. (C) Cell survival analysis following 24 h pre-treatment with IFN-β (0, 1, 10, 100, and 1,000 IU/mL) and subsequent SARS-CoV-2 infection. Cell viability was measured using CellTiter-Glo reagent. (D) Quantification of SARS-CoV-2 RNA levels (*N* and *orf1ab* genes) by qRT-PCR at the indicated

time points post-infection. (E) Representative Western blot analysis of SARS-CoV-2 N protein, ISGs (IFIT1 and IFITM1), and phosphorylation IRF3, STAT1, and STAT2 in Calu-3 and HSAEC1-KT/ACE2 cells, following IFN-β pre-treatment and SARS-CoV-2 infection. β-actin served as a loading control. (F) Quantitative analysis of phospho-Stat1 (Y701), phospho-Stat2 (Y689), and phospho-IRF3 (S386) normalized to β-actin, showing the impact of IFN-β pre-treatment on downstream signaling in both cell lines.

1.6.4 *Figure 4. IFN-β pre-treatment on ISG expression during SARS-CoV-2 infection.*

(A) Line plots showing the average LFC expression for ISGs identified in Figure 1D in Calu-3 and HSAEC1-KT/ACE2 cells pre-treated with IFN-β (10, 100, and 1,000 IU/mL) for 24 h before SARS-CoV-2 infection. (B) Heatmap of log CPM values for conserved ISGs across both cell lines during IFN-β pre-treatment. Annotations indicate whether each gene was significantly DE during IFN-β pre-treatment vs. infection at any time point. (C) Heatmap of log CPM values for Cluster 3 genes from panel B. (D) Average gene expression after SARS-CoV-2 (MOI:5) infection, stratified by IFN-β pre-treatment dose (0, 10, 100, and 1,000 IU/mL) for Calu-3 and HSAEC1-KT/ACE2 cells. Top pathways identified by enrichment analysis for each cluster are indicated.

1.6.5 Figure 5. *IFN-β post-treatment partly suppresses SARS-CoV-2 virus activity.*

(A) Schematic summary of IFN-β post-treatment. Calu-3 and HSAEC1-KT/ACE2 cells were infected with SARS-CoV-2 (MOI:5) for 1 h, incubated for 24 h, and then treated with increasing concentrations of IFN-β (10, 100, 1,000 IU/mL) for 6, 12, 24, or 48 h. (B) Plaque assay results quantifying SARS-CoV-2 viral activity in supernatants collected at 30, 36, 48, and 72 hpi. Viral titers are expressed as PFU/mL. Statistically significant differences are indicated by *$p<0.05$ and **$p<0.001$. (C) Cell survival analysis following SARS-CoV-2 infection and IFN-β post-

treatment (0, 1, 10, 100, and 1,000 IU/mL). Cell viability was measured using CellTiter-Glo reagent. (D) Quantification of SARS-CoV-2 RNA levels (*N* and *orf1ab* genes) by qRT-PCR at the indicated time points post-treatment. (E) Representative Western blot analysis of SARS-CoV-2 N protein, ISGs (IFIT1 and IFITM1), and phosphorylation levels of IRF3, STAT1, and STAT2 in Calu-3 and HSAEC1-KT/ACE2 cells. β-actin served as a loading control. (F) Quantitative analysis of phospho-STAT1 (Y701), phospho-STAT2 (Y689), and phospho-IRF3 (S386), normalized to β-actin, showing the impact of IFN-β post-treatment on downstream signaling in both cell lines.

1.6.6 *Figure 6. IFN-β inducible ISGs during an established SARS-CoV-2 infection.*

(A) Heatmap of average LFC expression for significant ISGs ($p \leq 0.01$, $LFC \geq 1$) in Calu-3 and HSAEC1-KT/ACE2 cells infected with SARS-CoV-2 (MOI:5) for 24 h, followed by IFN-β treatment (10, 100, 1,000 IU/mL). The first five columns provide a reference ISG expression profile during IFN-β treatment at 48 h or SARS-CoV-2 infection at 24 and 48 hpi. *Note: Gene names containing 'lncRNA' indicate long non-coding RNAs and NCL PSG refers to nucleolin pseudogene.* (B) Network of direct interactions among significant ISGs and their predicted TFs, including *STAT1*, *IRF3*, and *NONO.* Node color represents the LFC at 100 IU/mL IFN-β post-treatment, 6 hr post treatment.

1.6.7 *Figure 7. Identification of a viral load-associated gene module.*

(A) Heatmap of log CPM values for genes in the blue WGCNA module that were significantly DE in severe COVID-19 patients. (B) Lollipop plots of log CPM values comparing the expression of Cluster 6 genes across IFN-β treatment, SARS-CoV-2 infection, IFN-β pre-treatment, and IFN-β post-treatment in lung epithelial cells. (C) Box plots of normalized gene counts for Cluster 6 genes, comparing healthy controls and severe COVID-19 patients.

Statistically significant differences are indicated by *p<0.05, **p<0.001, ***p<0.001, ****p<0.0001.

1.7 SUPPLEMENTAL FIGURE LEGENDS

1.7.1 *Figure S1. PCA reveals sample clustering by time and treatment.*

(A) PCA of the per-time point mean LFC values using all expressed genes across all treatment conditions in Calu-3 and HSAEC1-KT/ACE2 cells. Each point represents a sample, with time indicated by color and treatment represented by symbol.

1.7.2 *Figure S2. Overlap of ISGs across transcriptional clusters.*

Bar chart showing the number of DE genes in each ISG cluster (IE, E, L, D1, D2) for Calu3 (transparent bars) and HSAEC1-KT/ACE2 (solid bars). Bars are grouped by cluster, with a dotted line indicating the number of shared genes in each cluster. The exact number of shared genes is labeled above each dotted line.

1.7.3 *Figure S3. Global transcriptomic response to SARS-CoV-2 in lung epithelial cells.*

(A) Heatmap of the average LFC expression of virus-stimulated genes (VSGs) in Calu-3 and HSAEC1-KT/ACE2 cells following SARS-CoV-2 infection (MOI:5). A total of 3,584 and 3,691 VSGs were identified in at least one time point ($p \leq 0.01$, $LFC \geq 1$) in Calu-3 and HSAEC1-KT/ACE2 cells, respectively. Hierarchical clustering was performed using Pearson and Ward.D2 linkage. The vertical bar chart reflects the number of upregulated and downregulated VSGs significantly DE at each time point. (B) Line plots of the average LFC for each VSG cluster at 0, 6, 12, 24 and 48 hpi in Calu-3 and HSAEC1-KT/ACE2 cells. (C) Heatmap of log CPM values for cytokines expressed during SARS-COV-2 infection at 0, 6, 12, 24 and 48 hpi in Calu-3 and HSAEC1-KT/ACE2 cells. Differential expression annotations are shown next to the heatmap. (D) Pathway enrichment analysis using ORA with GO, KEGG, and Hallmark databases for

clusters identified in panel A. Modules marked with an asterisk (*) did not meet the statistical significance threshold (FDR ≤ 0.05) for pathway enrichment, but associated GO terms are shown for biological context. (E) Upstream Regulator analysis of the VSG clusters identified in panel A, performed using IPA. TFs were filtered for significance, and significantly predicted TFs were assessed across ISG subsets. Dot color represents the VSG cluster where the TF was significant, dot size corresponds to the p-value, and TFs DE by SARS-CoV-2 are filled in.

1.7.4 *Figure S4. IFN-independent VSG responses in lung epithelial cells*

VSGs that were not significantly induced by IFN-β treatment were classified as IFN-independent VSGs. (A) Heatmap of the average LFC expression of IFN-independent VSGs in Calu-3 and HSAEC1-KT/ACE2 cells infected with SARS-CoV-2. Hierarchical clustering was performed using Pearson distance and Ward.D2 linkage. The vertical bar chart reflects the number of upregulated and downregulated IFN-independent VSGs that were significantly DE at each time point ($p \leq 0.01$, LFC ≥1). (B) Pathway enrichment analysis using ORA with GO, KEGG, and Hallmark databases for clusters identified in panel A. Modules marked with an asterisk (*) did not meet the statistical significance threshold (FDR ≤ 0.05) for pathway enrichment, but associated GO terms are shown for biological context. (C) Upstream Regulator analysis of the IFN-independent VSG clusters from panel A, performed using IPA. TFs were filtered for significance, and significantly predicted TFs were assessed across all clusters. Dot color represents the cluster where the TF was significant, dot size corresponds to the p-value, and TFs DE by SARS-CoV-2 are filled in.

1.7.5 *Figure S5. Global transcriptomic response to IFN-β pre-treatment*

(A) Heatmap of average LFC expression for significant DEGs (*p.adj* ≤ 0.01, LFC ≥ 1) identified at any time point in Calu-3 and HSAEC1-KT/ACE2 cells treated with IFN-β (10, 100, and 1,000

IU/mL). The first five columns provide a reference expression profile during IFN-β treatment at 48 h or SARS-CoV-2 infection at 24 and 48 hpi. The vertical bar chart reflects the number of upregulated and downregulated DEGs at each time point. (B) Heatmap of log CPM values for cytokines expressed during IFN-β pre-treatment (100 IU/mL) at 0, 6, 12, 24 and 48 hpi in Calu-3 and HSAEC1-KT/ACE2 cells. DE annotations are shown next to the heatmap. (C) Pathway enrichment analysis using ORA with GO, KEGG, and Hallmark databases for clusters identified in panel A. Modules marked with an asterisk (*) did not meet the statistical significance threshold (FDR ≤ 0.05) for pathway enrichment, but associated GO terms are shown for biological context. (D) Upstream Regulator analysis of the clusters from panel A, performed using IPA. TFs were filtered for significance, and significantly predicted TFs were assessed across all clusters. Dot color represents the cluster where the TF was significant, dot size corresponds to the p-value, and TFs DE by IFN-β pre-treatment are filled in.

1.7.6 Figure S6. *Global transcriptomic response to IFN-β post-treatment*

(A) Heatmap of the average LFC expression of significant DEGs identified in at least one time point ($p \leq 0.01$, LFC ≥ 1) in Calu-3 and HSAEC1-KT/ACE2 cells infected with SARS-CoV-2 (MOI:5) and subsequently treated with IFN-β (10, 100, and 1,000 IU/mL). The first five columns provide a reference expression profile during IFN-β treatment at 48 h or SARS-CoV-2 infection at 24 and 48 hpi. The vertical bar chart reflects the number of upregulated and downregulated DEGs at each time point.

1.7.7 Figure *S7. Co-expression modules highly correlated with SARS-CoV-2 viral load*

For this analysis, data from both cell lines were combined and normalized for a joint WGCNA. (A) Analysis of the scale-free topology index and mean connectivity for various soft-thresholding powers to identify the optimal power for network construction. (B) Gene

dendrogram generated using average linkage hierarchical clustering, with module assignments indicated by the underlying color map. (C) Heatmap showing the correlation between the module eigengenes (MEs) and the experimental trait, SARS-CoV-2 viral reads. The MEblue module (r^2 = 0.73, $p < 0.0001$) exhibited the strongest correlation with viral reads. (D) Scatterplot of gene significance (GS) for viral reads vs. module membership (MM) in the blue module. (E) Volcano plot of DE genes (*p.adj* < 0.05, LFC > 1) in severe COVID-19 patients compared to healthy controls. Whole blood RNA-seq data were obtained from the public dataset GSE171110. The top five genes with the most significant p-values and the top five genes with the greatest absolute LFC are labeled in the plot.

Chapter 2. TEMPORAL TRANSCRIPTOMIC PROFILING REVEALS AGE-ASSOCIATED IMPAIRMENTS IN ANTIVIRAL IMUNITY AND RECOVERY FOLLOWING SARS-COV-2 INFECTION

Chapter 2. SUMMARY

Age is the greatest risk factor for poor COVID-19 disease outcomes. While SARS-CoV-2 is transitioning into an endemic respiratory pathogen, older adults remain at risk for severe disease, hospitalization, and death. However, the molecular mechanisms underlying age-related susceptibility remain incompletely understood. We performed a temporally resolved transcriptomic analysis of SARS-CoV-2 infection across young, mature, and old mice to examine age-associated immune responses. Mice were infected with mouse-adapted SARS-CoV-2 (MA10) and lung tissues were collected across early and late stages of infection. Differential gene expression analysis, pathway enrichment, and immune cell deconvolution were performed. Aged mice exhibited prolonged viral persistence compared to younger mice. Transcriptomic profiling revealed age-dependent divergence in host responses, with older mice displaying

impaired induction of antiviral pathways during early infection. At 2 days post-infection, aged mice showed reduced activation of interferon-associated transcription factors and cytokine signaling pathways. By 7 days post-infection, aged mice failed to mount robust T cell activation signatures, suggesting impaired transition from innate to adaptive immunity. In addition to infection-induced defects, baseline differences among mock-infected samples highlighted chronic, low-grade inflammation in older mice, characterized by upregulation of immunoglobin-related genes, leukocyte migration pathways, and cytokine signaling signatures. Immune cell deconvolution further revealed increased baseline proportions of plasma cells and memory B cells in aged mice. Together, these findings reveal that age-associated impairments in both early innate and later adaptive immune responses, compounded by pre-existing inflammatory alterations, contribute to delayed viral clearance and poor COVID-19 outcomes in older hosts.

2.1 INTRODUCTION

2.1.1 *Age as a risk factor for COVID-19 severity*

The COVID-19 pandemic, caused by SARS-CoV-2, has disproportionately affected older adults, who account for the majority of COVID-19-related deaths. As of April 20, 2025, over 7 million deaths worldwide and 1.2 million deaths in the United States have been attributed to COVID-19[1]. Provisional death data from the Centers for Disease Control and Prevention's (CDC) National Center for Health Statistics (NCHS) covering January 1, 2020 through February 28, 2025, estimate that 76% of COVID-19 deaths occurred among individuals aged 65 and older, despite this group comprising only 17% of the U.S. population[2,3]. While COVID-19 appears to have transitioned into an endemic, seasonal respiratory infection, older adults and other vulnerable populations remain at heightened risk for severe disease, hospitalization, and death.

This disparity is particularly concerning given the rapid expansion of the global older adult population. According to the World Health Organization, the number of people aged 60 years and older is expected to double by 2050, reaching roughly 2.1 billion[4]. This demographic shift comes with additional challenges for public health systems, particularly in addressing age-related susceptibility to infectious diseases. Respiratory viruses including SARS-CoV-2, influenza, and respiratory syncytial virus (RSV), consistently cause more severe disease in older adults, who experience higher rates of hospitalization and death[5-8]. Despite this clear risk, the biological mechanisms by which aging drives severe disease outcomes is unclear.

2.1.2 *Immunosenescence*

Although increased age is one of the strongest predictors for severe COVID-19, it often coexists with chronic comorbidities that exacerbate risk. Conditions such as metastatic cancer, cardiovascular disease, liver disease, renal disease, and dementia both increase in prevalence with age and are associated with poor COVID-19 outcomes[9]. However, aging itself drives fundamental changes in immune function, collectively termed immunosenescence. These age-related immune alterations include impaired clearance of senescent cells, weakened anatomical barriers, increased circulation of pattern- and damage-associated molecular patterns (PAMPs and DAMPs), reduced lymphocyte function and chemotaxis, reduced naïve B and T cell pools, limited clonal expansion, and dysregulated antibody production[10-19]. These changes are often accompanied by a state of chronic low-grade inflammation known as inflammaging, characterized by elevated cytokine levels[20]. Together, immunosenescence and inflammaging compromise antiviral responses, but their effects are difficult to disentangle from comorbidities in human studies.

2.1.3 *Mice as model organisms*

To address this challenge, animal models offer a valuable platform to study the direct effects of aging on immune responses. While early SARS-CoV-2 strains such as the WA1 isolate could not naturally infect standard laboratory mice, later variants and mouse-adapted strains enabled the development of murine models of infection[21-24]. These models have successfully recapitulated key clinical manifestations of human COVID-19, including viral replication, lung pathology, and elevated cytokine production. Importantly, studies using aged mice have revealed age-dependent increases in viral persistence, lung damage, and mortality, coupled with blunted innate immune activation.[23,25] Our previous work demonstrated that aged mice infected with mouse-adapted SARS-CoV-2 exhibited greater susceptibility to infection, delayed weight recovery, sustained viral replication with systemic spread, and persistent inflammation compared to younger mice. Collectively, these results highlight failure to resolve infection and inflammation with age[23]. Although dysfunctional immune responses in aged individuals with COVID-19 have been widely documented, the molecular mechanisms underlying impaired antiviral immunity in aged animals remain incompletely characterized. Recent transcriptomic and proteomic studies in the lungs of infected mice have revealed elevated baseline inflammatory and tissue repair signatures in older mice, along with dampened antiviral responses and activation of complement and coagulation pathways following infection[26]. However, these studies were limited to a single early time point, constraining insights into the dynamic evolution of immune responses over the course of infection.

2.1.4 *Uncovering age-associated factors of severe COVID-19*

Here, we present a temporally resolved transcriptomic analysis of mouse-adapted SARS-CoV-2 infection across young, mature, and old mice, spanning early to late stages of infection. By capturing dynamic transcriptional responses across multiple time points, our study provides

insights into how aging shapes the kinetics of immune activation, viral control, and inflammatory resolution. We identify age-associated impairments in gene expression programs spanning both innate and adaptive arms of the immune response, offering a deeper understanding of the molecular mechanisms underlying age-dependent differences in antiviral control and disease progression.

2.2 RESULTS

2.2.1 *Distinct transcriptomic profiles by age*

To assess the transcriptomic landscape of SARS-CoV-2 infection in C57BL/6 mice, animals were challenged with 10^4 PFU of the mouse-adapted SARS-CoV-2-MA10 strain, as previously described[23]. Lung tissue was collected from infected and mock-infected controls for bulk RNA-sequencing at days 2, 4, and 7 post-infection (Fig. 1A). Principal component analysis (PCA) of all lung transcriptomes revealed that age contributed to variation in the dataset, with samples from 2-year-old mice forming a distinct cluster compared to 10-week-old and 20-week-old mice (Fig. 1B). We also observed a temporal separation of samples by days post-infection (dpi), mirroring trends in viral load measured by qPCR, which peaked at 2 dpi. Viral read counts confirmed peak viral load at 2 dpi, with additional age-related differences observed at 7 dpi. Both 2-year-old and 20-week-old mice retained significantly higher viral read counts compared to 10-week-old mice at this time point, suggesting ongoing viral persistence in older animals (Fig. 1C).

2.2.2 *Differential gene expression during infection*

To identify infection-responsive genes across age groups, we next performed differential gene expression analysis, comparing samples collected from 2, 4, and 7 dpi to their respective age-matched mock controls (Fig. 2A). At 2 dpi, the number of differentially expressed genes (DEGs)

increased with age, primarily driven by an expansion in downregulated genes in 2-year-old mice (Fig. 2B). Across all age groups, the number of DEGs declined over time, consistent with the resolution of infection and declining viral replication by 7 dpi. Despite variability in the total number of unique DEGs between age groups, more than 2,000 genes were significantly DE across all age groups, indicating a conserved SARS-CoV-2-responsive signature independent of age.

Across all age groups, we identified 4,957 significant DEGs at one or more time points. These genes were clustered based on expression profiles, resulting in six distinct co-expression modules. To characterize the biological functions associated with each module, we performed over representation analysis (ORA). Clusters 1 and 2 were enriched for genes involved in early innate immune responses, including cytokine-mediated signaling, type I IFN signaling, phagocytosis, and MHC protein binding. These clusters exhibited peak activation at 2 dpi, although a slight reduction in activation was observed in 2-year-old mice. In contrast, Clusters 5 and 6 captured late-stage responses peaking at 7 dpi, enriched for pathways related to DNA replication and repair, T cell receptor signaling, and regulation of leukocyte activation. Notably, expression within these late-response clusters was dampened in 2-year-old mice, suggesting impaired activation of crucial adaptive immune programs during recovery.

2.2.3 *Pathway enrichment during infection*

To further examine age-associated differences at the pathway-level, we extracted the DEGs from the top uniquely enriched pathways within each cluster and averaged expression by age group (Fig. 1E). With the exception of Cluster 3, the average expression of these pathway-associated DEGs was reduced in 2-year-old mice across the infection time course. Cluster 3, enriched for pathway related to proteasome function, angiogenesis, and oxidoreductase activity, and

glycolysis/gluconeogenesis, exhibited heightened activation in aged animals at 2dpi (Fig. 1D, Fig. 1E). This pattern suggests an age-related amplification of metabolic and stress response pathways that correlate with peak viral load and are more efficiently resolved in younger animals. In contrast, Cluster 6 pathway genes were notably downregulated during infection in 2-year-old mice, while younger mice exhibited peak upregulation at 7 dpi. These findings highlight impaired activation of late-stage immune pathways in older animals, potentially contributing to diminished viral clearance and delayed recovery.

2.2.4 *Baseline expression of enriched pathways by age*

Given the established association between aging and baseline inflammation, we next examined the expression of pathway-associated DEGs in mock-infected animals across age groups[20]. Cluster 2, encompassing early immune response pathways, was significantly upregulated at baseline in 2-year-old mice compared to both 10-week-old and 20-week-old mice. This cluster included genes involved in inflammation (SAA1, SAA3, LCN2, IL10), antiviral defense (OAS3, ZBP1, GBP11), and chemokine mediated leukocyte recruitment (CXCL9, CCL20, CXCL13), suggesting that aged lungs harbor a primed yet potentially dysregulated immune environment even prior to infection. This pre-activation of immune and stress-related pathways in aged mice may contribute to their impaired ability to mount effective responses upon SARS-CoV-2 infection.

2.2.5 *Impaired innate and adaptive immune coordination in aged mice*

Cluster 1, enriched for IFN and cytokine-mediated signaling pathways, exhibited peak expression at 2 dpi across all groups. To further characterize these responses, we curated a list of interferons and cytokines and assessed their expression dynamics across the infection time course. Type I and III IFNs, including IFNB, IRFA4, IFNA5, and IFNL2, exhibited prolonged

upregulation in 2-year-old mice, suggesting sustained antiviral signaling. However, key chemokines involved in immune cell recruitment, such as CXCL9, CXCL10, and CXCL5, were reduced at early time points in aged animals, potentially impairing effective immune cell mobilization. Similarly, proinflammatory cytokines TNF, IL-6, and IL-1β showed blunted early induction in older mice, indicating a dampened inflammatory response during the critical early window of infection.

2.2.6 *Cytokine and IFN network is attenuated in aged mice*

To further explore the cytokine signaling dynamics, we constructed a DEG network based on curated interactions from Ingenuity Pathway Analysis (IPA), centered on top predicted upstream regulators (IFN-β, IFN-γ, TNF-α, and IL-1β). Nodes were organized by cellular localization and colored according to $\log_2$ fold change (LFC) at 2 dpi for each age group. Notably, while IFN-β expression was elevated in 2-year-old mice, TFs critical for propagating antiviral responses– including IRF7, IRF9, and RELB, were markedly reduced. In parallel, immunomodulatory genes such as IL1R2, ZFP36, NFKBIZ, and TRIM30a were downregulated, suggesting impaired regulation of cytokine feedback loops. Components of the NLRP3 inflammasome, including CASP1, NLRP3, IL-1β, and IL-18, were also suppressed in older mice, potentially contributing to impaired IL-1 family cytokine production and reduced chemokine induction (CXCL10, CXCL11). Reduced IRF1 expression in aged mice may further explain diminished induction of IRF-stimulated chemokines and weakened early amplification of antiviral responses. Collectively, these findings reveal that despite elevated IFNβ expression, older mice demonstrate broader attenuation of IFN and cytokine activation at 2 dpi, characterized by reduced TF activation, impaired inflammasome signaling, and limited effector cell recruitment. Blunted early antiviral responses likely contribute to higher viral loads and delayed viral clearance in aged

animals, setting the stage for subsequent over compensatory immune activation observed at later time points.

2.2.7 *T-cell activation network is impaired with age*

Given these defects in early innate immunity, we next examined the adaptive immune responses during the resolution phase of infection. Cluster 6 encompassed genes involved in T cell receptor signaling and leukocyte activation, which were upregulated at 7 dpi in younger mice but remained blunted in 2-year-old mice. Several key genes regulating cytotoxicity (GZMB and NKG7) and leukocyte migration (CXCR3, CX3CR1, CXCR6, CCR2, and CCR4) exhibited progressive downregulation with increasing age (Fig. 3C). TFs essential for T cell differentiation and activation, including TCF7, IRF4, NFAT5, STAT3, TBX21, and GATA3, were also reduced in aged animals, suggesting a compromised transcriptional network required for effective T cell-mediated protection.

2.2.8 *Immune cell-type deconvolution*

To evaluate whether changes in immune cell composition contributed to these functional impairments, we performed CIBERSORT deconvolution analysis of lung transcriptomes. At 2 dpi, 2-year-old mice had reduced proportions of activated dendritic cells (DCs) and natural killer (NK) cells compared to younger counterparts (Fig. 3D, Fig.S1), likely contributing to early innate immune deficits. By 7 dpi, aged mice showed an increased proportion of activated $CD8^+$ T cells but concurrent decreases in $CD4^+$ follicular helper T (T_{FH}) cells, naïve $CD8^+$ T cells, and regulatory T cells (Tregs), suggesting impaired coordination of adaptive immunity (Fig. 3D, Fig. S1). Furthermore, 2-year-old mice showed elevated baseline levels of plasma cells, $CD8^+$ memory T cells, and $CD4^+$ memory T cells compared to younger mice, reflecting a skewed

homeostatic immune state characterized by ongoing antigen exposure and accumulation of long-lived immune cells (Fig. 3D, Fig. S1).

2.2.9 *Aged mice exhibit heightened immune activation at baseline*

During our analysis of the immune response to SARS-CoV-2 infection, we observed that several gene clusters were significantly upregulated at baseline in 2-year-old mice (Fig. 2G). This prompted broader investigation of transcriptional differences age groups at homeostatic conditions. We conducted DE analysis comparing mock-infected samples across age. We identified only 33 DEGs when comparing 20-week-old to 10-week-old mice(Fig. 4A). In contrast, 375 DEGs were observed when comparing 2-year-old to 20-week-old mice, and 510 DEGs were identified between 2-year-old and 10-week-old cohorts, with the majority of DEGs upregulated in older mice. Notably, the number of uniquely upregulated DEGs at baseline increased progressively with age (Fig. 4B).

2.2.10 *Pathway enrichment of baseline immune activation*

Co-expression analysis of all DEGs identified in at least one comparison (n=596) revealed three distinct clusters (Fig. 4C). Pathway analysis of the downregulated cluster identified circadian rhythm and rhythmic process with genes including PER1/2/3, RETN, and CIART. Cluster 2, although not enriched for canonical pathways, contained over 90 immunoglobulin-related genes, consistent with heightened plasma cell activity observed through CIBERSORT deconvolution analysis (Fig. 3D). Cluster 3 was enriched for pathways associated with leukocyte activation and migration, T cell activation, phagocytosis, immune modulation, and cation homeostasis (Fig. 4D). The predominance of immune-related DEGs at baseline in aged mice was unexpected, as we anticipated a broader range of age-associated transcriptional changes. However, over 80% of baseline DEGs by age overlapped with genes DE during SARS-CoV-2 infection (Fig. 4C). These

findings suggest that immune system alterations are a central feature of aging in the lung, potentially compromising the ability to mount effective responses to infections like SARS-CoV-2.

2.3 DISCUSSION

2.3.1 *Principle findings*

Age is the strongest risk factor for severe COVID-19 outcomes, yet the underlying mechanisms remain incompletely understood[40]. In this study, we utilized a C57BL/6 mouse model spanning various life stages to investigate age-related transcriptional differences throughout the course of SARS-CoV-2 infection. Our analyses revealed that transcriptional reprogramming correlates with age-associated changes in viral load dynamics, peaking at 2 dpi, with significantly higher viral loads observed in 2-year-old mice and 20-week-old mice compared to younger counterparts. Through transcriptomic profiling, we identified widespread age-associated dysregulation in immune responses. Older mice exhibited attenuated expression of proinflammatory cytokines and IFN signaling pathways at 2 dpi, coinciding with reduced activation of DCs and NK cells–key mediators of early innate immunity and viral clearance. By 7 dpi, aged mice showed impaired activation of T cell and leukocyte migration pathways, suggesting delayed or dysfunctional adaptive immune responses. Notably, several of these pathways were already upregulated at baseline in older animals, alongside increased expression of genes involved in phagocytosis, immunomodulation, and cellular cation homeostasis.

2.3.2 *Clinical implications*

Baseline DE analysis demonstrated that immune dysregulation is a predominant driver of transcriptional differences in the aged ling, with over 80% of baseline DEGs also participating in the infection response. Among baseline differences, we identified a strong enrichment for

immunoglobulin-related genes in aged mouse lungs, accompanied by elevated plasma cell frequencies. This finding mirrors previous reports showing >20-fold upregulation of immunoglobulin heavy chain genes (Igmh, Igha, Ighg) in aged lungs and establishing immunoglobin production as a signature of inflammaging[41]. Co-expression module analyses have similarly identified immunoglobulin-dominated networks, including kappa, lambda, heavy, and J chains, underscoring a fundamental remodeling of humoral immunity with age, even in the absence of infection[42]. This skewing toward constitutive antibody production likely reflects chronic immune activation and reduced immune flexibility, impairing the rapid generation of effective responses to novel pathogens such as SARS-CoV-2 and contributing to delayed viral clearance and worse disease outcomes.

We also identified disruption of circadian rhythm and rhythmic process pathways in aged lungs, consistent with emerging evidence that aging impairs cellular circadian clocks and reduces resilience to stressors[43]. This signature has recently been proposed as a new hallmark of aging. Collectively, these findings reveal that aged mice harbor a pre-activated yet dysfunctional immune landscape, priming them for impaired antiviral defense during SARS-CoV-2 infection.

In addition to baseline immune alterations, our findings align with previous studies identifying age-associated defects in the activation of key immune populations during aging. Reduced production of proinflammatory cytokines with age has previously been reported. For example, transcriptional profiling of blood mononuclear cells (PBMCs) from older adults had delayed and diminished induction of antiviral cytokines and chemokines, including TNF-α, IL-6, IL-1β, IFNγ, CCl2, and CCL7, upon stimulation with RIG-I agonists, a major pattern recognition receptor involved in SARS-CoV-2 sensing[44]. These results mirror our observation of attenuated early cytokine induction at infection onset in aged mice. Similarly, a study investigating

breakthrough SARS-CoV-2 infections in aged mice reported dysregulated IFN and adaptive antibody responses, leading to increased viral replication and more severe disease manifestations[45]. These patterns are consistent with studies on influenza infection in aged mice, where delayed induction of early cytokines, impaired IFN-stimulated gene expression, and prolonged inflammatory responses have been identified as key contributors to disease severity. Together, these observations reinforce that age-associated immune remodeling impairs both the timing and quality of antiviral responses.

Age-related alterations in T-cell function and subsets are well described. Aging is characterized by a loss of naïve $CD4^+$ and $CD8^+$ T cells and expansion of memory T cell compartments[46]. Our results validate these trends and extend them by demonstrating reduced cytotoxic potential of aged T cells, as evidenced by reduced GZMB and NKG7 expression. This decline in cytolytic function is consistent with *in vitro* analyses of naïve $CD8^+$ T cell responses in older adults, which revealed impaired priming and significantly reduced granzyme B expression following activation[47]. While we observed an increase in activated $CD8^+$ T cells in aged mice during infection, these findings suggest that aged T cells may be functionally compromised, limiting their ability to effectively clear virus-infected cells. Moreover, impaired induction of chemokine receptors critical for leukocyte trafficking, including CXCR3 and CCR2, suggests that aging not only compromises T cell effector function but also limits the efficient recruitment of immune cells to sites of infection.

T cell responses are also critical for generating robust vaccine-induced immunity and have been found to be compromised during the aging process. Zhou et al., reported reduced cytolytic T-cell responses to both seasonal and pandemic strains of influenza in vaccinated older adults[48]. Granzyme B activity, which we found to be attenuated during infection in aged mice, has been

identified as a predictor for influenza vaccine efficacy in older adults[49]. Moreover, responses to mRNA SARS-CoV-2 vaccination resemble the response to natural infection characterized by robust induction of antigen-specific T_{FH} and T_H1 cells[50]. However, older adults produced fewer spike-specific circulating T_H1 cells compared to younger adults following COVID-19 mRNA booster vaccination[51]. Our findings suggest that the age-related impairments identified here, both at baseline and during infection, not only reduce the ability to control viral replication but may also undermine vaccine efficacy in older individuals.

2.3.3 *Strengths and limitations*

While our study provides valuable insights into age-associated transcriptional dynamics across SARS-CoV-2 infection timepoints, several limitations should be acknowledged. First, although mouse models are widely used for aging studies due to their controlled environments and relatively short life spans, they do not recapitulate all age-associated diseases and physiological changes observed in humans[52]. Additionally, differences in immune cell composition, immune function, and viral pathogenesis between mice and humans may limit direct extrapolation of our findings to human aging. Second, our use of bulk RNA-sequencing captures average transcriptional changes across heterogenous cell populations, and future single-cell approaches could more precisely resolve the cell-type dynamics underlying age-associated antiviral responses. Despite these limitations, our findings reveal conserved patterns of immune impairment with aging and offer mechanistic insights into drivers of increased disease severity in older hosts.

2.3.4 *Conclusions*

Together, these data highlight the intersection of age-associated dysfunction across innate, humoral, and cellular arms of the immune system that collectively impair antiviral defense.

Given the ongoing circulation of SARS-CoV-2 and its disproportionate impact on older adults, our study underscores the urgent need to target age-related immune dysfunctions. By identifying specific immune pathways dysregulated with aging–including attenuated cytokine signaling, impaired T cell responses, and baseline humoral skewing–our findings offer a framework for developing interventions aimed at enhancing antiviral immunity and improving COVID-19 outcomes in older populations.

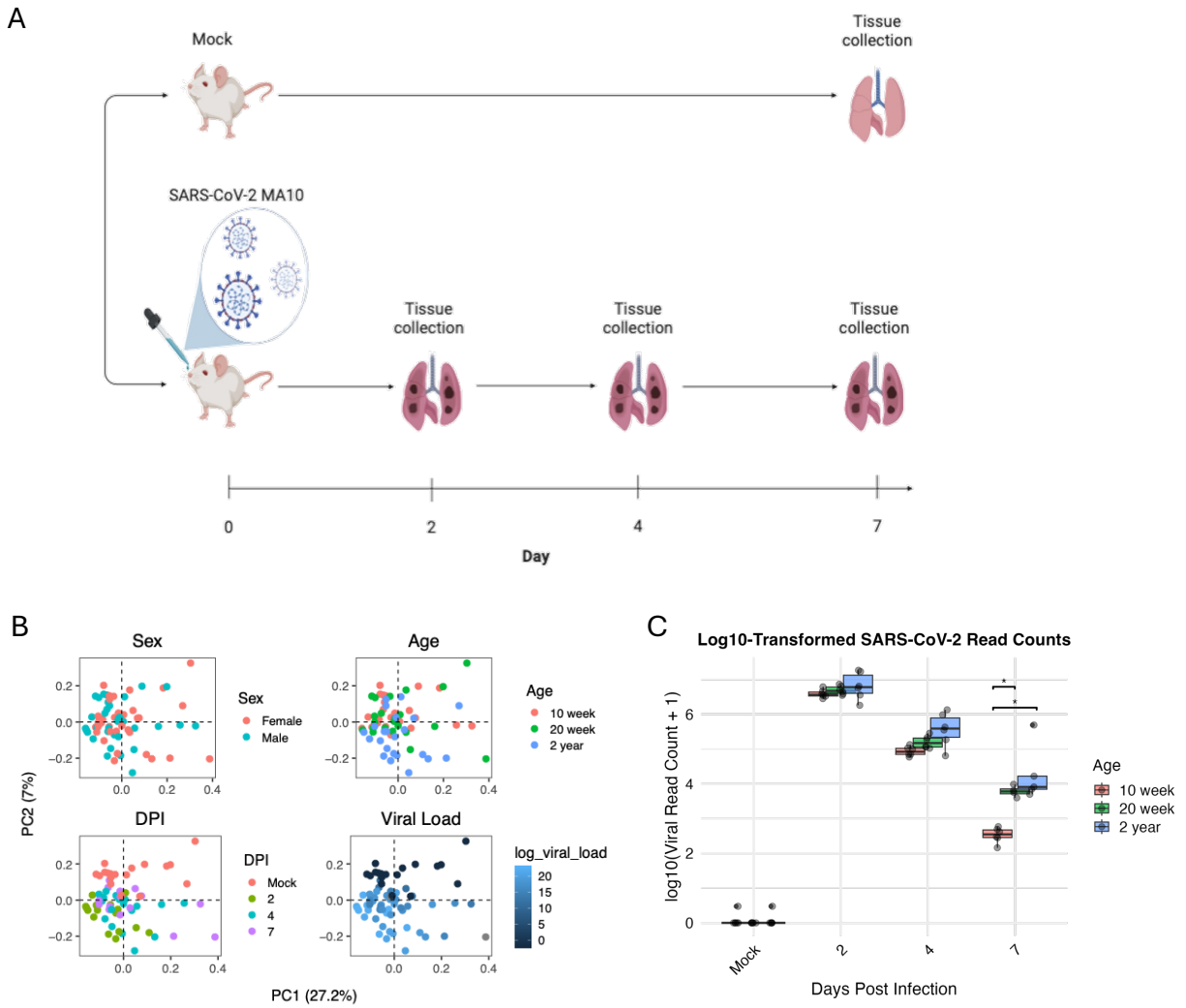
A
Mock
Tissue collection
SARS-CoV-2 MA10
Tissue collection
Tissue collection
Tissue collection
0
2
4
7
Day
B
Sex
Age
DPI
Viral Load
Sex
Female
Male
Age
10 week
20 week
2 year
DPI
Mock
2
4
7
log_viral_load
20
15
10
5
0
PC2 (7%)
PC1 (27.2%)
C
Log10-Transformed SARS-CoV-2 Read Counts
log10(Viral Read Count + 1)
Mock
2
4
7
Days Post Infection
Age
10 week
20 week
2 year

Fig. 1

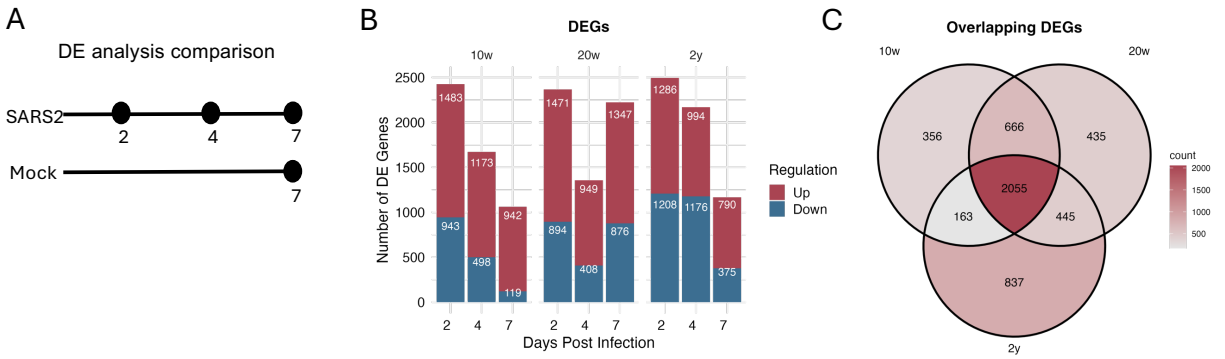
A
DE analysis comparison
SARS2
Mock
2
4
7
7
B
DEGs
10w
20w
2y
Number of DE Genes
Days Post Infection
Regulation
Up
Down
1483
943
1173
498
942
119
1471
894
949
408
1347
876
1286
1208
994
1176
790
375
C
Overlapping DEGs
10w
20w
2y
356
666
435
2055
163
445
837
count

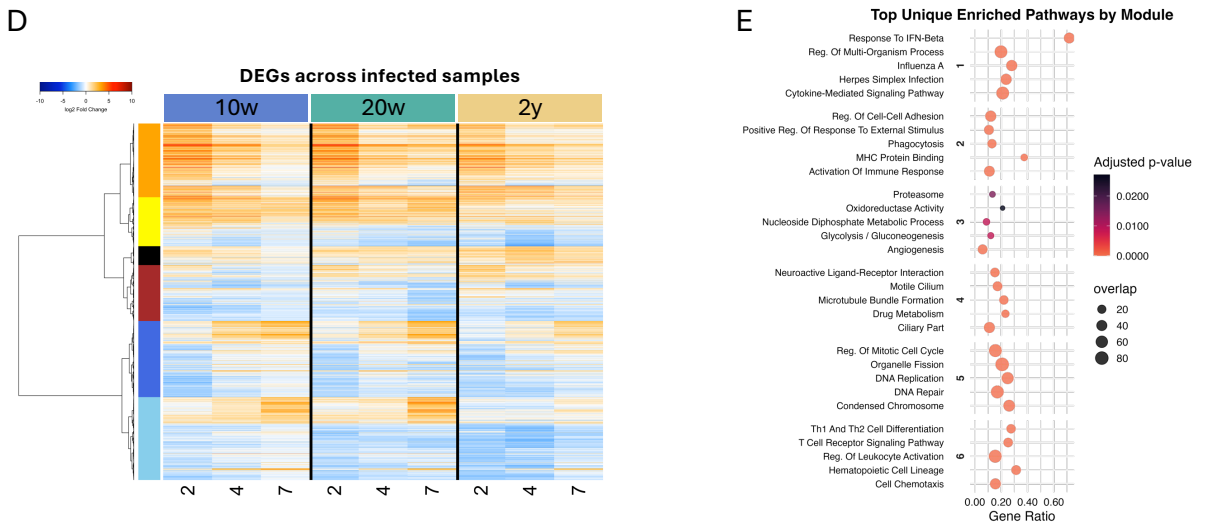
D
DEGs across infected samples
10w
20w
2y
E
Top Unique Enriched Pathways by Module
Response To IFN-Beta
Reg. Of Multi-Organism Process
Influenza A
Herpes Simplex Infection
Cytokine-Mediated Signaling Pathway
Reg. Of Cell-Cell Adhesion
Positive Reg. Of Response To External Stimulus
Phagocytosis
MHC Protein Binding
Activation Of Immune Response
Proteasome
Oxidoreductase Activity
Nucleoside Diphosphate Metabolic Process
Glycolysis / Gluconeogenesis
Angiogenesis
Neuroactive Ligand-Receptor Interaction
Motile Cilium
Microtubule Bundle Formation
Drug Metabolism
Ciliary Part
Reg. Of Mitotic Cell Cycle
Organelle Fission
DNA Replication
DNA Repair
Condensed Chromosome
Th1 And Th2 Cell Differentiation
T Cell Receptor Signaling Pathway
Reg. Of Leukocyte Activation
Hematopoietic Cell Lineage
Cell Chemotaxis
Gene Ratio
Adjusted p-value
overlap

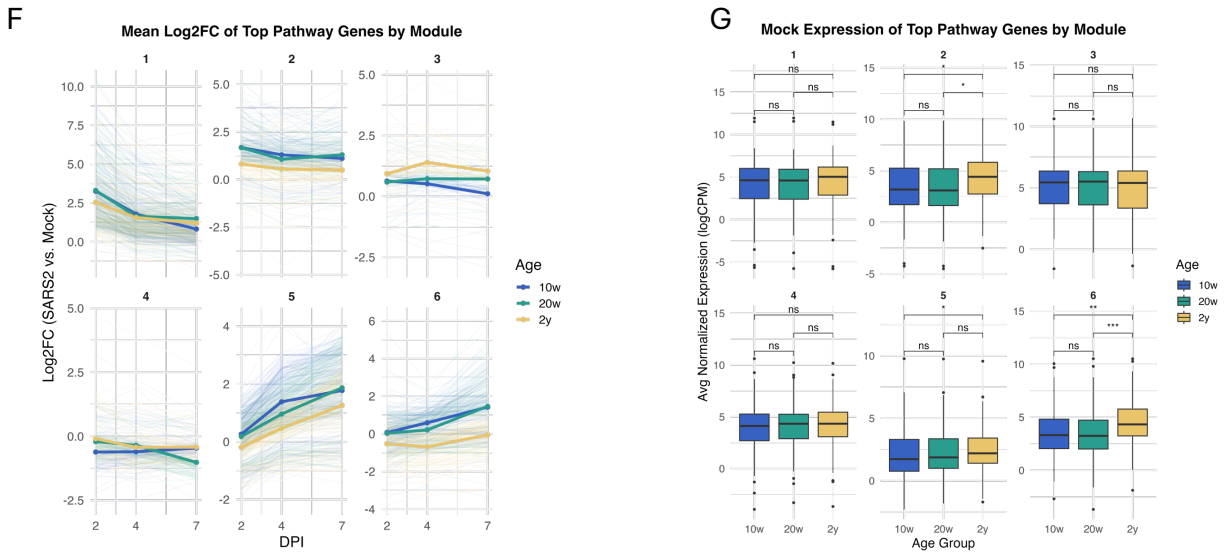
F
Mean Log2FC of Top Pathway Genes by Module
Log2FC (SARS2 vs. Mock)
DPI
Age
10w
20w
2y
G
Mock Expression of Top Pathway Genes by Module
Avg Normalized Expression (logCPM)
Age Group
ns

Fig. 2

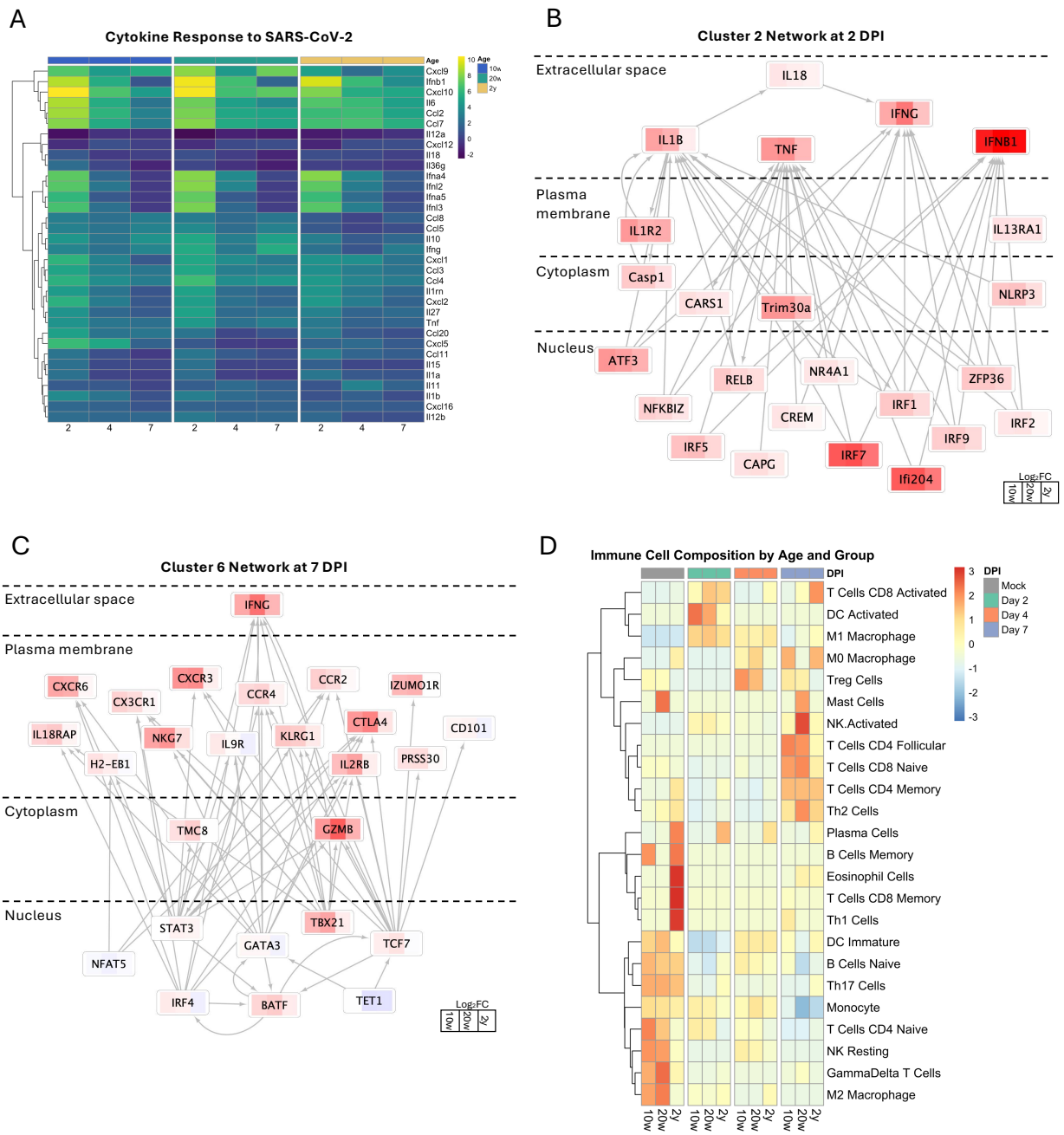
A
Cytokine Response to SARS-CoV-2
Age
10w
20w
2y
Cxcl9
Ifnb1
Cxcl10
Il6
Ccl2
Ccl7
Il12a
Cxcl12
Il18
Il36g
Ifna4
Ifnl2
Ifna5
Ifnl3
Ccl8
Ccl5
Il10
Ifng
Cxcl1
Ccl3
Ccl4
Il1rn
Cxcl2
Il27
Tnf
Ccl20
Cxcl5
Ccl11
Il15
Il1a
Il11
Il1b
Cxcl16
Il12b
2 4 7 2 4 7 2 4 7
B
Cluster 2 Network at 2 DPI
Extracellular space
Plasma membrane
Cytoplasm
Nucleus
IL18
IFNG
IL1B
TNF
IFNB1
IL1R2
IL13RA1
Casp1
CARS1
Trim30a
NLRP3
ATF3
RELB
NR4A1
ZFP36
NFKBIZ
CREM
IRF1
IRF2
IRF5
CAPG
IRF7
IRF9
Ifi204
Log2FC
10w
20w
2y
C
Cluster 6 Network at 7 DPI
Extracellular space
Plasma membrane
Cytoplasm
Nucleus
IFNG
CXCR6
CX3CR1
CXCR3
CCR4
CCR2
IZUMO1R
IL18RAP
NKG7
IL9R
KLRG1
CTLA4
CD101
H2-EB1
IL2RB
PRSS30
TMC8
GZMB
STAT3
TBX21
GATA3
TCF7
NFAT5
IRF4
BATF
TET1
Log2FC
10w
20w
2y
D
Immune Cell Composition by Age and Group
DPI
Mock
Day 2
Day 4
Day 7
3
2
1
0
-1
-2
-3
T Cells CD8 Activated
DC Activated
M1 Macrophage
M0 Macrophage
Treg Cells
Mast Cells
NK.Activated
T Cells CD4 Follicular
T Cells CD8 Naive
T Cells CD4 Memory
Th2 Cells
Plasma Cells
B Cells Memory
Eosinophil Cells
T Cells CD8 Memory
Th1 Cells
DC Immature
B Cells Naive
Th17 Cells
Monocyte
T Cells CD4 Naive
NK Resting
GammaDelta T Cells
M2 Macrophage
10w 20w 2y 10w 20w 2y 10w 20w 2y 10w 20w 2y

Fig. 3

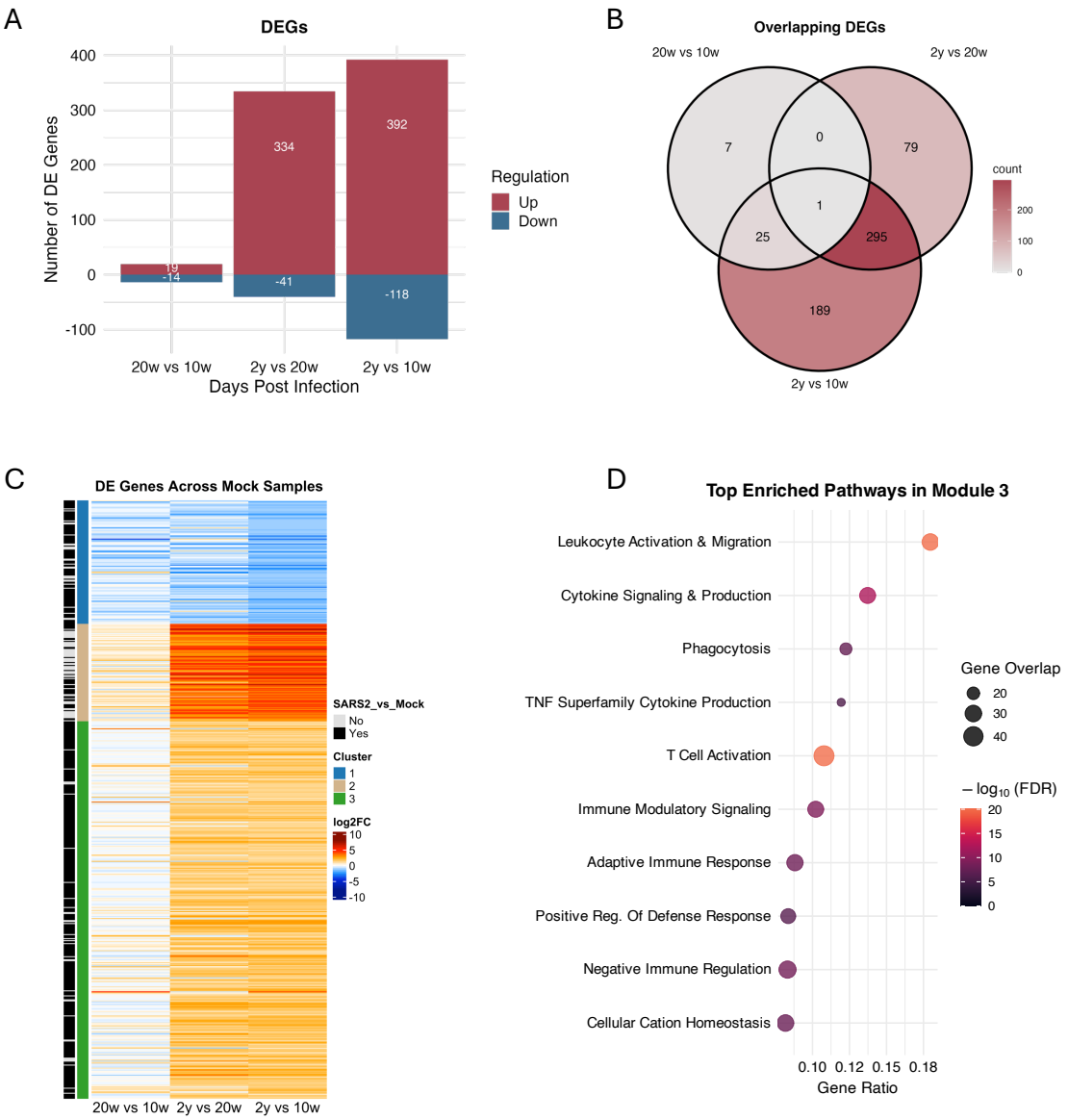
A
DEGs
Number of DE Genes
400
300
200
100
0
-100
334
392
19
-14
-41
-118
20w vs 10w
2y vs 20w
2y vs 10w
Days Post Infection
Regulation
Up
Down
B
Overlapping DEGs
20w vs 10w
2y vs 20w
2y vs 10w
7
0
79
1
25
295
189
count
200
100
0
C
DE Genes Across Mock Samples
SARS2_vs_Mock
No
Yes
Cluster
1
2
3
log2FC
10
5
0
-5
-10
20w vs 10w
2y vs 20w
2y vs 10w
D
Top Enriched Pathways in Module 3
Leukocyte Activation & Migration
Cytokine Signaling & Production
Phagocytosis
TNF Superfamily Cytokine Production
T Cell Activation
Immune Modulatory Signaling
Adaptive Immune Response
Positive Reg. Of Defense Response
Negative Immune Regulation
Cellular Cation Homeostasis
0.10
0.12
0.15
0.18
Gene Ratio
Gene Overlap
20
30
40
– log10 (FDR)
20
15
10
5
0

Fig. 4

A

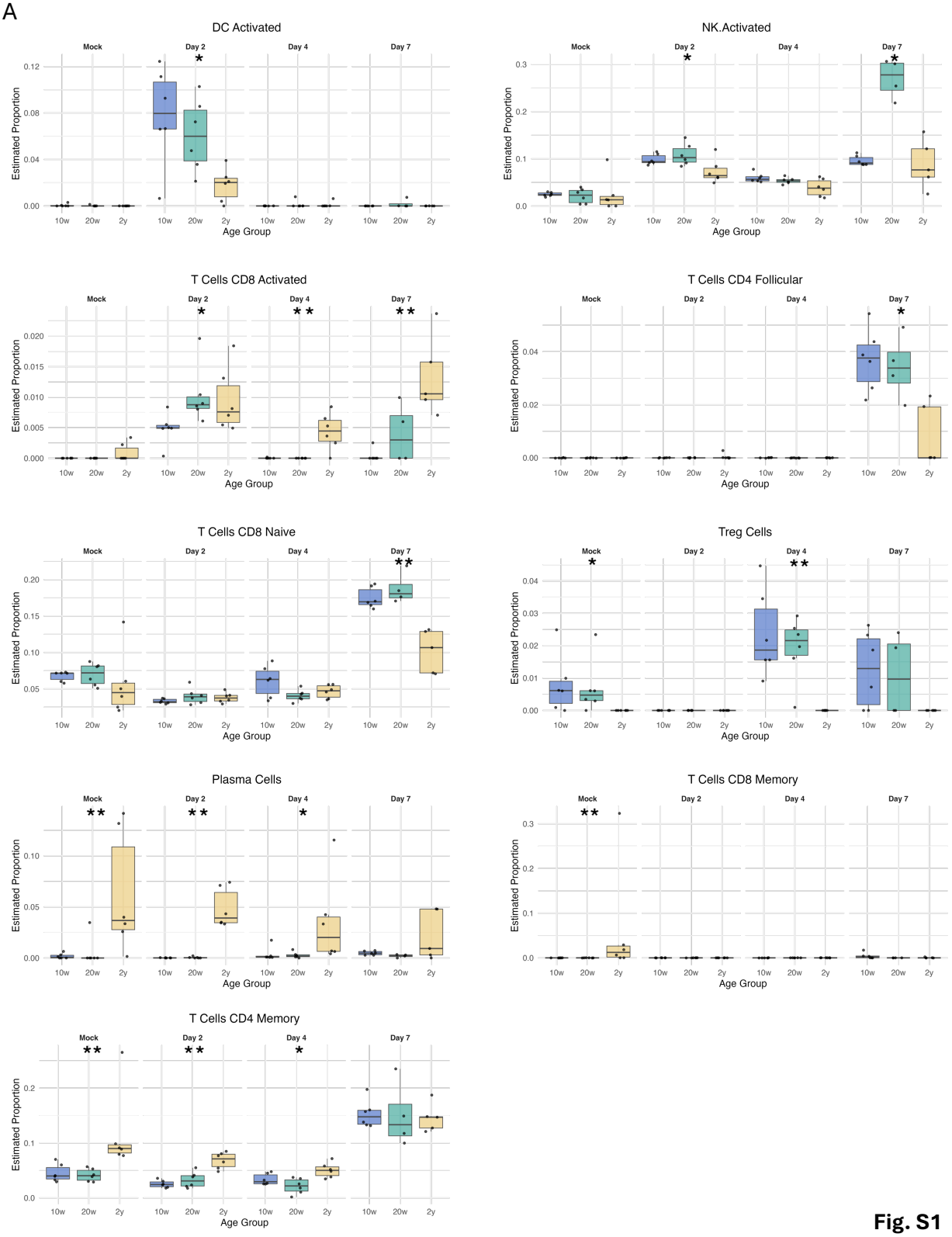
DC Activated
NK.Activated
T Cells CD8 Activated
T Cells CD4 Follicular
T Cells CD8 Naive
Treg Cells
Plasma Cells
T Cells CD8 Memory
T Cells CD4 Memory
Mock
Day 2
Day 4
Day 7
Estimated Proportion
Age Group
10w
20w
2y

Fig. S1

2.6 FIGURE LEGENDS

2.6.1 *Figure 1. Aged lung samples separate by age and viral load*

(A) Study design. (B) Principal component analysis of normalized log_2 CPM-transformed counts, overlaid with metadata including sex, age, day post-infection (DPI), and viral load. (C) Log_{10} transformed SARS-CoV-2 read counts by DPI and age group, highlighting significantly higher viral loads in aged mice at day 7. Statistical comparisons between age groups were conducted separately for each DPI using pairwise Wilcoxon rank-sum tests, with p-values adjusted for multiple comparisons using the false discovery rate (FDR) method. Significance thresholds were defined as $p.adj \leq 0.05$ (*), $p.adj \leq 0.01$(**), and $p.adj \leq 0.001$ (***).

2.6.2 *Figure 2. Infection transcriptomic responses are dysregulated with age*

(A) Differential expression (DE) analysis design. (B) Number of DEGs per time point across all age groups. (C) Venn diagram of overlapping DEGs per age group. (D) Hierarchical clustering of DEGs ($p.adj \leq 0.01$, $|log_2FC| \geq 1$) in aged lung samples. (E) Pathway enrichment analysis using over representation analysis (ORA) with KEGG and Gene Ontology databases. Pathways with ≥75% overlapping genes were removed to reduce redundancy. Dotplot visualization of the top uniquely enriched pathways in each cluster. The color of the dot represents the adjusted p-value, the size represents the number of overlapping DEGs in the total gene set. (F) Average log_2FC expression of cluster-specific DEGs within the uniquely enriched pathways by age. (G) Boxplots of the average normalized log_{10} CPM expression of cluster-specific DEGs within the uniquely enriched pathways by age. Statistical comparisons between age groups were conducted separately for each cluster using unpaired t-tests, with p-values were adjusted for multiple comparisons using the false discovery rate (FDR) method. Significance thresholds were defined as $p.adj \leq 0.05$ (*), $p.adj \leq 0.01$(**), and $p.adj \leq 0.001$ (***).

2.6.3 *Figure 3. Early and late antiviral programs are dysregulated with age*

(A) Heatmap of log_2FC values for cytokines and interferons differentially expressed (DE) during infection across DPI and age groups. (B) De novo network created from top cytokine upstream regulators (TNF, IL1B, IFNG, and IFNB) and direct interactions among DEGs from Cluster 2 (see Fig. 2D). Node color represents log_2FC values comparing infected samples to age-matched mock controls at 2 dpi for each age (10-week-old, 20-week-old, 2-year-old). (C) De novo network created from top transcription factors (NFAT, STAT3, GATA3, TBX21, TCF7, and TET1) and direct interactions among DEGs from Cluster 6 (see Fig. 2D). Node color represents log_2FC values comparing infected samples to age-matched mock controls at 7 dpi for each age. (D) Heatmap of immune cell composition by age group, scaled by z-score across cell types. Cell types with no variance across groups were excluded. Rows and columns were clustered using Ward's D2 hierarchical clustering.

2.6.4 *Figure 4. Aged mice have elevated inflammatory signatures at baseline*

(A) Number of baseline DEGs across age groups. (B) Venn diagram of overlapping baseline DEGs per age group. (C) Hierarchical clustering of baseline DEGs ($p.adj \leq 0.01$, $|log_2FC| \geq 1$) in aged lung samples. (D) Pathway enrichment analysis using over representation analysis (ORA) with KEGG and Gene Ontology databases. Pathways with ≥75% overlapping genes were removed to reduce redundancy. Dotplot visualization of the top enriched pathways in Cluster 3 (green cluster). The color of the dot represents the adjusted p-value, the size represents the number of overlapping DEGs in the total gene set.

2.7 SUPPLEMENTAL FIGURE LEGENDS

2.7.1 *Figure S1. Immune cell-type deconvolution by age*

(A) Boxplots represent the mean estimated proportion by day post-infection (DPI) and age group for the following cell types: activated dendritic cells (DCs), activated natural killer cells (NKs), activated $CD8^+$ T cells, CD^+ T follicular helper cells, naïve $CD8^+$ T cells, regulatory T cells (Tregs), plasma cells, $CD8^+$ memory T cells, and $CD4^+$ memory T cells. Statistical comparisons between age groups were conducted separately for each cell type at each DPI using Kruskal-Wallis tests. P-values were adjusted for multiple comparisons using the false discovery rate (FDR) method. Significance thresholds were defined as $p.adj \leq 0.05$ (*), $p.adj \leq 0.01$(**), and $p.adj \leq 0.001$ (***).

Chapter 3. AGE-BASED CRITERIA AND THE UNDERREPRESENTATION OF OLDER ADULTS IN SARS-COV-2 VACCINE CLINICAL TRIALS

Chapter 3. SUMMARY

Older adults (≥65 years) are historically underrepresented in clinical trials. Since the start of the pandemic, hundreds of SARS-CoV-2 vaccine clinical trials have been registered on ClinicalTrials.gov; however, the extent of older adult representation remains unclear. We conducted a cross-sectional analysis of SARS-CoV-2 vaccine clinical trials registered through November 23, 2024, to estimate the proportion of older adult enrollment. Of 337 identified trials, 93 met inclusion criteria and were analyzed. Among 524,452 enrolled participants, the weighted mean age was 44.2± 7.3 years. Despite adults ≥65 accounting for approximately 76% of COVID-19-related mortality, only 8% of trial participants were in this age group. Only 41% of studies had explicit upper age limits. However, we identified common study exclusion criteria, such as hypertension, diabetes, obesity, cancer, and chronic lung disease, that are significantly more prevalent among older adults and may contribute to their underrepresentation in these vaccine trials. These findings highlight potential reasons for the continued underrepresentation of

older adults in biomedical research and point to actionable opportunities to design more inclusive clinical trials by reconsidering exclusion criteria that disproportionately affect this high-risk population.

3.1 INTRODUCTION

3.1.1 *Vaccine development for COVID-19*

As of March 30, 2025, the COVID-19 pandemic has resulted in over 778 million cases and 7 million deaths.[1] However, the rapid development, approval, and distribution of COVID-19 vaccines in under a year represents one of the most remarkable achievements in modern medicine. The unmatched speed of vaccine development was driven by global urgency, decades of research in vaccine platforms, and unprecedented public and private collaboration that enabled parallel trial phases and accelerated regulatory review.

3.1.2 *Mass vaccination lead to remarkable protection*

COVID-19 vaccines have been instrumental in preventing severe illness and death, particularly among the most vulnerable populations. According to the Commonwealth Fund, from December 2020 to November 2022, COVID-19 vaccines in the U.S. prevented more than 3.2 million deaths and saved an estimated $1.15 trillion in medical costs.[2] A modeling study in Europe similarly estimated that between December 2020 and March 2023, COVID-19 vaccines saved approximately 1.6 million lives, with 96% of lives saved among individuals aged 60 or older, and 52% among those aged 80 or older.[3] These findings highlight the well-established observation that mortality rates throughout the pandemic have been disproportionately higher among older adults (≥65 years). Given their consistently elevated risk of COVID-19-related hospitalization and death, the CDC's Advisory Committee on Immunization Practices (ACIP) expanded its initial vaccination priority groups – originally focused on health care workers and

residents and staff of long-term care facilities – to include older adults, making them one of the first populations to be vaccinated at scale.[4-6] As of April 26, 2023, 94% of U.S. adults aged 65 and older were fully vaccinated against COVID-19, representing the highest vaccination coverage of any age group.[7]

3.1.3 *COVID-19 disease burden by age*

Despite bearing a disproportionate burden of many chronic and severe health conditions, older adults have historically been underrepresented in clinical research across the biomedical field.[8-14] Numerous studies have documented the frequent use of arbitrary upper age limits, poorly justified exclusion criteria, and inadequate age representation relative to the disease burden being studied.[8-14] Underrepresentation of any population in clinical trials limits the generalizability of findings and hinders a full understanding of a treatment's safety and efficacy once it becomes available to the broader public. This issue is especially critical for older adults, who not only experience the greatest disease burden but also account for the highest rates of medication use.[15] In response to this persistent disparity, the National Institutes of Health (NIH) implemented the *Inclusion Across the Lifespan* policy to require individuals of all ages, including older adults, be appropriately included in NIH-funded research and any age-related exclusions be scientifically justified.[16] However, early reviews of COVID-19-related clinical trials reported that this continued in these trials.[17-19] These early findings raised concerns that even the most well-funded, high-profile, and globally coordinated trials failed to meet longstanding calls for equitable age representation.

3.1.4 *Evaluation of COVID-19 vaccine clinical trials*

The objective of this study was to evaluate the representation of older adults in Phase II and higher SARS-CoV-2 vaccine clinical trials registered on ClinicalTrials.gov between November 1,

2019 and November 23, 2024. We compared the estimated proportion of older adults enrolled in these trials to the distribution of COVID-19-related mortality among older adults and found that older adults were significantly underrepresented relative to both their U.S. age distribution and disease burden. We extended prior research by evaluating potential reasons why older adults may be excluded despite recent policies highlighting the importance of greater inclusion. To do so, we evaluated exclusion criteria for their affect burden in older adults and compared the percentage of trials excluding each condition to its estimated prevalence among older adults in the U.S. These findings highlight ongoing barriers to older adult enrollment and suggest opportunities for more equitable clinical trial designs.

3.2 RESULTS

3.2.1 *Mean age of trial participants*

A total of 337 registered SARS-CoV-2 vaccine clinical trials were identified on ClinicalTrials.gov and screened according to predefined eligibility criteria (Fig. 1). Of these, 93 Phase II or higher SARS-CoV-2 trials with available enrollment and participant age data were included in the final analysis. Across these trials, the weighted mean age of participants was 44.2± 7.3 years, representing a total of 524,452 enrolled individuals (Table 1). When stratified by phase, Phase 2/3 trials had the highest mean age at enrollment (50.0±3.4 years), followed by Phase 4 (45.7±9.4 years), and Phase 2 (43.1±12.4). Phase 4 trials contributed just 1% (6,465) of enrolled individuals, but still reported a relatively higher mean age. While 54 (58%) trials reported the proportion of older adults enrolled, only 33 (35%) included age-adjusted analyses. Additionally, 38 (41%) trials imposed an upper age limit, and only 15 (16%) explicitly included an older adult enrollment requirement in their study design.

3.2.2 *Age distribution highlights older adult underrepresentation*

Based on the estimated proportion of participants in predefined older age groups, individuals younger than 65 accounted for 92% of SARS-CoV-2 vaccine clinical trial participants (Table 2). In contrast, an estimated 3.75% were aged 65-69, 2.17% were aged 70-74, 1.13% were aged 75-79, and only 0.89% were aged 80 or older.

To validate these estimates, we compared them to a subset of 46 trials that reported the true proportions of older adults in specific age categories of interest. Estimated and reported values were highly correlated across all age groups (Pearson's r range:0.96-1; p <0.001), supporting the reliability of our truncated normal distribution approach (Fig. S1).

3.2.3 *Older adults are underrepresented relative to disease burden and population size*

These older adult proportions were significantly lower than the corresponding age group distributions in the U.S. population (Fig. S2), and even more so when compared to the age distribution of COVID-19-related mortality (Fig. 2). For example, individuals aged 65 and older made up just 8% of trial participants but 76% of COVID-19-related mortality. The disparity between participation and mortality increased progressively with age, with the most pronounced underrepresentation observed among individuals aged 80 and older.

3.2.4 *Enrollment criteria significantly impacts older adult participation*

The number of studies excluding each of the top 10 chronic conditions affecting older adults, as identified by the NCOA, is summarized in **Table 3** and stratified by trial phase.[20,21] Heart failure (46%) was the most frequently excluded condition, followed by coronary heart disease (42%), chronic kidney disease (38%), hypertension (33%), and diabetes (29%). The prevalence of these conditions was significantly higher among adults aged ≥65 compared to those under 65, suggesting that at least one-third of SARS-CoV-2 clinical trials employed exclusion criteria that may disproportionately impact older adults. When stratified by trial phase, heart failure, coronary

heart disease, chronic kidney disease, hypertension, and obesity were most frequently excluded in Phase II trials, whereas diabetes, cognitive disorders, and mental health conditions were most commonly excluded in Phase IV trials. Stratified prevalence estimates across older adult subgroups further illustrate this disparity, with the prevalence of all conditions–except depression and other mental health conditions–increasing with age (Fig. S3). Nineteen trials (21%) excluded participants with cognitive disorders, and while this data was not assessed in NHANES, it is estimated that 10% of adults aged ≥65 have dementia and 22% have mild cognitive impairment.[22]

In addition to predefined chronic conditions, several studies excluded conditions that disproportionately affect older adults, including immunosuppressive therapy (83%), bleeding disorders (66%), and cancer or malignancy (55%) (Table 4). Among conditions excluded in clinical trials and assessed by NHANES, history of blood transfusion, cancer, heavy alcohol use, liver conditions, hepatitis B, chronic lung conditions, and thyroid conditions were all significantly more prevalent among older age groups (Fig. S4). The most frequently listed exclusion criteria overall was a vague descriptor, "according to PI discretion," which appeared in 85% of trials. History of COVID-19 and prior COVID-19 vaccination were also commonly listed, serving as exclusion criteria in 80% and 53% of studies, respectively. Notably, criteria such as prescription drug-use, technology access, group living, frailty, and transportation needs–often cited as potential barriers to older adult enrollment–were explicitly identified in fewer than 5% of trials, if at all. Taken together, these findings highlight the widespread use of exclusion criteria that may disproportionately restrict older adult participation in SARS-CoV-2 vaccine trials.

3.3 DISCUSSION

3.3.1 *Principle findings*

In this cross-sectional analysis of registered SARS-CoV-2 vaccine clinical trials, we found that older adults were routinely underrepresented, likely due to exclusion criteria other than age itself. The proportion of enrolled older adults was significantly lower than both their representation in the U.S. population and their share of COVID-19-related mortality. Among 93 trials and over half a million participants, only 8% of enrollees were aged ≥65, despite older adults accounting for 17% of the U.S. population and 76% of COVID-19-realted deaths. Stratified estimates revealed a striking decline in representation with increasing age, with the lowest participation among individuals aged 80+, the group at greatest risk for severe COVID-19 outcomes. This aligns with a prior analysis of ten SARS-CoV-2 vaccine RCTs published through 2021, which reported a mean age of 45.2±11.9 years, and in studies that reported participant age distributions, only 10% of participants were aged ≥65.[18] Despite clear prioritization of older adults for vaccination, our analysis demonstrates that they were significantly underrepresented in the clinical trials responsible for informing vaccine rollout.

3.3.2 *Relevance to previous work*

While upper age limits may account for a portion of this underrepresentation, we also found that 9 out 10 of the top chronic conditions affecting older adults were used as exclusion criteria in at least one study. Notably, conditions like hypertension, diabetes, and obesity, which are significantly more prevalent in older adults, were listed as exclusions in 33%, 29%, and 24% of studies, respectively. A study of COVID-19 clinical trials through 2020 found that among 18 vaccine trials, 100% of trials included either age cutoffs or vague exclusion language.[17] While the exclusion of participants with significant comorbidities may be justified in specific contexts, such decisions should be balanced by a deliberate effort to include older adults in vaccine

research. As our findings show, even trials without upper age limits can inadvertently impact older populations, ultimately limiting the generalizability of trial results to the groups most affected by COVID-19.

3.3.3 *Clinical implications*

In our review, the most frequently listed exclusion criterion was "according to PI discretion," which appeared in 85% of trials. This broad and non-specified phrasing lacks a transparent scientific rationale and is inconsistent with guidance from the NIH's *Inclusion Across the Lifespan* policy, which states that age-related exclusions must be clearly justified.[16] A subset of trials also included criteria allowing for the exclusion of participants deemed unable to adhere to the protocol or provide informed consent due to social or psychological conditions. While these considerations may be appropriate in certain contexts, they introduce subjectivity into enrollment decisions and may inadvertently contribute to age-related bias. Without clear documentation of who is excluded and why, these vague criteria undermine both the inclusivity and reproducibility of vaccine trials.

Clinical trials have shown that vaccine efficacy tends to be lower in older adults, including reduced concentrations of neutralizing antibodies.[23-25] Although COVID-19 vaccines were highly effective at preventing severe outcomes and death across all age groups, this diminished or more rapidly waning immunity in older adults highlights key biological differences that should be accounted for in clinical trial design. Such differences may inform decisions around vaccine dosing, scheduling, and booster recommendations specifically tailored to aging populations. Several recently registered clinical trials are now evaluating the safety and efficacy of combination vaccines targeting COVID-19 along with other respiratory viruses such as influenza and RSV–a shift that reflects the transition of SARS-CoV-2 into an endemic seasonal pathogen.

Given that these viruses disproportionately impact older adults, future vaccine trials must prioritize equitable inclusion of this population to ensure that combination vaccine strategies are both effective and generalizable.

3.3.4 *Strengths and limitations*

This study has several limitations. Our analysis was limited to trials registered on ClinicalTrials.gov, which may not capture all global SARS-CoV-2 vaccine trials or those without publicly available age-related data. We used a truncated normal distribution to estimate age subgroup proportions, which relies on reported mean age, standard deviation, and enrollment, and may not fully reflect actual participant age distributions. While we focused on listed enrollment criteria, this may not account for upstream barriers to participation, such as digital access, recruitment practices, or site-level bias. Some exclusion criteria could not be assessed using NHANES data and were therefore not included in our prevalence comparisons. In other cases, proxy variables were used. Lastly, exclusion criteria were often vaguely defined, limiting our ability to consistently categorize or quantify their frequency.

3.3.5 *Conclusions*

Despite these gaps, opportunities for improving older adult representation in clinical trials are both feasible and within reach. Of the 93 trials reviewed, only five were exclusively designed for older adults, underscoring how rarely this population is the focus of vaccine research, despite their vulnerability. Yet, at least four studies specifically allowed for flexible informed consent options, including video consent or consent via caregiver proxy, which may facilitate broader participation among older individuals. Additionally, providing more transparent justification for eligibility criteria and incorporating explicit inclusion targets for older adults, may mitigate barriers related to older adult enrollment. Additional proposed strategies that address barriers

upstream of formal eligibility include geriatric training for clinical trial personnel to address bias and ageism, improving federal monitoring and accountability, increasing incentives to enroll older adult participants, and expanding healthcare coverage of out-of-pocket costs associated with participation in clinical trials.[8,9]

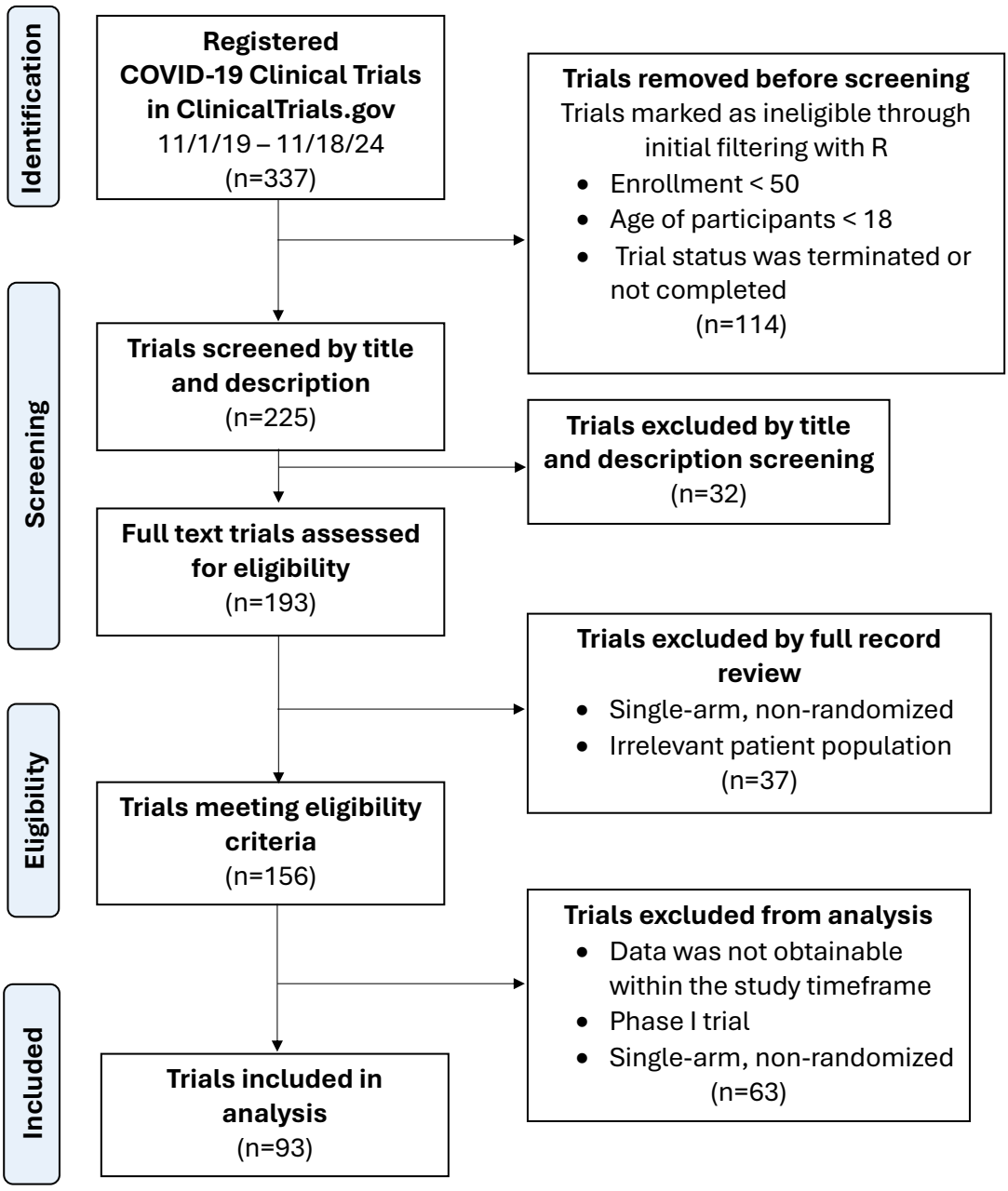
Identification
Screening
Eligibility
Included
Registered COVID-19 Clinical Trials in ClinicalTrials.gov
11/1/19 – 11/18/24
(n=337)
Trials removed before screening
Trials marked as ineligible through initial filtering with R
Enrollment < 50
Age of participants < 18
Trial status was terminated or not completed
(n=114)
Trials screened by title and description
(n=225)
Trials excluded by title and description screening
(n=32)
Full text trials assessed for eligibility
(n=193)
Trials excluded by full record review
Single-arm, non-randomized
Irrelevant patient population
(n=37)
Trials meeting eligibility criteria
(n=156)
Trials excluded from analysis
Data was not obtainable within the study timeframe
Phase I trial
Single-arm, non-randomized
(n=63)
Trials included in analysis
(n=93)

Fig. 1

Age-Related Characteristics of SARS-CoV-2 Vaccine Trials					
	Phase2	**Phase2/3**	**Phase3**	**Phase4**	**Total**
Participant Characteristics					
Age, mean (SD)	43.1 (12.4)	50 (3.4)	43.5 (7)	45.7 (9.4)	**44.2 (7.3)**
Total Participants	20642	53246	444099	6465	**524452**
Trial Characteristics					
Reports Older Age Proportion	16	4	28	6	**54 (58%)**
Upper Age Limit	21	0	10	6	**37 (40%)**
Reports Age Adjusted Analyses	8	4	16	5	**33 (35%)**
Includes Older Adults by Design	6	2	5	2	**15 (16%)**
Number of Trials	39	6	37	11	**93 (100%)**

Table 1

Estimated Age Distribution of SARS-CoV-2 Vaccine Trial Participants		
Age Cutoff	**Estimated Participants**	**Percent of Total (%)**
<65	480,856	92.06%
65-69	19,569	3.75%
70-74	11,314	2.17%
75-79	5,915	1.13%
80+	4,665	0.89%
All	522,319	100%

Table 2

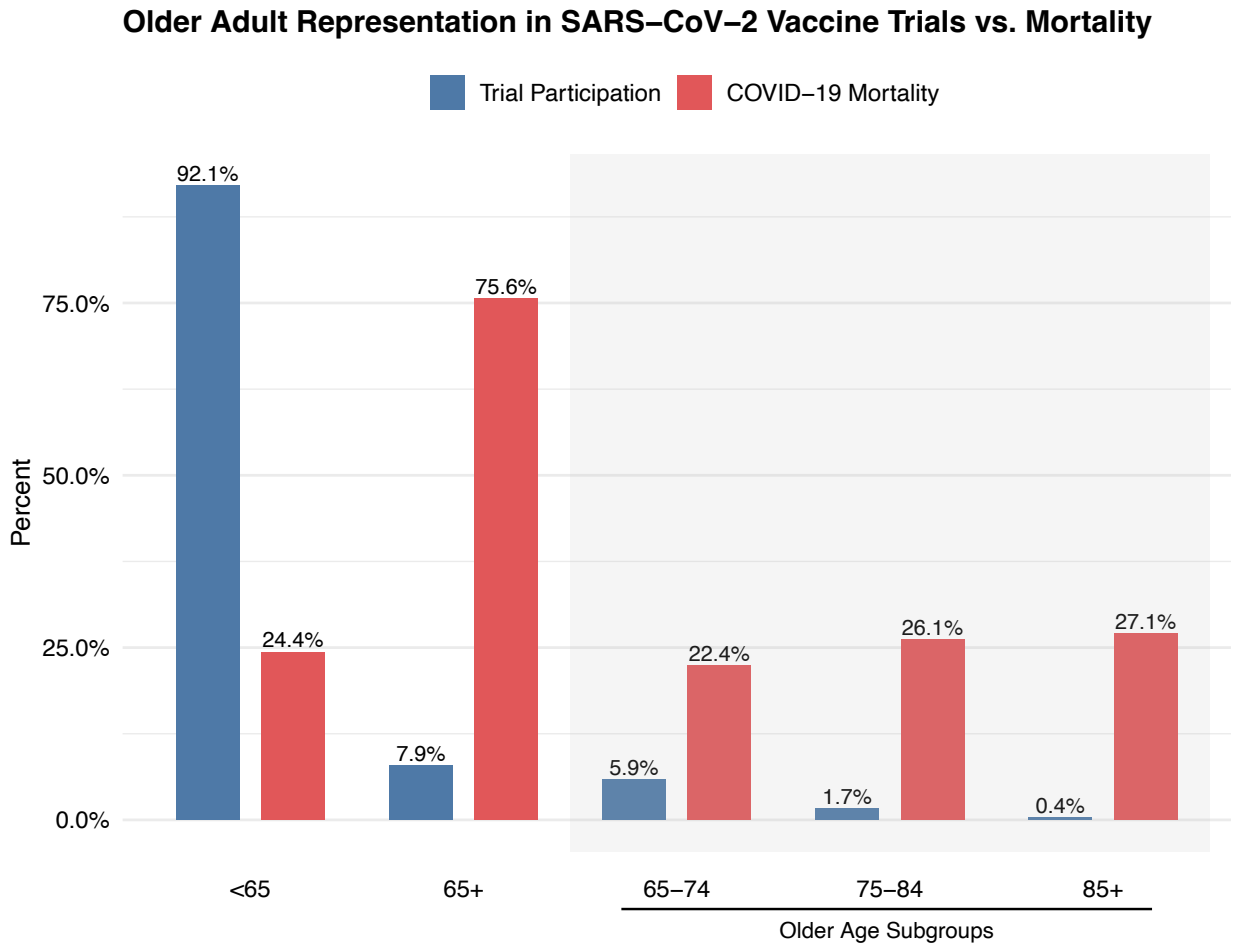
Older Adult Representation in SARS–CoV–2 Vaccine Trials vs. Mortality
Trial Participation
COVID–19 Mortality
Percent
75.0%
50.0%
25.0%
0.0%
92.1%
24.4%
7.9%
75.6%
5.9%
22.4%
1.7%
26.1%
0.4%
27.1%
<65
65+
65–74
75–84
85+
Older Age Subgroups

Fig. 2

Exclusion of Top Chronic Conditions Among Older Adults in SARS-CoV-2 Vaccine Trials vs. U.S. Prevalence							
	Excluded in SARS-CoV-2 Clinical Trials					U.S. Prevalence	
Characteristic	**Phase2**	**Phase2/3**	**Phase3**	**Phase4**	**Trials Excluded, N (%)**	**% of U.S. <65**	**% of U.S. ≥65**
Heart Failure	26	1	12	4	43 (47%)	1%	7%
Coronary Heart Disease	22	1	12	4	39 (42%)	2%	12%
Chronic Kidney Disease	19	2	12	2	35 (38%)	2%	7%
Hypertension	18	0	7	5	30 (33%)	24%	60%
Diabetes	16	1	4	6	27 (29%)	8%	28%
Obesity	18	1	2	1	22 (24%)	33%	41%
Cognitive Disorders	9	0	7	3	19 (21%)		
Mental Health Conditions	6	0	1	2	9 (10%)	9%	7%
Arthritis	0	0	1	0	1 (1%)	20%	56%
High Cholesterol	0	0	0	0	0 (0%)	8%	9%
Total	38	6	37	11	92 (100%)		

Table 3

Common Exclusion Criteria in SARS-CoV-2 Vaccine Trials vs. U.S. Prevalence							
	Excluded in SARS-CoV-2 Clinical Trials					U.S. Prevalence	
Characteristic	**Phase2**	**Phase2/3**	**Phase3**	**Phase4**	**Trials Excluded, N (%)**	**% of U.S. <65**	**% of U.S. ≥65**
According to PI	35	5	29	9	78 (85%)		
Immunosuppressive Therapy	33	6	28	9	76 (83%)		
History of COVID-19	30	5	29	9	73 (79%)		
Recent Blood Donation/Transfusion	29	4	28	8	69 (75%)	6%	21%
Bleeding Disorder	25	4	23	8	60 (65%)		
Cancer	25	2	17	6	50 (54%)	7%	29%
Prior COVID-19 Vaccination	20	1	22	5	48 (52%)		
HIV/AIDS	18	2	17	6	43 (47%)		
Immunocompromised	17	3	16	6	42 (46%)		
Drug or Alcohol Dependency	17	1	13	3	34 (37%)	13%	16%
Liver Disease	16	2	10	2	30 (33%)	4%	6%
Spleen Disorder	11	1	10	7	29 (32%)		
Hepatitis B	16	1	7	0	24 (26%)	3%	7%
Hepatitis C	15	1	7	0	23 (25%)	1%	1%
Chronic Lung Condition	17	0	3	1	21 (23%)	7%	16%
Angioedema	9	0	5	5	19 (21%)		
Asthma	12	0	3	1	16 (17%)	16%	12%
Gastrointestinal Disorder	8	1	6	0	15 (16%)		
Tuberculosis	9	0	3	3	15 (16%)		
Endocrine Disorder	7	1	6	0	14 (15%)		
Thyroid Disease	6	0	1	3	10 (11%)	10%	22%
Prescription Drug Use	4	0	0	0	4 (4%)	68%	98%
Technology-Related	1	0	3	0	4 (4%)		
Group Living	2	0	1	0	3 (3%)		
Frailty or Physical Limitations	0	0	0	0	0 (0%)		
Transportation-Related	0	0	0	0	0 (0%)		
Total	38	6	37	11	92 (100%)		

Table 4

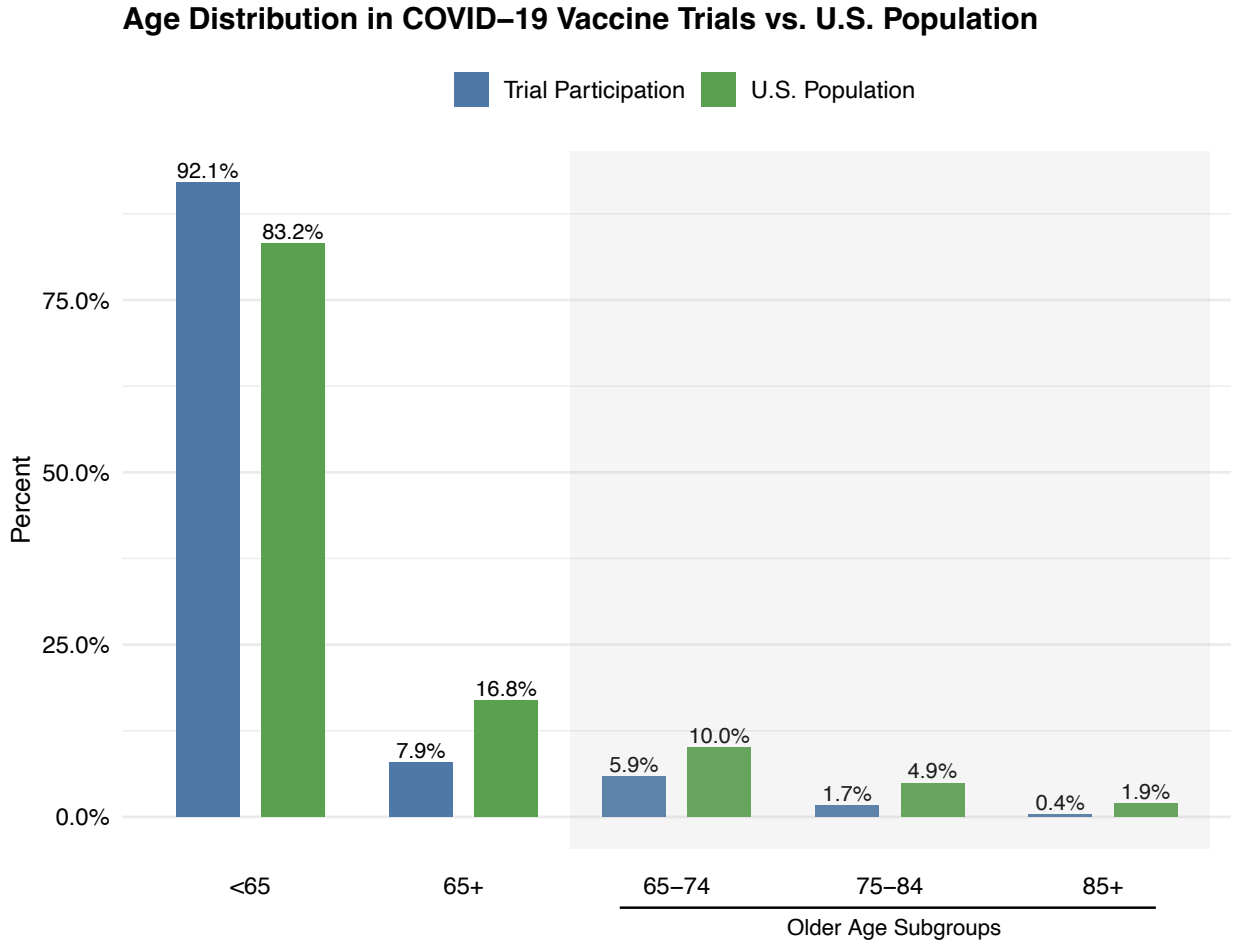
Age Distribution in COVID–19 Vaccine Trials vs. U.S. Population
Trial Participation
U.S. Population
Percent
75.0%
50.0%
25.0%
0.0%
92.1%
83.2%
7.9%
16.8%
5.9%
10.0%
1.7%
4.9%
0.4%
1.9%
<65
65+
65–74
75–84
85+
Older Age Subgroups

Fig. S1

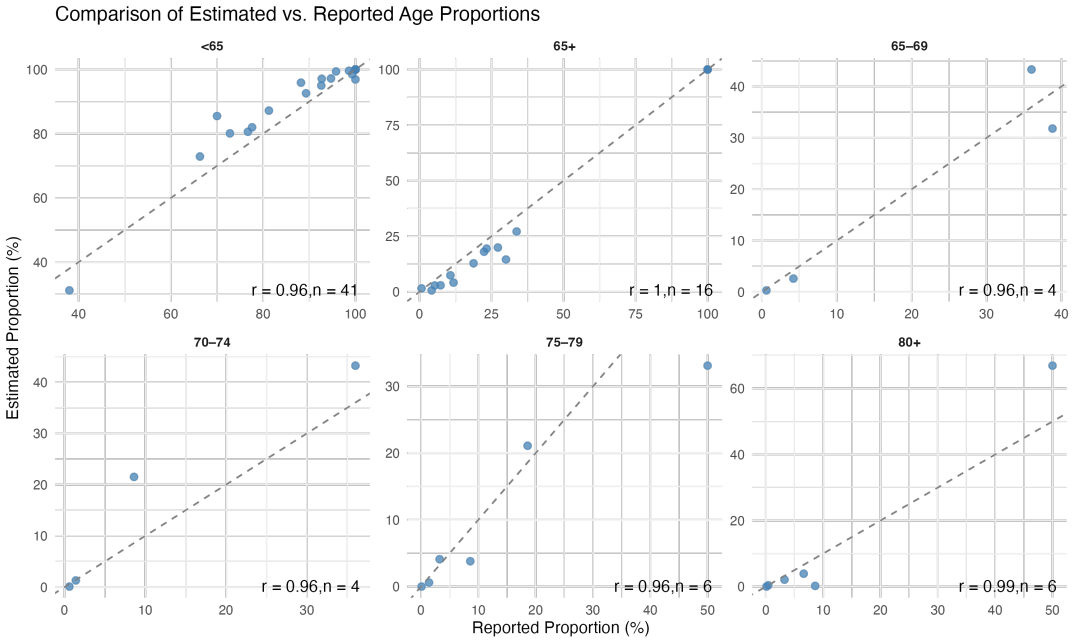
Comparison of Estimated vs. Reported Age Proportions
<65
65+
65–69
70–74
75–79
80+
r = 0.96,n = 41
r = 1,n = 16
r = 0.96,n = 4
r = 0.96,n = 4
r = 0.96,n = 6
r = 0.99,n = 6
Estimated Proportion (%)
Reported Proportion (%)

Fig. S2

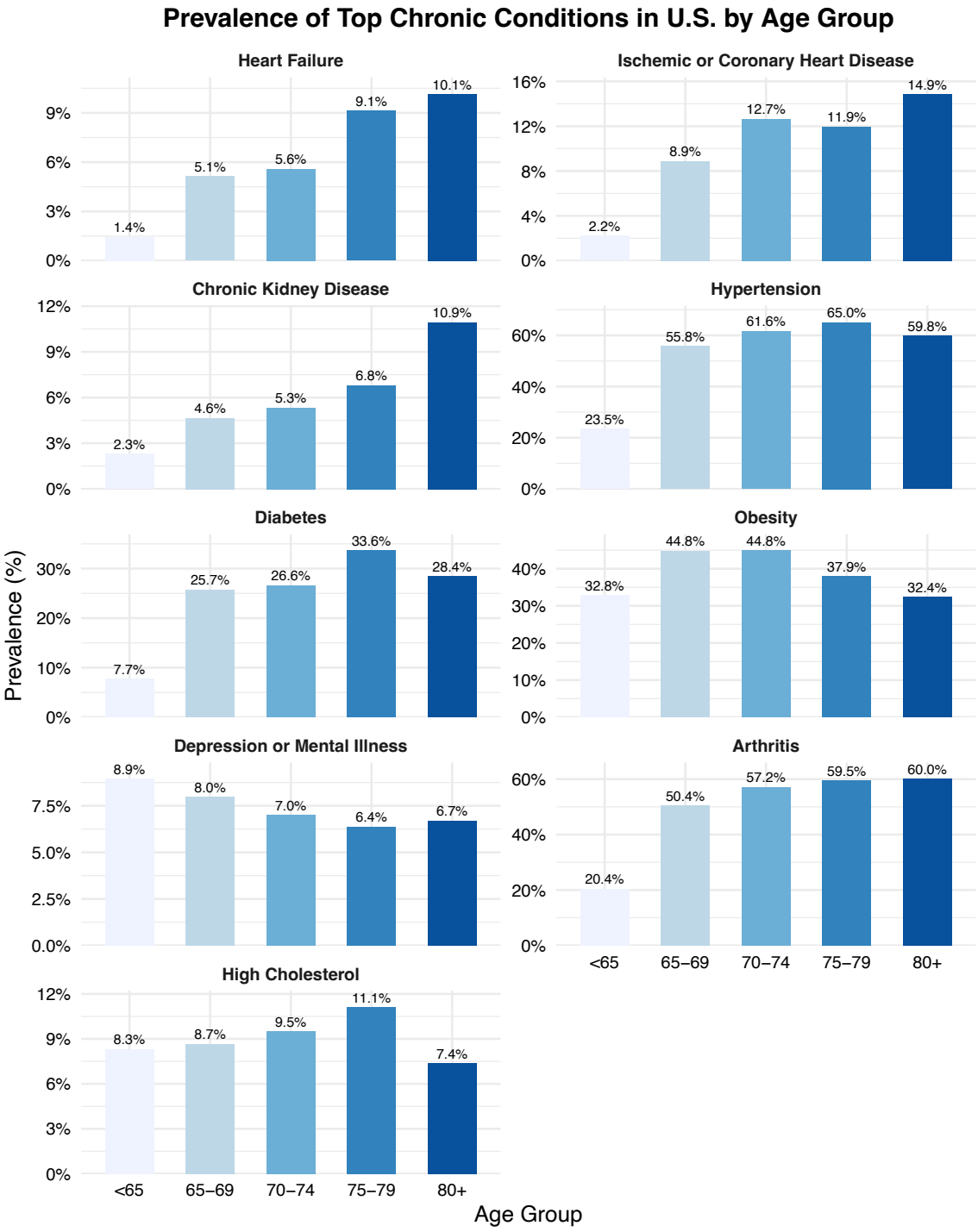
Prevalence of Top Chronic Conditions in U.S. by Age Group
Heart Failure
1.4%
5.1%
5.6%
9.1%
10.1%
Ischemic or Coronary Heart Disease
2.2%
8.9%
12.7%
11.9%
14.9%
Chronic Kidney Disease
2.3%
4.6%
5.3%
6.8%
10.9%
Hypertension
23.5%
55.8%
61.6%
65.0%
59.8%
Diabetes
7.7%
25.7%
26.6%
33.6%
28.4%
Obesity
32.8%
44.8%
44.8%
37.9%
32.4%
Depression or Mental Illness
8.9%
8.0%
7.0%
6.4%
6.7%
Arthritis
20.4%
50.4%
57.2%
59.5%
60.0%
High Cholesterol
8.3%
8.7%
9.5%
11.1%
7.4%
<65
65–69
70–74
75–79
80+
Prevalence (%)
Age Group

Fig. S3

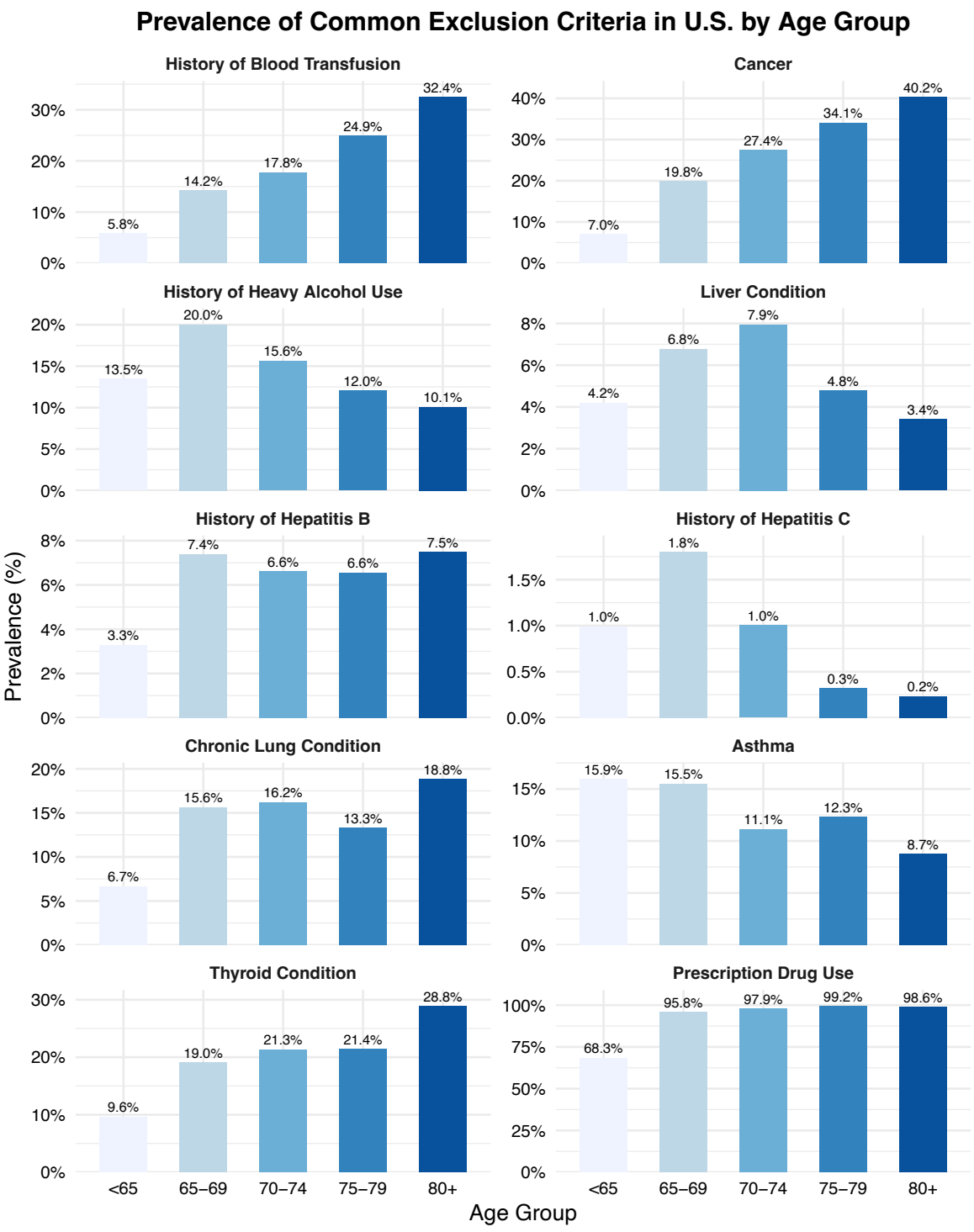
Prevalence of Common Exclusion Criteria in U.S. by Age Group
History of Blood Transfusion
5.8%
14.2%
17.8%
24.9%
32.4%
Cancer
7.0%
19.8%
27.4%
34.1%
40.2%
History of Heavy Alcohol Use
13.5%
20.0%
15.6%
12.0%
10.1%
Liver Condition
4.2%
6.8%
7.9%
4.8%
3.4%
History of Hepatitis B
3.3%
7.4%
6.6%
6.6%
7.5%
History of Hepatitis C
1.0%
1.8%
1.0%
0.3%
0.2%
Chronic Lung Condition
6.7%
15.6%
16.2%
13.3%
18.8%
Asthma
15.9%
15.5%
11.1%
12.3%
8.7%
Thyroid Condition
9.6%
19.0%
21.3%
21.4%
28.8%
Prescription Drug Use
68.3%
95.8%
97.9%
99.2%
98.6%
Prevalence (%)
<65
65–69
70–74
75–79
80+
Age Group

Fig. S4

2017-March 2020 NHANES Variables Used to Estimate U.S. Prevalence				
Characteristic	**Data Source**	**Documentation File**	**NHANES Variable(s)**	**Estimation Notes**
Heart Failure	Questionnaire	P_MCQ	MCQ160B	
Coronary Heart Disease	Questionnaire	P_MCQ	MCQ160C	
Chronic Kidney Disease	Questionnaire	P_KIQ_U	KIQ022	History of Weak/Failing Kidneys
Hypertension	Questionnaire	P_BPQ	BPQ020	
Diabetes	Questionnaire	P_DIQ	DIQ010	
Obesity	Examination	P_BMX	BMXBMI	BMI≥30 kg/m^2
Mental Health Conditions	Questionnaire	P_DPQ	DPQ010:DPQ090	PHQ-9≥10
Arthritis	Questionnaire	P_MCQ	MCQ160A	
High Cholesterol	Laboratory	P_TCHOL	LBXTC	≥240 mg/dL
Recent Blood Donation/Transfusion	Questionnaire	P_MCQ	MCQ092	History of Blood Transfusion
Cancer	Questionnaire	P_MCQ	MCQ220	
Drug or Alcohol Dependency	Questionnaire	P_ALQ	ALQ151	History of Heavy Drinking
Liver Disease	Questionnaire	P_MCQ	MCQ160L	
Hepatitis B	Laboratory	P_HEPBD	LBXHBC	History of Hepatitis B
Hepatitis C	Laboratory	P_HEPC	LBDHCI	History of Hepatitis C
Chronic Lung Condition	Questionnaire	P_MCQ	MCQ160P	History of COPD/Emphysema/Chronic Bronchitis
Thyroid Disease	Questionnaire	P_MCQ	MCQ160M	
Prescription Drug Use	Questionnaire	P_RXQ_RX	RXDUSE	

Table S1

3.6 FIGURE AND TABLE LEGENDS

3.6.1 *Figure 1. Clinical trial inclusion selection process.*

The diagram outlines the identification, screening, eligibility assessment, and inclusion of registered SARS-CoV-2 vaccine clinical trials used in this analysis.

3.6.2 *Table 1. Age-related characteristics of SARS-CoV-2 vaccine trials*

Mean participant age (SD) and total enrollment in SARS-CoV-2 vaccine clinical trials, stratified by trial phase. The table also summarizes the proportion of trails that reported key age-related characteristics.

3.6.3 *Table 2. Estimated age distribution of participants in SARS-CoV-2 vaccine clinical trials.*

Estimates are derived using truncated normal distributions based on reported mean age, standard deviation, and total enrollment, incorporating trial-specific lower and upper age limits. Age groups reflect clinically relevant older adult subcategories.

3.6.4 *Figure 2. Proportional representation versus COVID-19 mortality by age*

Participation estimates were generated using truncated normal distributions with trial-specific age limits, based on reported mean age, standard deviation, and enrollment per trial. Mortality data represent total COVID-19 deaths by age group as reported by the CDC from January 1, 2020 to June 14, 2023. [1] COVID-19 mortality was significantly higher than clinical trial participation for all age groups ≥65 ($p<0.001$). [2] Clinical trial participation was significantly higher than COVID-19 mortality among participants <65 years ($p <0.001$). [3] Differences between trial participation and mortality were significant across all age groups ($p<0.001$).

3.6.5 *Table 3. Exclusion of common chronic conditions among older adults in clinical trials compared to U.S. prevalence*

The table presents the top 10 chronic conditions affecting older adults in the U.S., as identified by the National Council on Aging, alongside the number of SARS-CoV-2 vaccine trials that listed each condition as an exclusion criterion, stratified by trial phase. Exclusion frequencies were extracted from trial eligibility criteria and categorized by condition. U.S prevalence estimates are based on NHANES 2017-2020 data for adults aged <65 and ≥65, where available.

3.6.6 *Table 4. Common exclusion criteria in clinical trials compared to U.S. prevalence*

The table presents frequently listed exclusion criteria across SARS-CoV-2 vaccine trials, along with the number of trials that excluded each condition, stratified by age. U.S. prevalence estimates are based on NHANES 2017-2020 data for adults aged <65 and ≥65, where available.

3.7 SUPPLEMENTAL FIGURE LEGENDS

3.7.1 Figure S1. *Comparison of estimated age distribution of participants in SARS-CoV-2 vaccine clinical trials and the U.S. population.*

Participation estimates were generated using truncated normal distributions with trial-specific age limits, based on reported mean age, standard deviation, and enrollment per trial. U.S. population estimates by age group were based on the 2023 U.S. Census Bureau data. [1] For all age groups ≥65, the proportion of individuals in the U.S. population was significantly higher than their representation in clinical trials ($p<0.001$). [2] Individuals <65 were significantly overrepresented in clinical trials compared to their proportion in the U.S. population ($p <0.001$). [3] Differences between trial participation and population distribution were statistically significant across all age groups ($p<0.001$).

3.7.2 *Figure S2. Correlation between estimated and reported age group proportions among participants in SARS-CoV-2 vaccine clinical trials.*

Each scatterplot shows the relationship between the estimated and reported proportion of participants in each age group, using only trials that reported the true values. Estimated proportions were derived using truncated normal distributions based on each trial's mean age, standard deviation, and enrollment size. Age groups reflect clinically relevant older adult subcategories.

3.7.3 *Figure S3. Prevalence of the top 10 chronic conditions affecting older adults in the U.S.*

Prevalence estimates were obtained from 2017-2020 NHANES data and stratified by age. Weighted estimates reflect the population-level burden across clinically relevant older adult subcategories. Conditions were selected based on National Council on Aging (NCOA) reports identifying the most common chronic conditions among adults aged ≥65.

3.7.4 *Figure S4. Prevalence of common exclusion criteria among U.S. adults.*

Prevalence estimates were obtained from 2017-2020 NHANES data and stratified by age. Weighted estimates reflect the population-level burden across clinically relevant older adult subcategories. Conditions were identified as frequently listed exclusion criteria across SARS-CoV-2 vaccine trials.

3.7.5 *Table S1. NHANES variables used to estimate U.S. prevalence of exclusion criteria.*

This table summarizes the NHANES source file, variable(s), and definition used to estimate the prevalence of exclusion criteria included in the analysis. Where applicable, notes clarify how

each condition was operationalized based on available NHANES data from the 2017-2020 pre-pandemic cycle.

Chapter 4. METHODS

4.1 CHAPTER 1 METHODS

4.1.1 *Experimental design*

The experiments reported in this study were performed in human lung epithelial cells, Calu-3 and HSAEC1-KT, using an identical protocol. Prior to the experiment, human ACE2 gene was stably introduced into parental HSAEC1-KT cells using a lentivirus system followed by cell sorting. We evaluated the effect of both IFN-β and SARS-CoV-2(WA1) on Calu-3 and HSAEC1-KT cells. Furthermore, we investigated the effect of IFN-β administration 24 hours before and 24 hours after SARS-CoV-2 infection. Cells were treated with IFN-β at 10, 100, or 1000 IU/mL. SARS-CoV-2 Isolate USA-WA1/2020 was derived from BEI Resources. Viral infections were performed as previously described [28]. Three biological replicates were harvested at each time point for each treatment group. Supernatant was collected from each sample for transcriptomic analysis.

4.1.2 *Cell culture*

Human lung adenocarcinoma cell line Calu-3 and immortalized normal human lung-derived small airway epithelium cell line HSAEC1-KT were obtained from The American Type Culture Collection (ATCC) (Manassas, VA, USA). Calu-3 cells were cultured in Opti-MEM supplemented with 4% fetal bovine serum, 20 mM HEPES, 10 mM GlutaMAX (Gibco Catalog No. 35050), and 1X penicillin-streptomycin. HSAEC1-KT were cultured in Small Airway Epithelial Cell Growth Medium (MilliporeSigma, St. Louis, MO, USA) supplemented with

penicillin-streptomycin. Both cells were split using trypsin (0.05%) in phosphate-buffered saline (PBS) following PBS wash.

4.1.3 *Viral preparation*

All experiments using live virus were performed in the Biosafety Level-3 (BSL-3) facility at the University of Washington in compliance with the BSL-3 laboratory safety protocols (CDC BMBL 5th ed.) and the recent CDC guidelines for handling SARS-CoV-2. The preparation of SARS-CoV-2 was described previously. [28] In brief, SARS-Related Coronavirus 2, Isolate USA-WA1/2020 (SARS-CoV-2) was obtained from BEI Resources (NR-52281) and propagated in VERO cells (USAMRIID), and the concentrated viral stock was stored at -80 °C.

4.1.4 *Plaque assay*

Viral preparations and culture supernatant from SARS-CoV-2-infected epithelial cells were titered using a plaque assay. Briefly, Vero cells (250,000 cells/well) were seeded in a 12-well plate and incubated for 1 h at 37 °C with serial 10-fold dilutions of virus-containing media. A solution of 1:1 2.4% Avecil-RC-591 and 2X DMEM supplemented with 4% heat-inactivated FBS, L-glutamine, 1X penicillin-streptomycin (Gibco), and 220 mg/mL sodium pyruvate was layered on top of the cells, followed by incubation at 37 °C for 48 h. After washing PBS and fixing the cells with 10% formaldehyde, the layer was removed, and cells were stained with 1% crystal violet solution in 20% ethanol. Plaques were counted, and the virus titer in the original sample was assessed as plaque formation unit per mL (PFU/mL).

4.1.5 *Viral infection*

Calu-3 and HSAEC1-KT/ACE2 cells were seeded into 6-, 12- or 96-well plates. After 2 days, the cells were infected with diluted SARS-CoV-2 (MOI = 5) in Opti-MEM and incubated for 1 h at

37 °C. (non-infected [mock] control cells were incubated without virus). Cells were then washed with PBS and cultured in the culture medium for the indicated times.

4.1.6 *Cell viability assay*

Calu-3 and HSAEC1-KT/ACE2 cells (5 x10^3 cells/well) were seeded to an optical-bottom plate (Thermo Scientific™) and were incubated for 48 h. For the IFN-β followed by SARS-CoV-2 infection group, cells were incubated in a fresh culture medium in the presence of various concentration of IFN-β (0, 10, 100, and 1000 IU/mL) for 24 h. Cells were then infected with SARS-CoV-2 (MOI = 5) for 1h. After infection, the cells were further incubated for 72 h. For the SARS-CoV-2 infection followed by IFN-β treatment group, cell viability was assayed with Real-time Glo reagent (Promega). Relative percentages of cell viability were calculated after normalization to a mock treatment group.

4.1.7 *Immunoblot*

Cells were lysed with RIPA Buffer (25 mM Tris, 1mM EDTA, 1% Triton X100, 150 mM NaCl) supplemented with protease inhibitor (Sigma-Aldrich) and phosphatase inhibitor cocktail (Sigma-Aldrich) on ice for 15 min. Lysates were then centrifuged at 20,000 g for 10 min at 4 °C. Protein concentration was measured with Bradford Assay (Bio-Rad). Immune complexes were detected using SuperSignal™ West Pico PLUS Chemiluminescent Substrate (Thermofisher-Life Technologies) and band intensities were measured using a ChemiDoc Imaging Systems (Bio-Rad, Hercules, CA, USA). Each blot was independently performed for three times. Relative protein levels were calculated after normalization to an internal standard, β-actin.

4.1.8 *RT-qPCR*

Cells were washed once with PBS and incubated with 300 µL per well of RNA lysis buffer (Zymo Research, Irvine, CA 92614, USA) for 10 min at room temperature. The lysates were

stored at -80 °C until further use. RNA was extracted using Quick-RNA kit (Zymo). cDNA was prepared with iScript cDNA synthesis kit (Bio-Rad). qPCR for virus detection was performed with Premix Ex Taq™ (TaKaRa, Shiga, Japan). Using 10 ng of cDNA and 400 nM of each primer and a specific probe labelled with a dye label (FAM) on the 5' end and a minor groove binder (MGB) and non-fluorescent quencher (NFQ) on the 3' end. qPCR was run on a ViiA 7 Real-Time PCR System (Thermofisher-Life Technologies). Data was analyzed using the ΔΔCt method. Gene expression of *GAPDH* was used as an internal control.

4.1.9 *Bulk RNA sequencing*

For each cell line, we designed experimental groups for transcriptomic analysis as follows; (i) IFN-β treatment (0, 10, 100, and 1000 IU/mL) for 0, 6, 12, 24, and 48 h, (ii) SARS-CoV-2 infection (MOI=5) for 0, 6, 12, 24 and 48 hpi, (iii) IFN-β treatment (0, 10, 100, and 1000 IU/mL) for 24 h followed by SARS-CoV-2 infection (MOI = 5) for 0, 6, 12, 24, and 48 hpi, and (iv) SARS-CoV-2 infection (MOI = 5) for 24 h followed by IFN-β treatment (0, 10, 100, and 1000 IU/mL) for 30, 36, 48, and 72 hpi. Total RNA was extracted from the cells as described above. Bulk mRNA-seq data were generated by constructing mRNA-seq libraries using the KAPA mRNA HyperPrep kit (Kapa Biosystems). 250 ng of RNA was used for Calu-3 cells and 180 ng of RNA was used for ACE2/HSAEC1-KT cells. The RNA and resulting libraries were quality controlled and quantified using a 4200 TapeStation System (Agilent Technologies, Inc.) and a Qubit Fluorometer (Invitrogen). Libraries were sequenced on an Illumina NovaSeq using S2 v1.5 200 cycle flow cell which generates paired-end reads of one hundred nucleotides. Each sample was sequenced to a minimum of twenty million mapped reads.

4.1.10 *Differential gene expression analysis*

Identical bioinformatic analyses were completed on the Calu-3 and HSAEC1-KT/ACE2 samples using the R statistical programming language (v 4.3.1). Genes with less than ten raw counts averaged across all samples were removed. Counts were normalized using Trimmed Mean of M-values (TMM) via edgeR [29] and transformed into $\log_2$ CPM with the voom function in the R library *limma* [30]. Differential expression analysis was performed using the *lmFit* function in *limma* to test the following comparisons at matched time points: (i) IFN-β treatment relative to mock, (ii) SARS-CoV-2 infection relative to mock, (iii) IFN-β treatment 24 h before SARS-CoV-2 infection relative to SARS-CoV-2 infection, and (iv) IFN-β treatment 24 h after SARS-CoV-2 infection relative to SARS-CoV-2 infection. Genes with a Benjamini-Hocberg (BH)-adjusted p-value of ≤ 0.01 and absolute $\log_2$ fold change (LFC) above 1 in at least one time point were considered significantly differentially expressed (DE). We also ran DE analysis on the public dataset GSE171110 to obtain LFCs of genes associated with severe COVID-19 compared to healthy controls.

4.1.11 *Principal component analysis*

The prcomp function from the R library *stats* was used to perform principal component analysis (PCA) on the transformed $\log_2$ CPM using all genes that passed initial filtering.

4.1.12 *Pathway enrichment analyses*

The union of all differentially expressed genes were grouped into co-expression clusters using Ward clustering and Pearson distance on the LFC values using the *WGCNA* and *heatmap.2* packages in R[31,32] .Over-representation analysis (ORA) was performed on each cluster using WebGestaltR[33]. Functional categories among the Kyoto Encyclopedia of Genes and Genomes (KEGG) pathways, the non-redundant Gene Ontology database, and the Hallmark Community Contributed 50 database were tested for enrichment[34-36]. Upstream regulator analysis was

performed on the co-expression clusters of DE genes using QIAGEN Ingenuity Pathway Analysis (QIAGEN Inc., https://digitalinsights.qiagen.com/IPA). For each co-expression module, bar plots of highly significant pathways and bubble plots of significant upstream regulators were created using *ggplot2* [37]. For the IFN-β post-treatment networks, significant transcription factors (*STAT1*, *IRF3*, and *NONO*) were defined as central nodes interconnected with cell line-specific DE genes using IPA, in conjunction with Cytoscape[38].

4.1.13 *Weighted gene co-expression network analysis*

Weighted gene correlation network analysis (WGCNA) is a method used to identify modules of co-expressed genes and their association with external traits of interest. To identify a viral-load associated gene signature in lung epithelial cells, we used the *WGCNA* R package to construct a gene co-expression network and correlated these modules to SARS-CoV-2 viral reads across all samples. We identified a highly correlated co-expression module, whose eigengene showed a significant association with viral load. A scatterplot of Gene Significance (GS) vs. Module Membership (MM) confirmed that hub genes within this module were highly correlated with viral reads.

4.1.14 *Additional analyses*

The average gene expression of each ISG cluster was presented as line plots using *ggplot2*[37]. When IFN-β treatment was present, the average expression was calculated using the LFC values from the 100 IU/ml dose. A curated list of cytokines including various interleukins and interferons was generated using public literature. Cytokines with more than ten raw counts averaged across all samples were transformed using the ntile function from the *dplyr* R package[39]. Heatmaps displaying normalized cytokine expression values were also created using *ggplot2*[37]. Lollipop plots of normalized gene counts for the viral-load associated gene signature

and box plots of normalized gene counts for severe COVID-19 patients vs. healthy controls (GSE17110) were created using ggplot2.[37] Statistically significant differences are indicated by *p<0.05, **p<0.001, ***p<0.001, ****p<0.0001.

4.2 CHAPTER 2 METHODS

4.2.1 *Experimental design*

Lung samples from C57BL/6 mice infected with SARS-CoV-2 were collected and prepared for RNA-sequencing as previously described in Davis et al. (2022)[23]. Processing of the raw read counts was conducted in-house. Our analysis began with the normalized count matrix and focused on differential expression, co-expression network analysis, pathway enrichment, and cell-type deconvolution to characterize age-associated immune responses during infection.

4.2.2 *Data processing and differential gene expression analysis*

All bioinformatic analyses were conducted in R using RStudio (v2024.12.0.467). Genes with low expression were filtered prior to normalization. After transforming raw counts to counts per million (CPM), genes with CPM >2 greater in at least three samples were retained. Normalization was performed using the trimmed mean of M-values (TMM) method implemented in *edgeR* package[27]. Differential expression (DE) analysis was performed using the *limma* package with voom transformation to model the mean-variance relationship of log-transformed expression values[28]. Contrasts were fit using contrasts.fit and empirical Bayes moderation (eBayes) with robust estimated was applied. DEGs were identified using decideTests with a Benjamini-Hochberg (BH)-adjusted p-value of ≤0.01 and absolute $\log_2$ fold change (LFC) ≥ 1 in at least one time point.

4.2.3 *Pathway enrichment analyses*

The union of all differentially expressed genes were grouped into co-expression clusters using Ward's D2 hierarchal clustering and Pearson distance on the LFC values using *WGCNA* and *heatmap.2* packages[29,30]. Over-representation analysis (ORA) was performed on each cluster using *WebGestaltR*[31]. Functional categories among the Kyoto Encyclopedia of Genes and Genomes (KEGG) pathways and the non-redundant Gene Ontology (GO) database[32,33]. To reduce redundancy in pathway enrichment results, a custom function was implemented to filter overlapping gene sets. Pathways with ≥75% overlap in genes relative to the smaller gene set were compared, and the term with the higher false discovery rate (FDR) was removed. Pathways unique to a single co-expression cluster were further selected and visualized as dotplots using *ggplot2*[34]. Upstream regulator analysis was performed on the co-expression clusters of DEGs using QIAGEN Ingenuity Pathway Analysis (IPA) (QIAGEN Inc., https://digitalinsights.qiagen.com/IPA). *De novo* networks were created using IPA's curated knowledge base to predict connections between top upstream regulators and DEGs. Cytoscape was used for network visualization[35].

4.2.4 *Immune cell-type deconvolution*

Immune cell composition was estimated using *CIBERSORT* with a mouse-specific ImmuCC signature matrix[36,37]. CPM-normalized, non-log transformed lung expression values were used as input, with quantile normalization disabled and 100 permutations performed. Immune cell composition was visualized using a heatmap of mean estimated cell type proportions across age groups, scaled by z-score across cell types. Cell types with no variance across groups were excluded. Rows and columns were clustered using Ward's D2 hierarchical clustering and visualized using *pheatmap*[38].

4.2.5 *Additional analyses*

Venn diagrams of DEGs were created using *ggVennDiagam*[39]. Average $\log_2$ fold change ($\log_2$FC) line plots, mock expression boxplots, and cell-type-specific proportion boxplots were also generated using *ggplot2*.

4.3 CHAPTER 3 METHODS

4.3.1 *Clinical trial selection*

The selection process is outlined in Figure 1. Clinical trials were identified using ClinicalTrials.gov by searching the condition/disease terms, “COVID-19”, “SARS-CoV-2”, and “COVID,” along with additional intervention-related terms including, “vaccine”, “vaccination”, “inoculation”, and “immunization.” The search was restricted to trials registered between November 1, 2019 and November 23, 2024. Phase I, observational, and non-randomized trials were excluded, resulting in an initial pool of 337 studies.

Each trial was reviewed for relevance and eligibility. We excluded studies that: (1) did not include adult participants, (2) focused exclusively on populations that implicitly excluded older adults (e.g., pregnant individuals, healthcare workers), (3) were withdrawn, not yet recruiting, recruiting, active but not recruiting, or terminated, (4) had fewer than 50 participants, or (5) were not SARS-CoV-2 vaccine trials. After applying these criteria, 156 trials remained.

We conducted a literature search to identify published data on participant enrollment and mean age for each study. Trials without publicly available information were excluded unless data could be obtained from study investigators. Of those contacted, only one investigator responded and provided the requested information. In total, 93 trials were included in the final analysis.

4.3.2 *Data extraction*

The following information was abstracted for each eligible study by a trained researcher (TJ): ClinicalTrials.gov identifier (NCT number), principal investigator, study title, study status,

intervention(s), outcome measures, study phase, design, sex, enrollment number, location(s), and study URL. For studies with publicly available enrollment data, additional variables were recorded, including: start date, actual enrollment number, participant gender distribution, reported mean age (SD), median age, participant age range, lower and upper age limits, and whether an explicit older adult inclusion criterion was present.

We also documented whether trials reported the proportion of older adults enrolled, stratified age group data, and whether age-adjusted analyses were conducted. When trials reported age-based proportions (e.g., <65, 65+, 65-74,), these were extracted into corresponding columns. From this, we derived discrete age bins (<65, 65-69, 70-74,75-79,≥80, and ≥65) for downstream comparisons with our estimated age proportions.

All inclusion and exclusion criteria were reviewed and recorded. Studies were flagged if they included criteria likely to disproportionately impact older adults, such as upper age limits or exclusions based on chronic conditions in aging populations (**Table 4**). We identified the top 10 chronic conditions identified by the National Council on Aging, as well as other factors such as history of COVID-19 vaccination or infection, transportation-related exclusions, technology access or literacy requirements, group-living exclusions, and frailty-related criteria. To do this, we analyzed free-text exclusion criteria from the 93 trials using a keyword tokenization and grouping approach. Terms were cleaned, tokenized, and grouped into clinically relevant exclusion categories to common patterns (e.g., “hepatic” and “liver” grouped under “Liver disease”).

4.3.3 *Trial participant age distribution*

The weighted mean age and pooled SD across all 93 trials were calculated using each trial’s reported mean age and actual enrollment number. The weighted mean reflects the average

participant age across trials, adjusted for sample size. The pooled SD represents the variability in mean age between trials, weighted by the number of participants in each study.

To estimate the proportion of participants in predefined older age subgroups, we used a truncated normal distribution to model the age distribution for each trial based on its reported mean age, SD, and trial-specific lower and upper age limits. Proportions of participants aged <65, 65-69, 70-74,75-79, and 80+ were calculated and aggregated across all trials. To validate this approach, we identified a subset of 46 trials that reported participant proportions within these discrete age groups. Estimated proportions were then compared to the reported values by age group. Pearson correlation analysis demonstrated a strong agreement between estimated and reported values (r range: 0.96-1, p <0.0001), supporting the reliability of our modeling approach.

4.3.4 *COVID-19 mortality by age*

To compare the proportion of older adults enrolled in SARS-CoV-2 vaccine trials to their representation in the U.S. population, we obtained 2023 U.S. age distribution estimates from the U.S. Census Bureau. We calculated the distribution of participants across the following age groups in both clinical trials and the U.S. population: <65, 65+, 65-74, 75-84, and 85+. We also compared trial age distributions to COVID-19 mortality by age group using data from the Centers for Disease Control and Prevention (CDC) “Deaths by Select Demographics and Geographic Characteristics ,” covering January 1, 2020 to June 14, 2023. To assess statistical significance, we used two-sample proportion tests to compare estimated trial participation proportions to both population and mortality proportions within each age group.

4.3.5 *U.S. Prevalence data comparisons*

We compared the top 10 chronic conditions affecting older adults, as defined by the NCOA, to their estimated prevalence in the U.S. population using data from the 2017-2020 National Health

and Nutrition Examination Survey (NHANES). When a direct match to NHANES variables was not available, the most appropriate proxy variable was used. A full list of NHANES variable IDs used in comparison analyses is provided in **Supplementary Table 1**.

Additionally, we compared the frequency of variables corresponding to the exclusion criteria previously reported to disproportionately affect older adult enrollment to estimated prevalence of these conditions in the U.S. population based on NHANES.

For estimates with corresponding NHANES variables, U.S. prevalence estimates were compared across the following age groups: <65, 65-69, 70-74, 75-79, and 80+. To assess statistical differences, we used two-sample tests for proportions to compare the prevalence in each older age group to the <65 reference group.

4.3.6 *Computational tools and data visualization*

Initial clinical trial filtering, statistical analyses, bar plot generation, scatterplots, and table formatting were performed in RStudio (version 2024.12.0.467) using R (version 4.4.1). Visualizations were created using the ggplot2 package (version 3.5.1), and summary tables were formatted with the gt package (version 0.11.1).

Chapter 5. References

5.1 CHAPTER 1 REFERENCES

1. Zhou, P., Yang, X.L., Wang, X.G., Hu, B., Zhang, L., Zhang, W., Si, H.R., Zhu, Y., Li, B., Huang, C.L., et al. (2020). A pneumonia outbreak associated with a new coronavirus of probable bat origin. Nature *579*, 270-273. 10.1038/s41586-020-2012-7.

2. Holshue, M.L., DeBolt, C., Lindquist, S., Lofy, K.H., Wiesman, J., Bruce, H., Spitters, C., Ericson, K., Wilkerson, S., Tural, A., et al. (2020). First Case of 2019 Novel Coronavirus in the United States. N Engl J Med *382*, 929-936. 10.1056/NEJMoa2001191.

3. Bedford, T., Greninger, A.L., Roychoudhury, P., Starita, L.M., Famulare, M., Huang, M.-L., Nalla, A., Pepper, G., Reinhardt, A., Xie, H., et al. (2020). Cryptic transmission of SARS-CoV-2 in Washington State. medRxiv, 2020.2004.2002.20051417. 10.1101/2020.04.02.20051417.

4. Chen, N., Zhou, M., Dong, X., Qu, J., Gong, F., Han, Y., Qiu, Y., Wang, J., Liu, Y., Wei, Y., et al. (2020). Epidemiological and clinical characteristics of 99 cases of 2019 novel coronavirus pneumonia in Wuhan, China: a descriptive study. Lancet *395*, 507-513. 10.1016/S0140-6736(20)30211-7.

5. Gottlieb, M., Sansom, S., Frankenberger, C., Ward, E., and Hota, B. (2020). Clinical Course and Factors Associated With Hospitalization and Critical Illness Among COVID-19 Patients in Chicago, Illinois. Acad Emerg Med *27*, 963-973. 10.1111/acem.14104.

6. Report of the WHO - China Joint Mission on Coronavirus Disease 2019 (COVID-19). (2020). World Health Organization. 16-24 February 2020. https://www.who.int/docs/default-source/coronaviruse/who-china-joint-mission-on-covid-19-final-report.pdf.

7. Zhang, J.J., Dong, X., Liu, G.H., and Gao, Y.D. (2023). Risk and Protective Factors for COVID-19 Morbidity, Severity, and Mortality. Clin Rev Allergy Immunol *64*, 90-107. 10.1007/s12016-022-08921-5.

8. Mehta, P., McAuley, D.F., Brown, M., Sanchez, E., Tattersall, R.S., and Manson, J.J. (2020). COVID-19: consider cytokine storm syndromes and immunosuppression. Lancet *395*, 1033-1034. 10.1016/s0140-6736(20)30628-0.

9. Ye, Q., Wang, B., and Mao, J. (2020). The pathogenesis and treatment of the `Cytokine Storm' in COVID-19. J Infect *80*, 607-613. 10.1016/j.jinf.2020.03.037.

10. Hadjadj, J., Yatim, N., Barnabei, L., Corneau, A., Boussier, J., Smith, N., Péré, H., Charbit, B., Bondet, V., Chenevier-Gobeaux, C., et al. (2020). Impaired type I interferon activity and inflammatory responses in severe COVID-19 patients. Science *369*, 718-724. 10.1126/science.abc6027.

11. Blanco-Melo, D., Nilsson-Payant, B.E., Liu, W.C., Uhl, S., Hoagland, D., Moller, R., Jordan, T.X., Oishi, K., Panis, M., Sachs, D., et al. (2020). Imbalanced Host Response to SARS-CoV-2 Drives Development of COVID-19. Cell *181*, 1036-1045 e1039. 10.1016/j.cell.2020.04.026.

12. Channappanavar, R., Fehr, A.R., Vijay, R., Mack, M., Zhao, J., Meyerholz, D.K., and Perlman, S. (2016). Dysregulated Type I Interferon and Inflammatory Monocyte-Macrophage Responses Cause Lethal Pneumonia in SARS-CoV-Infected Mice. Cell Host Microbe *19*, 181-193. 10.1016/j.chom.2016.01.007.

13. Shaw, A.C., Goldstein, D.R., and Montgomery, R.R. (2013). Age-dependent dysregulation of innate immunity. Nat Rev Immunol *13*, 875-887. 10.1038/nri3547.

14. Yang, L., Xie, X., Tu, Z., Fu, J., Xu, D., and Zhou, Y. (2021). The signal pathways and treatment of cytokine storm in COVID-19. Signal Transduct Target Ther *6*, 255. 10.1038/s41392-021-00679-0.

15. Mangalmurti, N., and Hunter, C.A. (2020). Cytokine Storms: Understanding COVID-19. Immunity *53*, 19-25. 10.1016/j.immuni.2020.06.017.

16. Janeway, C.A., Jr., and Medzhitov, R. (2002). Innate immune recognition. Annu Rev Immunol *20*, 197-216. 10.1146/annurev.immunol.20.083001.084359.

17. Yamada, T., and Takaoka, A. (2023). Innate immune recognition against SARS-CoV-2. Inflamm Regen *43*, 7. 10.1186/s41232-023-00259-5.

18. Schneider, W.M., Chevillotte, M.D., and Rice, C.M. (2014). Interferon-stimulated genes: a complex web of host defenses. Annu Rev Immunol *32*, 513-545. 10.1146/annurev-immunol-032713-120231.

19. Mesev, E.V., LeDesma, R.A., and Ploss, A. (2019). Decoding type I and III interferon signalling during viral infection. Nat Microbiol *4*, 914-924. 10.1038/s41564-019-0421-x.

20. Viox, E.G., Hoang, T.N., Upadhyay, A.A., Nchioua, R., Hirschenberger, M., Strongin, Z., Tharp, G.K., Pino, M., Nguyen, K., Harper, J.L., et al. (2023). Modulation of type I interferon responses potently inhibits SARS-CoV-2 replication and inflammation in rhesus macaques. Sci Immunol *8*, eadg0033. 10.1126/sciimmunol.adg0033.

21. AbdelHamid, S.G., Refaat, A.A., Benjamin, A.M., Elmawardy, L.A., Elgendy, L.A., Manolly, M.M., Elmaksoud, N.A., Sherif, N., and Hamdy, N.M. (2021). Deciphering epigenetic(s) role in modulating susceptibility to and severity of COVID-19 infection and/or outcome: a systematic rapid review. Environ Sci Pollut Res Int *28*, 54209-54221. 10.1007/s11356-021-15588-6.

22. Behura, A., Naik, L., Patel, S., Das, M., Kumar, A., Mishra, A., Nayak, D.K., Manna, D., Mishra, A., and Dhiman, R. (2023). Involvement of epigenetics in affecting host immunity during SARS-CoV-2 infection. Biochim Biophys Acta Mol Basis Dis *1869*, 166634. 10.1016/j.bbadis.2022.166634.

23. Woods, E., Mena, A., Sierpinska, S., Carr, E., Sttar, B., Hagan, R., Crowley, J., Bergin, C., Clark, D., Brophy, C., et al. (2024). Reduced IFNL1 and/or IFNL2, but not IFNL3 is associated with worse outcome in patients with COVID-19. Clin Exp Immunol *218*, 300-307. 10.1093/cei/uxae047.

24. Jabeen, A., Ahmad, N., and Raza, K. (2022). Global Gene Expression and Docking Profiling of COVID-19 Infection. Front Genet *13*, 870836. 10.3389/fgene.2022.870836.

25. Lu, L., Liu, L.P., Gui, R., Dong, H., Su, Y.R., Zhou, X.H., and Liu, F.X. (2022). Discovering common pathogenetic processes between COVID-19 and sepsis by bioinformatics and system biology approach. Front Immunol *13*, 975848. 10.3389/fimmu.2022.975848.

26. deAndres-Galiana, E.J., Fernandez-Martinez, J.L., Alvarez-Machancoses, O., Bea, G., Galmarini, C.M., and Kloczkowski, A. (2022). Analysis of transcriptomic responses to SARS-CoV-2 reveals plausible defective pathways responsible for increased susceptibility to infection and complications and helps to develop fast-track repositioning of drugs against COVID-19. Comput Biol Med *149*, 106029. 10.1016/j.compbiomed.2022.106029.

27. Takashima, Y., Inaba, T., Matsuyama, T., Yoshii, K., Tanaka, M., Matsumoto, K., Sudo, K., Tokuda, Y., Omi, N., Nakano, M., et al. (2024). Potential marker subset of blood-circulating cytokines on hematopoietic progenitor-to-Th1 pathway in COVID-19. Front Med (Lausanne) *11*, 1319980. 10.3389/fmed.2024.1319980.

28. Marchiano, S., Hsiang, T.Y., Khanna, A., Higashi, T., Whitmore, L.S., Bargehr, J., Davaapil, H., Chang, J., Smith, E., Ong, L.P., et al. (2021). SARS-CoV-2 Infects Human Pluripotent Stem Cell-Derived Cardiomyocytes, Impairing Electrical and Mechanical Function. Stem Cell Reports *16*, 478-492. 10.1016/j.stemcr.2021.02.008.

29. Robinson, M.D., McCarthy, D.J., and Smyth, G.K. (2010). edgeR: a Bioconductor package for differential expression analysis of digital gene expression data. Bioinformatics *26*, 139-140. 10.1093/bioinformatics/btp616.

30. Law, C.W., Chen, Y., Shi, W., and Smyth, G.K. (2014). voom: Precision weights unlock linear model analysis tools for RNA-seq read counts. Genome Biol *15*, R29. 10.1186/gb-2014-15-2-r29.

31. Wan, Q., Tang, J., Han, Y., and Wang, D. (2018). Co-expression modules construction by WGCNA and identify potential prognostic markers of uveal melanoma. Exp Eye Res *166*, 13-20. 10.1016/j.exer.2017.10.007.

32. Langfelder, P., and Horvath, S. (2008). WGCNA: an R package for weighted correlation network analysis. BMC Bioinformatics *9*, 559. 10.1186/1471-2105-9-559.

33. Wang, J., Duncan, D., Shi, Z., and Zhang, B. (2013). WEB-based GEne SeT AnaLysis Toolkit (WebGestalt): update 2013. Nucleic Acids Res *41*, W77-83. 10.1093/nar/gkt439.

34. Kanehisa, M., Furumichi, M., Tanabe, M., Sato, Y., and Morishima, K. (2017). KEGG: new perspectives on genomes, pathways, diseases and drugs. Nucleic Acids Res *45*, D353-D361. 10.1093/nar/gkw1092.

35. Liberzon, A., Birger, C., Thorvaldsdottir, H., Ghandi, M., Mesirov, J.P., and Tamayo, P. (2015). The Molecular Signatures Database (MSigDB) hallmark gene set collection. Cell Syst *1*, 417-425. 10.1016/j.cels.2015.12.004.

36. Ashburner, M., Ball, C.A., Blake, J.A., Botstein, D., Butler, H., Cherry, J.M., Davis, A.P., Dolinski, K., Dwight, S.S., Eppig, J.T., et al. (2000). Gene ontology: tool for the unification of biology. The Gene Ontology Consortium. Nat Genet *25*, 25-29. 10.1038/75556.

37. Wickham, H. (2016). ggplot2: Elegant Graphics for Data Analysis (Springer-Verlag).

38. Shannon, P., Markiel, A., Ozier, O., Baliga, N.S., Wang, J.T., Ramage, D., Amin, N., Schwikowski, B., and Ideker, T. (2003). Cytoscape: a software environment for integrated models of biomolecular interaction networks. Genome Res *13*, 2498-2504. 10.1101/gr.1239303.

39. Wickham, H., François, R., Henry, L., Müller, K., and Vaughan, D. (2023). dplyr: A Grammar of Data Manipulation.

5.2 CHAPTER 2 REFERENCES

1. World Health Organization (2025). WHO Coronavirus (COVID-19) Dashboard. https://data.who.int/dashboards/covid19.

2. Prevention, U.S.C.f.D.C.a. (2023). Deaths by Select Demographic and Geographic Characteristics. https://www.cdc.gov/nchs/nvss/vsrr/covid_weekly/index.htm.

3. Bureau, U.S.C. (2023). American Community Survey 5-Year Estimates Subject Tables, Table S0101, 2023. https://data.census.gov/table/ACSST5Y2023.S0101?q=people.

4. World Health Organization (2017). Global Strategy and Action Plan on Ageing and Health. World Health Organization. https://www.who.int/publications/i/item/global-strategy-and-action-plan-on-ageing-and-health.

5. Langer, J., Welch, V.L., Moran, M.M., Cane, A., Lopez, S.M.C., Srivastava, A., Enstone, A.L., Sears, A., Markus, K.J., Heuser, M., et al. (2023). High Clinical Burden of Influenza Disease in Adults Aged >/= 65 Years: Can We Do Better? A Systematic Literature Review. Adv Ther *40*, 1601-1627. 10.1007/s12325-023-02432-1.

6. Prevention, C.f.D.C.a. (2024). Flu and People 65 Years and Older. https://www.cdc.gov/flu/highrisk/65over.htm.

7. Prevention, C.f.D.C.a. (2024). Preliminary Estimated Flu Disease Burden 2023-2024 Flu Season. https://www.cdc.gov/flu-burden/php/data-vis/2023-2024.html.

8. Prevention, C.f.D.C.a. (2024). RSV in Older Adults. https://www.cdc.gov/rsv/older-adults/.

9. Bucholc, M., Bradley, D., Bennett, D., Patterson, L., Spiers, R., Gibson, D., Van Woerden, H., and Bjourson, A.J. (2022). Identifying pre-existing conditions and multimorbidity patterns associated with in-hospital mortality in patients with COVID-19. Sci Rep *12*, 17313. 10.1038/s41598-022-20176-w.

10. Ovadya, Y., Landsberger, T., Leins, H., Vadai, E., Gal, H., Biran, A., Yosef, R., Sagiv, A., Agrawal, A., Shapira, A., et al. (2018). Impaired immune surveillance accelerates accumulation of senescent cells and aging. Nat Commun *9*, 5435. 10.1038/s41467-018-07825-3.

11. Yoshida, K., Cologne, J.B., Cordova, K., Misumi, M., Yamaoka, M., Kyoizumi, S., Hayashi, T., Robins, H., and Kusunoki, Y. (2017). Aging-related changes in human T-cell repertoire over 20years delineated by deep sequencing of peripheral T-cell receptors. Exp Gerontol *96*, 29-37. 10.1016/j.exger.2017.05.015.

12. Martin, V., Bryan Wu, Y.C., Kipling, D., and Dunn-Walters, D. (2015). Ageing of the B-cell repertoire. Philos Trans R Soc Lond B Biol Sci *370*. 10.1098/rstb.2014.0237.

13. Kruglikov, I.L., and Scherer, P.E. (2018). Skin aging as a mechanical phenomenon: The main weak links. Nutr Healthy Aging *4*, 291-307. 10.3233/NHA-170037.

14. Huang, J., Xie, Y., Sun, X., Zeh, H.J., 3rd, Kang, R., Lotze, M.T., and Tang, D. (2015). DAMPs, ageing, and cancer: The 'DAMP Hypothesis'. Ageing Res Rev *24*, 3-16. 10.1016/j.arr.2014.10.004.

15. Aprahamian, T., Takemura, Y., Goukassian, D., and Walsh, K. (2008). Ageing is associated with diminished apoptotic cell clearance in vivo. Clin Exp Immunol *152*, 448-455. 10.1111/j.1365-2249.2008.03658.x.

16. Tseng, C.W., Kyme, P.A., Arruda, A., Ramanujan, V.K., Tawackoli, W., and Liu, G.Y. (2012). Innate immune dysfunctions in aged mice facilitate the systemic dissemination of methicillin-resistant S. aureus. PLoS One *7*, e41454. 10.1371/journal.pone.0041454.

17. Wenisch, C., Patruta, S., Daxbock, F., Krause, R., and Horl, W. (2000). Effect of age on human neutrophil function. J Leukoc Biol *67*, 40-45. 10.1002/jlb.67.1.40.

18. van Beek, A.A., Van den Bossche, J., Mastroberardino, P.G., de Winther, M.P.J., and Leenen, P.J.M. (2019). Metabolic Alterations in Aging Macrophages: Ingredients for Inflammaging? Trends Immunol *40*, 113-127. 10.1016/j.it.2018.12.007.

19. Gayoso, I., Sanchez-Correa, B., Campos, C., Alonso, C., Pera, A., Casado, J.G., Morgado, S., Tarazona, R., and Solana, R. (2011). Immunosenescence of human natural killer cells. J Innate Immun *3*, 337-343. 10.1159/000328005.

20. Santoro, A., Bientinesi, E., and Monti, D. (2021). Immunosenescence and inflammaging in the aging process: age-related diseases or longevity? Ageing Res Rev *71*, 101422. 10.1016/j.arr.2021.101422.

21. Leist, S.R., Dinnon, K.H., 3rd, Schafer, A., Tse, L.V., Okuda, K., Hou, Y.J., West, A., Edwards, C.E., Sanders, W., Fritch, E.J., et al. (2020). A Mouse-Adapted SARS-CoV-2 Induces Acute Lung Injury and Mortality in Standard Laboratory Mice. Cell *183*, 1070-1085 e1012. 10.1016/j.cell.2020.09.050.

22. Dinnon, K.H., 3rd, Leist, S.R., Schafer, A., Edwards, C.E., Martinez, D.R., Montgomery, S.A., West, A., Yount, B.L., Jr., Hou, Y.J., Adams, L.E., et al. (2020). A mouse-adapted model of SARS-CoV-2 to test COVID-19 countermeasures. Nature *586*, 560-566. 10.1038/s41586-020-2708-8.

23. Davis, M.A., Voss, K., Turnbull, J.B., Gustin, A.T., Knoll, M., Muruato, A., Hsiang, T.Y., Dinnon Iii, K.H., Leist, S.R., Nickel, K., et al. (2022). A C57BL/6 Mouse Model of SARS-CoV-2 Infection Recapitulates Age- and Sex-Based Differences in Human COVID-19 Disease and Recovery. Vaccines (Basel) *11*. 10.3390/vaccines11010047.

24. Zhang, Y., Huang, K., Wang, T., Deng, F., Gong, W., Hui, X., Zhao, Y., He, X., Li, C., Zhang, Q., et al. (2021). SARS-CoV-2 rapidly adapts in aged BALB/c mice and induces typical pneumonia. J Virol *95*. 10.1128/JVI.02477-20.

25. Gu, H., Chen, Q., Yang, G., He, L., Fan, H., Deng, Y.Q., Wang, Y., Teng, Y., Zhao, Z., Cui, Y., et al. (2020). Adaptation of SARS-CoV-2 in BALB/c mice for testing vaccine efficacy. Science *369*, 1603-1607. 10.1126/science.abc4730.

26. Ma, L., Lin, X., Xu, M., Ke, X., Liu, D., and Chen, Q. (2025). Exploring the biological mechanisms of severe COVID-19 in the elderly: Insights from an aged mouse model. Virulence *16*, 2487671. 10.1080/21505594.2025.2487671.

27. Robinson, M.D., McCarthy, D.J., and Smyth, G.K. (2010). edgeR: a Bioconductor package for differential expression analysis of digital gene expression data. Bioinformatics *26*, 139-140. 10.1093/bioinformatics/btp616.

28. Ritchie, M.E., Phipson, B., Wu, D., Hu, Y., Law, C.W., Shi, W., and Smyth, G.K. (2015). limma powers differential expression analyses for RNA-sequencing and microarray studies. Nucleic Acids Res *43*, e47. 10.1093/nar/gkv007.

29. Wan, Q., Tang, J., Han, Y., and Wang, D. (2018). Co-expression modules construction by WGCNA and identify potential prognostic markers of uveal melanoma. Exp Eye Res *166*, 13-20. 10.1016/j.exer.2017.10.007.

30. Langfelder, P., and Horvath, S. (2008). WGCNA: an R package for weighted correlation network analysis. BMC Bioinformatics *9*, 559. 10.1186/1471-2105-9-559.

31. Wang, J., Duncan, D., Shi, Z., and Zhang, B. (2013). WEB-based GEne SeT AnaLysis Toolkit (WebGestalt): update 2013. Nucleic Acids Res *41*, W77-83. 10.1093/nar/gkt439.

32. Kanehisa, M., Furumichi, M., Tanabe, M., Sato, Y., and Morishima, K. (2017). KEGG: new perspectives on genomes, pathways, diseases and drugs. Nucleic Acids Res *45*, D353-D361. 10.1093/nar/gkw1092.

33. Ashburner, M., Ball, C.A., Blake, J.A., Botstein, D., Butler, H., Cherry, J.M., Davis, A.P., Dolinski, K., Dwight, S.S., Eppig, J.T., et al. (2000). Gene ontology: tool for the unification of biology. The Gene Ontology Consortium. Nat Genet *25*, 25-29. 10.1038/75556.

34. Wickham, H. (2016). ggplot2: Elegant Graphics for Data Analysis (Springer-Verlag).

35. Shannon, P., Markiel, A., Ozier, O., Baliga, N.S., Wang, J.T., Ramage, D., Amin, N., Schwikowski, B., and Ideker, T. (2003). Cytoscape: a software environment for integrated models of biomolecular interaction networks. Genome Res *13*, 2498-2504. 10.1101/gr.1239303.

36. Newman, A.M., Liu, C.L., Green, M.R., Gentles, A.J., Feng, W., Xu, Y., Hoang, C.D., Diehn, M., and Alizadeh, A.A. (2015). Robust enumeration of cell subsets from tissue expression profiles. Nat Methods *12*, 453-457. 10.1038/nmeth.3337.

37. Chen, Z., Huang, A., Sun, J., Jiang, T., Qin, F.X., and Wu, A. (2017). Inference of immune cell composition on the expression profiles of mouse tissue. Sci Rep *7*, 40508. 10.1038/srep40508.

38. Kolde, R. (2018). pheatmap: Pretty Heatmaps.

39. Gao, C.H., Yu, G., and Cai, P. (2021). ggVennDiagram: An Intuitive, Easy-to-Use, and Highly Customizable R Package to Generate Venn Diagram. Front Genet *12*, 706907. 10.3389/fgene.2021.706907.

40. Rosenthal, N., Cao, Z., Gundrum, J., Sianis, J., and Safo, S. (2020). Risk Factors Associated With In-Hospital Mortality in a US National Sample of Patients With COVID-19. JAMA Netw Open *3*, e2029058. 10.1001/jamanetworkopen.2020.29058.

41. He, M., and Borlak, J. (2023). A genomic perspective of the aging human and mouse lung with a focus on immune response and cellular senescence. Immun Ageing *20*, 58. 10.1186/s12979-023-00373-5.

42. Hernandez, A.M., Mossman, J.A., Toapanta, F.R., Previte, D.M., Ross, T.M., and Nau, G.J. (2022). Altered transcriptional responses in the lungs of aged mice after influenza infection. Immun Ageing *19*, 27. 10.1186/s12979-022-00286-9.

43. Wolff, C.A., Gutierrez-Monreal, M.A., Meng, L., Zhang, X., Douma, L.G., Costello, H.M., Douglas, C.M., Ebrahimi, E., Pham, A., Oliveira, A.C., et al. (2023). Defining the age-dependent and tissue-specific circadian transcriptome in male mice. Cell Rep *42*, 111982. 10.1016/j.celrep.2022.111982.

44. Metcalf, T.U., Cubas, R.A., Ghneim, K., Cartwright, M.J., Grevenynghe, J.V., Richner, J.M., Olagnier, D.P., Wilkinson, P.A., Cameron, M.J., Park, B.S., et al. (2015). Global analyses revealed age-related alterations in innate immune responses after stimulation of pathogen recognition receptors. Aging Cell *14*, 421-432. 10.1111/acel.12320.

45. Chen, Y., Li, C., Liu, F., Ye, Z., Song, W., Lee, A.C.Y., Shuai, H., Lu, L., To, K.K., Chan, J.F., et al. (2022). Age-associated SARS-CoV-2 breakthrough infection and changes in immune

response in a mouse model. Emerg Microbes Infect *11*, 368-383. 10.1080/22221751.2022.2026741.

46. Lee, N., Shin, M.S., and Kang, I. (2012). T-cell biology in aging, with a focus on lung disease. J Gerontol A Biol Sci Med Sci *67*, 254-263. 10.1093/gerona/glr237.

47. Briceno, O., Lissina, A., Wanke, K., Afonso, G., von Braun, A., Ragon, K., Miquel, T., Gostick, E., Papagno, L., Stiasny, K., et al. (2016). Reduced naive CD8(+) T-cell priming efficacy in elderly adults. Aging Cell *15*, 14-21. 10.1111/acel.12384.

48. Zhou, X., and McElhaney, J.E. (2011). Age-related changes in memory and effector T cells responding to influenza A/H3N2 and pandemic A/H1N1 strains in humans. Vaccine *29*, 2169-2177. 10.1016/j.vaccine.2010.12.029.

49. McElhaney, J.E., Ewen, C., Zhou, X., Kane, K.P., Xie, D., Hager, W.D., Barry, M.B., Kleppinger, A., Wang, Y., and Bleackley, R.C. (2009). Granzyme B: Correlates with protection and enhanced CTL response to influenza vaccination in older adults. Vaccine *27*, 2418-2425. 10.1016/j.vaccine.2009.01.136.

50. Painter, M.M., Mathew, D., Goel, R.R., Apostolidis, S.A., Pattekar, A., Kuthuru, O., Baxter, A.E., Herati, R.S., Oldridge, D.A., Gouma, S., et al. (2021). Rapid induction of antigen-specific CD4(+) T cells is associated with coordinated humoral and cellular immunity to SARS-CoV-2 mRNA vaccination. Immunity *54*, 2133-2142 e2133. 10.1016/j.immuni.2021.08.001.

51. Kometani, K., Yorimitsu, T., Jo, N., Yamaguchi, E., Kikuchi, O., Fukahori, M., Sawada, T., Tsujimoto, Y., Sunami, A., Li, M., et al. (2024). Booster COVID-19 mRNA vaccination ameliorates impaired B-cell but not T-cell responses in older adults. Front Immunol *15*, 1455334. 10.3389/fimmu.2024.1455334.

52. Vanhooren, V., and Libert, C. (2013). The mouse as a model organism in aging research: usefulness, pitfalls and possibilities. Ageing Res Rev *12*, 8-21. 10.1016/j.arr.2012.03.010.

5.3 CHAPTER 3 REFERENCES

1. World Health Organization (2025). WHO Coronavirus (COVID-19) Dashboard. https://data.who.int/dashboards/covid19.

2. Fitzpatrick, M.C., Moghadas, S.M., Pandey, A., and Galvani, A.P. (2022). Two Years of U.S. COVID-19 Vaccines Have Prevented Millions of Hospitalizations and Deaths. https://doi.org/10.26099/whsf-fp90.

3. Mesle, M.M.I., Brown, J., Mook, P., Katz, M.A., Hagan, J., Pastore, R., Benka, B., Redlberger-Fritz, M., Bossuyt, N., Stouten, V., et al. (2024). Estimated number of lives directly saved by COVID-19 vaccination programmes in the WHO European Region from December, 2020, to March, 2023: a retrospective surveillance study. Lancet Respir Med *12*, 714-727. 10.1016/S2213-2600(24)00179-6.

4. Freed, M., Cubanski, J., Ochieng, N., and Neuman, T. (2021). Vaccinating Older Adults in the US Against COVID-19: A Work in Progress. https://www.kff.org/coronavirus-covid-19/issue-brief/vaccinating-older-adults-in-the-us-against-covid-19-a-work-in-progress/.

5. Prevention, C.f.D.C.a. (2025). COVID-19: COVID-NET interactive dashboard. https://gis.cdc.gov/grasp/COVIDNet/COVID19_3.html.

6. Prevention, U.S.C.f.D.C.a. (2023). Deaths by Select Demographic and Geographic Characteristics. https://www.cdc.gov/nchs/nvss/vsrr/covid_weekly/index.htm.

7. Prevention, C.f.D.C.a. (2025). COVID Data Tracker. https://covid.cdc.gov/covid-data-tracker/#datatracker-home.

8. Herrera, A.P., Snipes, S.A., King, D.W., Torres-Vigil, I., Goldberg, D.S., and Weinberg, A.D. (2010). Disparate inclusion of older adults in clinical trials: priorities and opportunities for policy and practice change. Am J Public Health *100 Suppl 1*, S105-112. 10.2105/AJPH.2009.162982.

9. Hurria, A., Levit, L.A., Dale, W., Mohile, S.G., Muss, H.B., Fehrenbacher, L., Magnuson, A., Lichtman, S.M., Bruinooge, S.S., Soto-Perez-de-Celis, E., et al. (2015). Improving the Evidence Base for Treating Older Adults With Cancer: American Society of Clinical Oncology Statement. J Clin Oncol *33*, 3826-3833. 10.1200/JCO.2015.63.0319.

10. Talarico, L., Chen, G., and Pazdur, R. (2004). Enrollment of elderly patients in clinical trials for cancer drug registration: a 7-year experience by the US Food and Drug Administration. J Clin Oncol *22*, 4626-4631. 10.1200/JCO.2004.02.175.

11. Lockett, J., Sauma, S., Radziszewska, B., and Bernard, M.A. (2019). Adequacy of Inclusion of Older Adults in NIH-Funded Phase III Clinical Trials. J Am Geriatr Soc *67*, 218-222. 10.1111/jgs.15786.

12. Cruz-Jentoft, A.J., Carpena-Ruiz, M., Montero-Errasquin, B., Sanchez-Castellano, C., and Sanchez-Garcia, E. (2013). Exclusion of older adults from ongoing clinical trials about type 2 diabetes mellitus. J Am Geriatr Soc *61*, 734-738. 10.1111/jgs.12215.

13. Bourgeois, F.T., Orenstein, L., Ballakur, S., Mandl, K.D., and Ioannidis, J.P.A. (2017). Exclusion of Elderly People from Randomized Clinical Trials of Drugs for Ischemic Heart Disease. J Am Geriatr Soc *65*, 2354-2361. 10.1111/jgs.14833.

14. Cherubini, A., Oristrell, J., Pla, X., Ruggiero, C., Ferretti, R., Diestre, G., Clarfield, A.M., Crome, P., Hertogh, C., Lesauskaite, V., et al. (2011). The persistent exclusion of older patients

from ongoing clinical trials regarding heart failure. Arch Intern Med *171*, 550-556. 10.1001/archinternmed.2011.31.

15. Khezrian, M., McNeil, C.J., Murray, A.D., and Myint, P.K. (2020). An overview of prevalence, determinants and health outcomes of polypharmacy. Ther Adv Drug Saf *11*, 2042098620933741. 10.1177/2042098620933741.

16. Health, N.I.o. (2017). Revision: NIH Policy and Guidelines on the Inclusion of Individuals Across the Lifespan as Participants in Research Involving Human Subjects. U.S. Department of Health and Human Services.

17. Helfand, B.K.I., Webb, M., Gartaganis, S.L., Fuller, L., Kwon, C.S., and Inouye, S.K. (2020). The Exclusion of Older Persons From Vaccine and Treatment Trials for Coronavirus Disease 2019-Missing the Target. JAMA Intern Med *180*, 1546-1549. 10.1001/jamainternmed.2020.5084.

18. Veronese, N., Petrovic, M., Benetos, A., Denkinger, M., Gudmundsson, A., Knol, W., Marking, C., Soulis, G., Maggi, S., Cherubini, A., et al. (2021). Underrepresentation of older adults in clinical trials on COVID-19 vaccines: A systematic review. Ageing Res Rev *71*, 101455. 10.1016/j.arr.2021.101455.

19. Prendki, V., Tau, N., Avni, T., Falcone, M., Huttner, A., Kaiser, L., Paul, M., Leibovici-Weissmann, Y., Yahav, D., and Elderly, E.S.G.f.I.i.t. (2020). A systematic review assessing the under-representation of elderly adults in COVID-19 trials. BMC Geriatr *20*, 538. 10.1186/s12877-020-01954-5.

20. National Council on Aging (2024). The Top 10 Most Common Chronic Conditions in Older Adults. https://www.ncoa.org/article/the-top-10-most-common-chronic-conditions-in-older-adults/.

21. U.S. Department of Health and Human Services, Centers for Disease Control and Prevention (2017-2020). https://wwwn.cdc.gov/nchs/nhanes/continuousnhanes/default.aspx?Cycle=2017-2020.

22. Manly, J.J., Jones, R.N., Langa, K.M., Ryan, L.H., Levine, D.A., McCammon, R., Heeringa, S.G., and Weir, D. (2022). Estimating the Prevalence of Dementia and Mild Cognitive Impairment in the US: The 2016 Health and Retirement Study Harmonized Cognitive Assessment Protocol Project. JAMA Neurol *79*, 1242-1249. 10.1001/jamaneurol.2022.3543.

23. Bates, T.A., Leier, H.C., Lyski, Z.L., Goodman, J.R., Curlin, M.E., Messer, W.B., and Tafesse, F.G. (2021). Age-Dependent Neutralization of SARS-CoV-2 and P.1 Variant by Vaccine Immune Serum Samples. JAMA *326*, 868-869. 10.1001/jama.2021.11656.

24. Baden, L.R., El Sahly, H.M., Essink, B., Kotloff, K., Frey, S., Novak, R., Diemert, D., Spector, S.A., Rouphael, N., Creech, C.B., et al. (2021). Efficacy and Safety of the mRNA-1273 SARS-CoV-2 Vaccine. N Engl J Med *384*, 403-416. 10.1056/NEJMoa2035389.

25. Nanishi, E., Levy, O., and Ozonoff, A. (2022). Waning effectiveness of SARS-CoV-2 mRNA vaccines in older adults: a rapid review. Hum Vaccin Immunother *18*, 2045857. 10.1080/21645515.2022.2045857.